



LUDWIG-
MAXIMILIANS-
UNIVERSITÄT
MÜNCHEN

H2A.Z-Dependent Cellular Responses to a Persistent DNA Double-Strand Break

**Dissertation zur Erlangung des Doktorgrades der
Fakultät für Biologie der Ludwig-Maximilians-Universität München**

vorgelegt von
**Diplom-Biochemikerin
Natalie Jasmin Hiller**

6. Mai 2010



Ehrenwörtliche Erklärung

Hiermit erkläre ich, dass ich die vorliegende Dissertation selbstständig und ohne unerlaubte Hilfe angefertigt habe. Ich habe weder anderweitig versucht, eine Dissertation einzureichen oder eine Doktorprüfung durchzuführen, noch habe ich diese Dissertation oder Teile derselben einer anderen Prüfungskommission vorgelegt.

München, den

.....
(Unterschrift)

Promotionsgesuch eingereicht am: 6. Mai 2010

Datum der mündlichen Prüfung: 16. Juni 2010

Erster Gutachter: Prof. Dr. Stefan Jentsch

Zweiter Gutachter: Prof. Dr. Peter Becker

Die vorliegende Arbeit wurde zwischen September 2006 und Mai 2010 unter der Anleitung von Prof. Dr. Stefan Jentsch am Max-Planck-Institut für Biochemie in Martinsried durchgeführt.

Wesentliche Teile dieser Arbeit sind in der folgenden Publikation veröffentlicht:

Kalocsay, M.* , Hiller, N. J.* & Jentsch, S. Chromosome-Wide Rad51 Spreading and SUMO-H2A.Z-Dependent Chromosome Fixation in Response to a Persistent DNA Double-Strand Break. *Molecular Cell* 33, 335-43 (2009).

** these authors contributed equally to this work.*

Note on results obtained in collaboration:

For the statistical analysis in figures 7A, 11, 12 and 15, data from experimental repetitions performed by M. Kalocsay and N. Hiller in collaboration were used. Experiments solely done by M. Kalocsay are not shown in figures here but referenced by (Kalocsay, 2010; Kalocsay et al., 2009) when mentioned in the text.

Dedicated to my parents

TABLE OF CONTENTS

SUMMARY	1
1 INTRODUCTION	2
1.1 Chromatin structure and function	2
1.1.1 Basic organization of chromatin.....	2
1.1.2 Chromatin dynamics	3
1.2 Sister chromatid cohesion	11
1.2.1 The cohesin complex.....	11
1.2.2 Establishment of sister chromatid cohesion	12
1.2.3 Cohesion establishment in response to DSBs	14
1.3 DNA damage and repair	15
1.3.1 Repair of double-strand breaks by homologous recombination.....	15
1.3.2 The DNA damage checkpoint	18
1.3.3 Adaptation to DNA damage.....	20
1.3.4 DNA repair in the context of chromatin	20
1.4 Nuclear compartmentalization	23
2 AIM OF THIS STUDY	25
3 RESULTS	26
3.1 H2A.Z directs DSB processing and DNA damage checkpoint activation	26
3.1.1 H2A.Z is implicated in DSB repair	26
3.1.2 H2A.Z is required for proper resection of DSB ends	27
3.1.3 H2A.Z is required for proper DNA damage checkpoint activation.....	29
3.2 Role of H2A.Z in DSB repair	30
3.3 A persistent DSB relocates to the nuclear envelope	33
3.3.1 DSB movement to the nuclear envelope can be visualized in vivo	33
3.3.2 Nuclear envelope protein Mps3 binds to the persistent DSB	34
3.3.3 DSB tethering requires H2A.Z, Rad51, and the DNA damage checkpoint.	35
3.4 H2A.Z SUMOylation is required for DSB relocation	37
3.5 Interactors of Mps3 at the nuclear envelope	39
3.5.1 Mps3 binds to H2A.Z	39
3.5.2 Mps3 binds to DSB repair factors	42
3.5.3 Dissecting the function of the Mps3 nucleoplasmic domain.....	42

3.6	Possible functions of DSB relocation to the nuclear envelope	46
3.6.1	The fixed DSB end does not acquire telomere-like features	46
3.6.2	Mps3, DSB tethering and adaptation	47
3.7	Cohesion establishment in response to DSBs	52
3.7.1	H2A.Z binds Eco1, the key player in cohesion establishment	52
3.7.2	H2A.Z-SUMOylation represses cohesion establishment	56
3.7.3	H2A.Z is required for Eco1-mediated cohesion at DSBs	60
4	<u>DISCUSSION</u>	<u>62</u>
4.1	H2A.Z directs DSB-resection, checkpoint activation & repair	62
4.2	A persistent DSB relocates to the nuclear periphery.....	66
4.2.1	Mechanism of break relocation to the nuclear periphery.....	66
4.2.2	Possible functions of break anchoring at the nuclear periphery	69
4.3	H2A.Z and sister chromatid cohesion	72
5	<u>MATERIALS AND METHODS.....</u>	<u>77</u>
5.1	Microbiology	77
5.1.1	<i>Escherichia coli</i> techniques	77
5.1.2	<i>Saccharomyces cerevisiae</i> techniques.....	78
5.2	Molecular biological techniques	85
5.3	Biochemistry techniques	87
5.3.1	Protein methods	87
5.3.2	Chromatin methods	91
5.4	Cell biological techniques	97
5.4.1	Live-cell microscopy.....	97
5.4.2	Cohesion assays.....	97
5.5	Computer-aided analysis	98
6	<u>REFERENCES.....</u>	<u>99</u>
7	<u>ABBREVIATIONS</u>	<u>117</u>
8	<u>ACKNOWLEDGEMENTS.....</u>	<u>122</u>
9	<u>CURRICULUM VITAE</u>	<u>123</u>

SUMMARY

DNA double-strand breaks (DSB) pose an extreme threat to genome stability. Nevertheless, they occur frequently, being inflicted by γ -irradiation and certain genotoxins, but also arising sporadically during faulty replication. If left unrepaired, DSBs can cause chromosome-loss-associated lethality or translocation-driven tumorigenesis. To overcome this fundamental, genotoxic insult, cells have evolved elaborate DNA repair systems, most importantly, homologous recombination (HR), which needs homologous sequences to guide repair and non-homologous end-joining (NHEJ), which involves ligation of DSB ends and is error-prone. By default, DSB repair must function in the context of chromatin. Only recently it is appreciated, how repair pathways have in fact harnessed the preexisting, vast regulatory potential of epigenetics to fine-tune and diversify the cellular DNA damage response (DDR).

This study identified the histone-variant H2A.Z as an important new and early factor in the DDR, being positioned at the vertex of DSB-processing and DNA damage checkpoint activation. Mutants in the gene for H2A.Z are severely sensitive to DSB-inducing agents and defective in both DSB-resection and DSB repair via single-strand annealing. Research over the past decades has established a detailed choreography of events during HR-directed DSB repair. However, little is known about how cells cope with a persistent DSB, when homology-search fails. In the second part of this thesis work, monitoring a single DSB in live cell microscopy and by chromatin immunoprecipitation (ChIP) reveals that when no homology is found and a DSB persists, it relocates to the nuclear periphery. Intriguingly, this process requires not only the recombinase Rad51, but also the DNA damage checkpoint, H2A.Z and its SUMO-modification. The function of sequestering persistent DNA damage to the nuclear periphery might be to prevent deleterious recombination.

Sister chromatid cohesion is a prerequisite for chromosome segregation and DSB repair. Cohesion is established by Eco1, which however needs to be targeted to its chromatin template. In S-phase this occurs via direct interaction with PCNA at the replication fork. How Eco1 is recruited to DSBs is unknown. In its final part, this study reveals and characterizes the interaction between Eco1 and H2A.Z. Remarkably, cells that fail to incorporate H2A.Z into chromatin are specifically defective in DSB-induced cohesion. Moreover, H2A.Z-SUMOylation seems to be a negative regulator of cohesion establishment. Taken together this suggests that besides guiding resection of DSB-ends, an additional function of H2A.Z at the DSB might be to facilitate Eco1 recruitment for cohesion establishment to ensue.

1 INTRODUCTION

1.1 Chromatin structure and function

DNA encodes the blueprint for all cellular functions and is therefore considered to be the central molecule of life. In eukaryotic cell nuclei, genomic DNA is packaged into chromosomes, which ensures faithful replication and transmission during cell division. Moreover, packaging solves a complex and serious challenge for the cell: accommodating 2m of linear DNA in the confined space of a human nucleus, which is only about 6 μm in diameter. Astoundingly, this tight packaging still allows for DNA-transactions such as transcription, replication and DNA repair to occur. Research within the last decades has spurred a renaissance of interest into DNA transactions and chromatin dynamics, placing the nucleosome as a complex regulatory switchboard at the crossroads of virtually all DNA-linked activities.

1.1.1 Basic organization of chromatin

About 40 years ago, nucleosomes were discovered to be the principal repeating unit of chromatin (Kornberg, 1974). Notably, they present the first level of chromosome compaction. The nucleosome core particle comprises 147 bp of DNA being wrapped in a left-handed superhelical fashion around a protein octamer containing 2 molecules each of the canonical histones H2A, H2B, H3 and H4 (Fig. 1A and Luger et al., 1997).

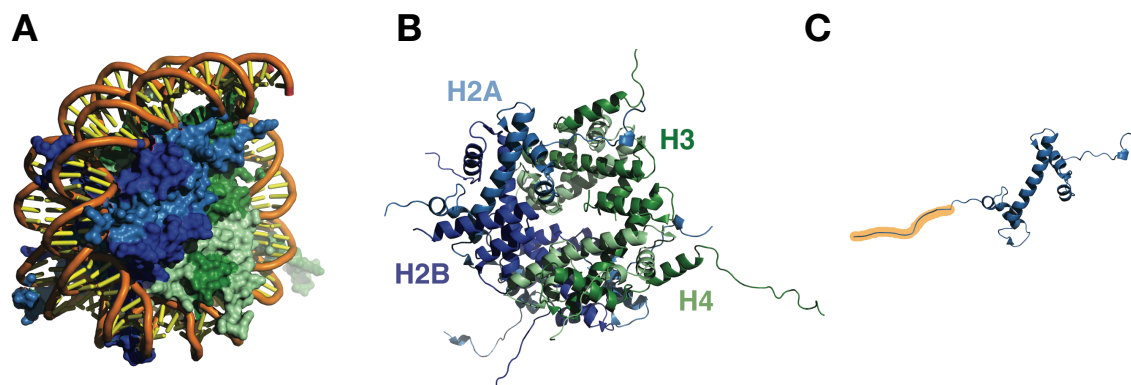


Figure 1. Structure of the nucleosome core particle

The depicted structure was obtained by X-ray crystallography of *Xenopus laevis* reconstituted nucleosomes (PDB-ID: 1AOI; Luger et al., 1997). Histones are color-coded as indicated in (B).

(A) Space-filling representation of the histone octamer core, with the 147nt of DNA making 1.7 tight turns around it. Most of the DNA remains accessible.

(B) Ribbon representation of the histone octamer containing two molecules each of H2A, H2B, H3 and H4. The flexible N-terminal tails emanate from the disc-shaped histone octamer core structure.

(C) A single H2A within the histone octamer shown in (B). The histone fold is formed by three α -helices connected by two loops. This structural motif is shared by all other histones. The very N-terminal tail was too flexible to be resolved in the structure; here it was appended manually (yellow shading).

The protein-DNA contact surface is extensive, however, involves mostly the DNA sugar-phosphate backbone, leaving around 75% of the DNA accessible to solvent and therefore capable of interacting with DNA-binding proteins. Histones are very small (ca. 11-15 kD), highly basic proteins containing, next to a globular core domain (also known as the ‘histone fold’), flexible N-terminal “tails”, which emanate from the nucleosome core (Fig. 1B and 1C). The histone tails are subject to a multitude of posttranslational modifications and serve as binding and signaling platforms thereby controlling various, chromatin-related processes. Indicative of their elemental role in chromosome packaging and chromatin regulation, histones are among the most highly evolutionary conserved proteins known.

Individual nucleosome core particles are connected via “linker DNA”, which can vary in length from 8 to 114 bp. In vivo, chromatin rarely adopts the 11 nm “beads on a string” conformation described above, which is only apparent at low ionic strength. Rather, nucleosomal arrays compact further to form the so-called 30 nm fiber in which nucleosome core particles pack against each other presumably forming a solenoid with ~6 nucleosomes per turn (Khorasanizadeh, 2004). In higher eukaryotes, this structure is stabilized and facilitated by the linker-histone protein H1, which binds to both linker DNA and core histones, thereby bringing together DNA entry and exit paths on the nucleosome. Moreover, H1, which has been reported to have 8 isoforms in higher eukaryotes, is believed to promote condensation by shielding off the negative charge of free linker-DNA. The final mode of chromatin compaction is brought about by higher-order chromatin organization into radial loops. These looped chromatin domains are probably anchored to nuclear scaffolds, such as the lamin-meshwork at the nuclear periphery, however, how exactly this gives rise to the functionally important chromosome territories remains unclear (Cremer et al., 2006).

1.1.2 Chromatin dynamics

The chromatin higher order structure described above is inherently stable. However, it is now well established, that cells modify chromatin structure to confer specificity to many DNA-linked processes. Of these, the best understood today is to determine and index transcriptionally active and inactive regions. Site-specific access to chromatin is often mediated via the nucleosomes packaging the DNA. Three mechanistically distinct classes of factors (Fig. 2) can be distinguished in this context: (1) ATP-dependent chromatin remodeling complexes use energy derived

from ATP-hydrolysis to alter nucleosome-DNA interactions (Clapier and Cairns, 2009). This enables them to disassemble, remodel or reposition nucleosomes on the DNA. (2) Enzymes catalyzing covalent modifications of various histone N-terminal tails set the so-called histone code and contribute profoundly to the diversification of chromatin structure, accessibility and protein factor recruitment. (3) A final mode of chromatin diversification is the deposition of histone variants, which, like histone posttranslational modifications, may directly impact on nucleosome structure *in cis* or act *in trans* by recruiting distinct DNA-transacting proteins.

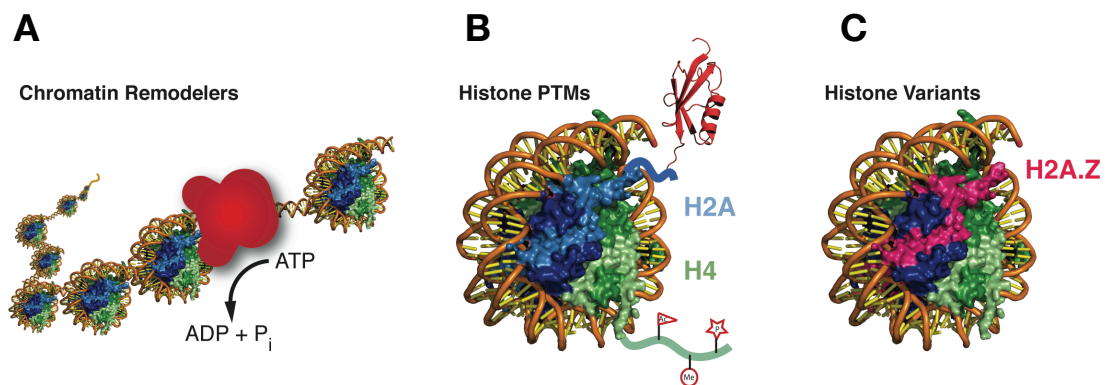


Figure 2. Chromatin dynamics and diversification in its three manifestations

(A) Nucleosome sliding, removal and exchange is catalyzed by ATP-dependent chromatin remodelers (the Luger et al., 1997 structure, PDB-ID: 1AOI, was used to illustrate nucleosome arrays shown here).

(B) Covalent, histone post-translation modifications (PTMs) take place mostly on histone tails. These PTMs include but are by far not limited to: acetylation, methylation, phosphorylation (bottom) and modification by ubiquitin and SUMO (top, PDB-ID: 1EUV; Mossessova and Lima, 2000).

(C) A third mode of chromatin diversification is the deposition of histone variants, here exemplified by an H2A.Z containing nucleosome (PDB-ID: 1F66; Suto et al., 2000).

1.1.2.1 Chromatin remodeling

The inherently rigid structure of chromatin, poses a barrier to essentially all DNA-linked processes occurring within the cell. Therefore, cells have evolved powerful chromatin remodeling activities to bestow the system with the necessary dynamics and flexibility (Fig. 2A). However, cells must hereby strike a delicate balance between on the one hand facilitating access of factors to the DNA substrate and on the other hand, maintaining chromatin structure and epigenetic states.

DNA sequence seems to influence nucleosome positioning. The basic nucleosome structure requires the DNA to be sharply bended and sequences that facilitate this associate preferentially with the histone octamer. This prompted Segal and Widom to put forward a ‘positioning code’ hypothesis (Kaplan et al., 2009; Segal et al., 2006; Segal and Widom, 2009). However, *in vivo*, only 50% of genome-wide nucleosome positions can be predicted on sequence base (Segal et al., 2006) and therefore other, additional factors must exist that govern nucleosome

positioning. In particular, competition with sequence-specific DNA-binding factors and the activity of chromatin remodelers can overrule the observed octamer-DNA sequence preference substantially. Signifying their impact on chromatin dynamics, chromatin remodelers are highly abundant proteins: estimates predict ~1 remodeler per 12 nucleosomes (Ghaemmaghami et al., 2003; Huh et al., 2003; van Vugt et al., 2007).

Chromatin remodelers are multi-subunit, high molecular weight protein machines that harness the energy of ATP hydrolysis to move, evict, destabilize or reassemble nucleosomes (Becker and Horz, 2002). They exhibit several key features: (1) a conserved SWI2/SNF2-family ATPase subunit, (2) preferential nucleosome- versus DNA-binding affinity, (3) regulatory domains for the ATPase activity, and (4) targeting domains recognizing specific histone modifications or chromatin features. According to the exact domain architecture of their ATPase subunit, one can distinguish four remodeling families, which are conserved from yeast to human: SWI/SNF (switching defective/sucrose nonfermentable), ISWI (imitation switch), CHD (chromodomain, helicase, DNA binding) and INO80 (inositol requiring).

In *S. cerevisiae*, the INO80 subfamily is represented by its two only members, the INO80 and the SWR (SWI/SNF-related) complex. Next to transcriptional regulation, these complexes have been implicated in diverse nuclear processes ranging from DNA repair, checkpoint activation, and chromosome segregation to telomere maintenance and DNA replication (Morrison and Shen, 2009). However, the major function of the SWR1 complex is to exchange H2A for the non-canonical variant H2A.Z in chromatin (Kobor et al., 2004; Krogan et al., 2003; Mizuguchi et al., 2004; s. section 1.1.2.3). SWR1 contains next to H2A.Z 11-12 additional proteins and is far less abundant than its sibling, the INO80 complex (656 and 6850 copies per cell, respectively). What exactly recruits SWR1 to chromatin to deposit H2A.Z is unclear, however one subunit, Bdf1, contains bromodomains which were shown to bind the acetylated tails of histone H3 and H4. The defining feature of the entire INO80 subfamily is a split ATPase domain. As noted above, all chromatin remodelers belong to the super family (SF) 2 of DEAD/H-box ATPases. This protein family includes next to type I restriction enzymes also DNA/RNA translocases (Eisen et al., 1995), which often display helicase activity. Despite the apparent homology to helicases, so far, no chromatin remodeler ATPase subunit could be attributed with helicase activity in vitro. INO80 and SWR1 are

special in that they contain helicase activity, which, however, is due to the presence of two RuvB-like helicase subunits in the complex (Jha and Dutta, 2009). Interestingly, the bacterial homolog, the RuvB helicase, catalyzes Holliday junction migration in recombinational repair and was shown to assemble as a double hexamer around the Holliday junction. Intriguingly, the stoichiometry of each RuvB protein in the INO80/SWR complexes is also 1:6, possibly suggesting a functional conservation in DNA repair. Finally, INO80 and the SWR1 complexes contain actin-related proteins (ARPs), which can also be found in other chromatin remodelers like SWI/SNF, RSC but also the NuA4 histone acetyltransferase complex. The exact function of these nuclear ARPs is enigmatic (Dion et al., 2010) but seemingly relates to chaperone activity and binding of histone posttranslational modifications (Chen and Shen, 2007; Downs et al., 2004; Shen et al., 2003).

Taken together, chromatin remodelers are positioned at the crossroads of many nuclear functions that all necessitate chromatin dynamics. Their activities often seem to be redundant but sometimes also oppose each other. More research will be required to decipher the exact function and mechanisms of action of the diverse chromatin remodeling complexes *in vivo*.

1.1.2.2 Histone posttranslational modifications

Histones are subject to a bewildering array of posttranslational modifications (Fig. 2B) of which over 100 have been reported to date (Allis et al., 2006). These include but are not limited to: lysine acetylation, methylation, ubiquitylation, SUMOylation and biotinylation, as well as arginine methylation, serine phosphorylation, proline isomerization and glutamate ADP-ribosylation. By and large, modifications can be grouped into active and repressive chromatin marks. For example, H2B ubiquitylation and H3K4 and K36 methylation are strongly correlated with transcriptional activation. By contrast, H3K9, K27 and H4K20 methylation seem to mediate transcriptional repression (Berger, 2007). Specialized enzymes set each of these modifications and many of them are transient, being reversed again by the respective demodifying enzymes.

The extensive posttranslational modifications (PTMs) on histone tails can have diverse effects. On the one hand they may act *in cis*, by directly impacting on chromatin structure. For instance, lysine acetylation neutralizes the highly positive charge of histone tails and is thought to thereby promote localized dilation of the chromatin template. In line with this hypothesis, lysine acetylation is generally linked to transcriptional activation. Another prominent example is histone phosphorylation,

which by the introduction of a negative charge impedes histone packaging thereby altering higher order structure. Harnessing the converse mechanism, linker histone H1 is suspected to promote packaging by shielding off the negative charge of linker DNA.

However, probably the most prominent effects of histone modifications are mediated *in trans*, by recruitment of modification-binding proteins to specific chromosomal loci. These can 'dock on' to the chromatin marks by distinctive domains, which specifically recognize, i.e. 'read', certain modifications (Taverna et al., 2007). For example, bromodomains recognize acetylated residues whereas chromo-, tudor and MBT-domains as well as PHD-fingers read methylation marks. Similarly 14-3-3 proteins recognize phosphorylated histone tails and ubiquitylation and SUMOylation presumably act in part by recruiting UIM and SIM (ubiquitin and SUMO interacting motif, respectively) –containing proteins. Interestingly, 'reader' domains often co-exist in large multiprotein complexes with 'writers', i.e. histone modifying enzymes. This allows for example in the case of a bromodomain-containing histone acetyltransferase (HAT) complex the spread of the acetylation mark along the chromatin template by a feed forward mechanism (Dhalluin et al., 1999). But many other examples of so-called histone modification crosstalk exist: for instance, H3K36 trimethylation, an active mark associated with transcriptional elongation, is read by concerted PHD-chromodomains within the RPD3-S histone deacetylase complex (HDAC). The thus achieved lysine deacetylation was demonstrated to prevent cryptic initiation of transcription within coding regions (Carrozza et al., 2005; Li et al., 2007).

In summary, the various histone posttranslational modifications seem to correlate with different biological outputs. This spurred the formulation of the 'histone code' hypothesis (Strahl and Allis, 2000), which predicts that the vast array and combinatorial diversity in histone PTMs serves to index chromatin, launching via a 'decoding machinery' distinct and locus-specific functional programs.

1.1.2.3 Histone variants

Next to the chromatin remodeling and posttranslational modification of histone tails, a third mode of chromatin diversification is the deposition of histone variants (Henikoff and Ahmad, 2005; Sarma and Reinberg, 2005; Talbert and Henikoff, 2010). In contrast to canonical histones, whose synthesis and incorporation is tightly controlled and strictly coupled to replication, cells have evolved a range of histone variants, which are expressed and incorporated locally in a rapid and on-demand

fashion throughout the cell cycle. Variants for both H2A and H3 are described, however, interestingly, so far (apart from a single testis-specific case) no variants exist for H2B and H4. This might attribute to their more protected localization within the nucleosome core, which is thought to hinder their exchange for a variant.

The most important and best-studied H3 variants are the centromere-specific CenH3 (Cse4 in yeast, CENP-A in mammals), and H3.3. Strikingly, CenH3 is exclusively incorporated into the centrosomal nucleosomes, where it governs kinetochore assembly. Whereas CenH3 shares only 40-50% sequence identity with canonical H3, the H3 'replacement variant' H3.3 highly resembles its canonical sibling, with only four amino acids being different. Nevertheless, H3.3 incorporation is independent of replication and this histone variant is enriched in transcriptionally active regions and gene regulatory elements. A general theme in H3.3 chromatin biology seems to be its inherent instability and elevated turnover rate, which endows the affected chromosomal loci with high flexibility and provides access for DNA-binding factors.

Among the core histones, H2A has the largest number of variants, including H2AX, MacroH2A, H2A-Bbd and H2A.Z (Fig. 1C). Interestingly, bulk H2A in yeast is of H2AX-type and therefore does not resemble canonical H2A from other species. In mammals ~10% of all nucleosomes contain H2AX instead of H2A. During the rise of the DNA damage response, the PI-3K-related ATM (ataxia telangiectasia mutated, Tel1 in yeast) and ATR (ataxia telangiectasia and RAD3-related, Mec1 in yeast) kinases phosphorylate H2AX-like histones within [S/T]Q consensus motifs in the C-terminal tail (Burma et al., 2001; Ward and Chen, 2001). This seems to be an early, important step in the DNA damage response, especially in mammals (s. section 1.3.4). Interestingly, as first noted by Malik and Henikoff (2003), the H2AX gene copy number seems to correlate well with the dominance of homologous recombination pathways in an organism. Along these lines, yeast, which is highly recombination-proficient relies entirely on H2AX instead of H2A, whereas in humans, with moderate recombination rates, H2A is present in 90% of nucleosomes. Nematodes, which have negligible levels of homologous recombination lack H2AX completely.

H2A.Bbd and MacroH2A are only present in mammals and vertebrates, respectively. Being the most recent addition to the H2A-variant family, H2A.Bbd (bar body deficient) is excluded from the inactive X-chromosome in females and predominantly localizes to euchromatin (Chadwick and Willard, 2001). By contrast, MacroH2A, whose name alludes to the large C-terminal (macro domain) extension

(Pehrson and Fried, 1992), is a hallmark of heterochromatin, and is found at CpG methylation sites (Choo et al., 2006) and on the inactive X-chromosome (Costanzi and Pehrson, 1998).

Unlike other histone variants H2A.Z is highly conserved throughout eukarya. Notably, H2A.Z-like variants across species are more homologous to each other than e.g. *S. cerevisiae* H2A.Z to canonical H2A (Malik and Henikoff, 2003). Seemingly, H2A.Z arose early during eukaryotic evolution and has been distinct from H2A ever since. This ancient evolutionary specialization implies that H2A.Z has an important role, which cannot be substituted for by canonical H2A. Not surprisingly thus, H2A.Z is an essential histone variant in most organisms. By contrast, in budding and fission yeast, deletion mutants of H2A.Z (HTZ1 in yeast) are viable, however, severely sensitive to various cellular stresses.

The structure of the H2A.Z nucleosome (Suto et al., 2000) indicates at least three features distinguishing H2A.Z from the canonical H2A: (1) a unique C-terminal tail, which binds to the Swc2 subunit of the SWR1 complex and specifies Htz1 deposition (Wu et al., 2005). This C-terminal domain also mediates H2A.Z's critical functions next to H2A (Adam et al., 2001), (2) an extended negative surface patch facing outside of the nucleosome which seems to facilitate specific protein-protein interactions (Fan et al., 2004) and (3) sterical clashes within the loop1 region of H2A.Z which supposedly preclude heterodimerization of H2A and H2A.Z in the same nucleosome. In summary, the crystallographic comparison of H2A- and H2A.Z-containing nucleosomes suggests a subtle destabilization of the interaction between the H2A.Z/H2B dimer with the H3/H4 tetramer.

Over the last decade, H2A.Z has emerged as a potent regulator of such diverse processes as transcriptional activation, silencing and even chromosome segregation. In yeast euchromatin, H2A.Z was shown to occupy the two nucleosomes flanking and thereby marking the nucleosome-free regions at transcriptional start sites of most genes (Raisner et al., 2005). Moreover, early studies on H2A.Z and its role in transcription revealed that mutants in H2A.Z had difficulties to induce gene expression from previously repressed loci (Santisteban et al., 2000). In addition, H2A.Z facilitates S-phase progression by directing the timely and full activation of the cell cycle genes *CLN2* and *CLB5* (Dhillon et al., 2006). ChIP-on-chip profiling (Guillemette et al., 2005; Raisner et al., 2005; Zhang et al., 2005) showed that H2A.Z is in fact highly localized, being enriched at intergenic regions and depleted from silenced, subtelomeric loci. Microarray studies pointed

towards a prominent role of H2A.Z in antagonizing the spread of SIR-protein mediated gene silencing (Meneghini et al., 2003). Together with the fact that H2A.Z seems to be excluded from heterochromatic loci, this suggests that H2A.Z acts as a barrier to the spread of silencing. However, despite its high degree of evolutionary conservation between species, the overall role of H2A.Z in transcription remains enigmatic as, depending on the experimental system used, H2A.Z correlates with both active and repressed chromatin (Raisner and Madhani, 2006).

In addition, studies on the stability of H2A.Z nucleosomes compared to the canonical H2A-containing nucleosome are also conflicting (Zlatanova and Thakar, 2008). In mammals, H2A.Z homozygous knockout is lethal, the embryos fail to develop beyond gastrulation (Faast et al., 2001). More recently, RNAi depletions in mammalian cell culture revealed a role for H2A.Z in chromosome segregation (Rangasamy et al., 2004). In addition H2A.Z seems to direct the normal confinement of the HP1 α protein to heterochromatin, and is therefore implicated in the maintenance of facultative heterochromatin (Fan et al., 2004). H2A.Z incorporation is facilitated by the H2A.Z-specific chaperone Chz1, which was only recently identified. Interestingly, histone variant deposition seems to be linked to subsequent acetylation of H2A.Z on lysine (K) 14 by the NuA4 histone acetyl transferase complex (Keogh et al., 2006b; Kobor et al., 2004). This modification seems to be specifically required for stable chromosome propagation but not for other H2A.Z related processes.

In summary, the avalanche of genome-wide nucleosome positioning data has provided us with a very detailed picture of H2A.Z distribution. However, more research is needed to unravel the mechanics of H2A.Z function in its various epigenetic contexts. Conspicuously lacking thus far are e.g. specific binding factors, which could be recruited to H2A.Z-containing nucleosomes.

1.2 Sister chromatid cohesion

Faithful and equal segregation of the genome to both daughter cells during mitosis is fundamental to maintain genomic stability. To preserve the identity of sister chromatids throughout G₂, cells support an intricate machinery that tethers sister chromatids after replication (Fig. 3A). This physical linkage was termed sister chromatid cohesion and is constituted by a protein complex called cohesin (Nasmyth and Haering, 2009; Onn et al., 2008; Peters et al., 2008). Importantly, this allows for the build-up of tension at the metaphase plate, as the spindle exerts force on the bioriented, cohesed sister chromatids. Only when cohesion is dissolved at the metaphase to anaphase transition, can the two sister chromatids migrate to the opposite poles of the mitotic spindle. In consequence, the process of sister chromatid cohesion is essential for cell viability, with faulty cohesion leading to chromosome missegregation, aneuploidy and genome instability.

1.2.1 The cohesin complex

The cohesin complex belongs to the structural maintenance of chromosome (SMC) family, which contains in addition the Mre11-Rad50-Nbs1 (MRN) complex (Mre11-Rad50-Xrs2 (MRX) in yeast), condensin (Smc2/4) and the Smc5/6 repair complex. All these complexes share a conserved architecture. Cohesin is composed of Smc1 and Smc3, two rod-like coiled-coil proteins, which possibly embrace the DNA, the kleisin subunit Scc1 (Mcd1), connecting the two Smc proteins, and the accessory protein, Scc3 (Fig. 3B). The complex is assumed to adopt a ring shaped conformation with a proposed diameter of 35nm, wide enough to accommodate two 10 nm chromatin fibers. Ring closure occurs via the Smc head domains, which contain ABC-transporter-like walker A and B -type ATPases that dimerize upon nucleotide binding. Elegant experiments by the laboratory of Kim Nasmyth in particular suggest a model in which cohesin encircles the two sister chromatids after replication (Gruber et al., 2003; Haering et al., 2008). However, the exact structure and mechanism underlying sister chromatid cohesion by the cohesin complex is still a matter of lively debate. By contrast, the mode of cohesion dissolution in anaphase is undisputed and has been studied in great detail. The key step is the cleavage of Scc1 by the cysteine protease separase, which is otherwise kept inactive through most of the cell cycle, there being sequestered by its inhibitor, securin. Triggered by the anaphase-promoting complex (APC/C), securin is degraded at the metaphase to anaphase transition, thereby setting off chromosome segregation.

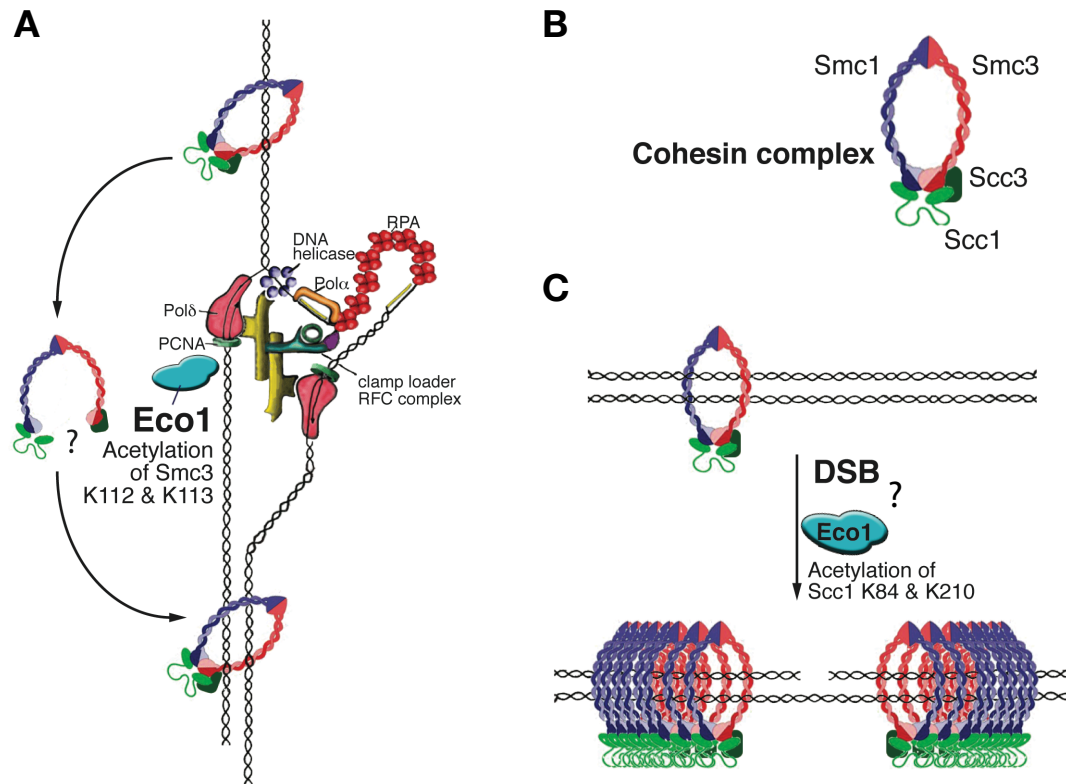


Figure 3. Sister chromatid cohesion

(A) Concomitant to S-phase, sister chromatid cohesion is established by the acetyltransferase Eco1, which travels with the replication fork and acts on pre-loaded cohesin complexes. Eco1 interacts directly via an N-terminal PIP-box with PCNA, the DNA-sliding clamp for the replicative polymerase. The crucial substrate for cohesion establishment in S-phase is the cohesin subunit Smc3, which Eco1 acetylates on K112 and K113 (replication fork model adapted from Witte, 2004).

(B) The large multiprotein complex called cohesin mediates tethering of sister chromatids. Smc1 and Smc3 are coiled-coil proteins with ATPase domains. Scc1 and Scc2 connect the ATPase head domains; thereby the complex adopts a ring-shaped structure.

(C) A second way of cohesion establishment is in response to DSBs. Cohesin complexes are loaded specifically around the DSB. However, for them to become cohesive, Eco1 activity is needed. The crucial substrate in this case seems to be the cohesin subunit Scc1, which Eco1 acetylates on K84 and K210. How Eco1 is recruited to DSBs is unknown (denoted by a question mark).

1.2.2 Establishment of sister chromatid cohesion

Considerably less is known about the initiation of cohesion. Unexpectedly, cohesin is already found on chromatin in telophase, being reloaded onto DNA by the Scc2/Scc4 loading complex immediately after chromosome separation. This association of cohesin with chromatin occurs pericentric and at lower density along chromosome arms, being concentrated at so-called cohesion-associated regions (CARs) (Lengronne et al., 2004). Intriguingly, CARs predominate at sites of convergent transcription, which has been attributed to transcribing PolIII complexes actively pushing cohesin complexes during elongation (Lengronne et al., 2004). Besides being AT-rich, no sequence-specific determinants for CARs could be identified to date. Notably, this initial cohesion loading onto CARs is only of transient nature, with a more stable cohesin-chromatin linkage being established only

concomitant to replication (Fig. 3A and Gerlich et al., 2006). Importantly, this establishment of cohesion during S-phase is strictly dependent on the essential protein factor Eco1 (Skibbens et al., 1999; Toth et al., 1999). How cohesion establishment is linked to replication was solved by the discovery of a direct interaction between PCNA, the ring-shaped DNA polymerase cofactor, and Eco1 (Moldovan et al., 2006). In fact, this interaction is of vital importance, as single amino acid exchanges in the conserved PIP (PCNA-interacting protein)-box of Eco1 lead to inviability or precocious sister chromatid cohesion. Interestingly, Moldovan et al. (2006) could demonstrate that PCNA SUMOylation represses cohesion presumably by blocking Eco1 binding to PCNA. This could constitute a mechanism to ensure that certain chromosomal regions, e.g. highly transcribed ones, remain free of cohesion.

The Eco1 protein contains a C2H2-type zinc finger and an acetyl transferase domain (Ivanov et al., 2002), which acetylates the cohesin subunit Smc3 on lysines K112 and K113 in the nucleotide-binding head-domain (Ben-Shahar et al., 2008; Rowland et al., 2009; Unal et al., 2008; Zhang et al., 2008). This modification takes place in S-phase and is essential for cohesion establishment and cell viability in both humans and yeast. Remarkably, the acetylation-mimicking alterations in Smc3 entirely bypass the requirement for Eco1-function in cohesion establishment, indicating that Smc3 is indeed the critical *in vivo* target. The modification seems to counteract an 'anti-establishment' activity exerted by Wapl and Pds5, which, when deleted, suppress the lethality of $\Delta eco1$ cells as well (Ben-Shahar et al., 2008; Rowland et al., 2009; Sutani et al., 2009).

All domains of the yeast Eco1 protein are conserved in its mammalian homologs, ESCO1 and ESCO2. Mutations in ESCO2 were shown to cause severe developmental diseases, the Roberts and SC phocomelia syndromes, characterized by growth retardation, microcephaly and craniofacial anomalies (Schule et al., 2005; Vega et al., 2005). Cells from Roberts syndrome patients show defects in centromeric sister chromatid cohesion and chromosome segregation, corroborating that Eco1 function is indeed well conserved.

1.2.3 Cohesion establishment in response to DSBs

In *S. cerevisiae*, cohesion is required for efficient double strand break repair via sister chromatid recombination (Sjogren and Nasmyth, 2001; Strom et al., 2004). In undamaged cells, cohesion establishment is limited to S-phase, presumably by its PCNA-mediated linkage to the progressing replication fork (Fig. 3A), even though cohesin complexes continue to be loaded onto chromatin by the Scc2/Scc4 loading complex post-replicatively. Notably, upon irradiation, cohesin complexes are recruited and cohesion is established *de novo* at DSBs (Fig. 3C) in an ATM and ATR dependent manner in yeast (Strom et al., 2004; Unal et al., 2004). Similarly, also in human cells, DNA damage signaling via the MRN complex is required for recruitment of cohesin to laser-induced DNA damage (Kim et al., 2002). Furthermore, DSBs arising in S-phase by replication through a nick were shown to be repaired by a cohesion-mediated sister chromatid exchange mechanism (Cortes-Ledesma and Aguilera, 2006). CHIP-on-chip profiling revealed that cohesin accumulates in a broad chromatin domain (50-100 kb) surrounding the DSB (Strom et al., 2004; Unal et al., 2004). Remarkably, this damage-induced cohesion is not restricted to the DSB site. Rather, cohesion is also established across the entire yeast genome in response to a single DSB (Unal et al., 2007). Recently, it was demonstrated that the cohesin subunit Scc1 directs the damage-induced cohesion pathway. Its phosphorylation on Ser83 by the Chk1 kinase seems to be a critical determinant for cohesion establishment outside of S-phase (Heidinger-Pauli et al., 2008). Remarkably, expression of the phospho-mimicking *scc1*^{S83D} mutant variant resulted in *de novo* cohesion establishment in G2 even in the absence of DNA damage. Similarly, overexpression of Eco1 also allows for post-replicative cohesion establishment (Unal et al., 2007). Notably, DSB-induced cohesion in the G2 phase strictly depends on Eco1, however, not on PCNA or replication (Strom et al., 2007; Unal et al., 2007). Together, this indicates that an alternative, yet undiscovered, recruitment pathway for Eco1 must exist outside of S-phase.

1.3 DNA damage and repair

Both extracellular as well as intracellular damage sources constantly threaten the integrity of our genome. DNA-lesions can arise from replication errors, metabolic byproducts, such as reactive oxygen species, but also clastogenic agents and UV or γ -irradiation. The damage can manifest itself as single strand nicks, base alterations or whole chromosome breakage. By far the most toxic type of DNA lesion is the DNA double strand break (DSB). There are estimates that a single human cell encounters 10 DSBs per day on average (Bernstein and Bernstein, 1991), and a single one, if left unrepaired, can be lethal or lead to translocation-driven tumorigenesis. Interestingly, in special cases, cells also deliberately create DSBs for chromosomal rearrangements to ensue, as is the case in meiosis, V(D)J recombination of immunoglobulin genes and yeast mating type switching. However, in the vast majority of cases, DSBs are unwanted, toxic and deleterious events. Therefore, it comes as no surprise that cells have evolved powerful DNA repair pathways. DSBs are repaired either by non-homologous end-joining, an error-prone process involving ligation of the broken ends, or homologous recombination (Fig. 4), which uses homologous sequences to guide repair and is therefore error-free. For space constrains, only the latter repair mechanism will be introduced in detail in the following.

1.3.1 Repair of double-strand breaks by homologous recombination

The first step in homologous recombination (HR) is the recognition of the DNA lesion by so-called sensor proteins, which initiate the DNA damage response (DDR) by recruiting repair and checkpoint proteins to relay the signal onwards. The paramount DSB sensor protein is the MRN or MRX (in yeast) complex, which fulfills a tripartite function in the DDR: (1) the extended Rad50 coiled-coils directly bind and physically tether DSB ends, (2) the Mre11 nuclease facilitates the initiation of DSB resection i.e. the formation of single-stranded DNA (ssDNA), and (3) the Nbs1 subunit (Xrs2 in yeast) recruits and activates the key checkpoint kinase ATM (Tel1 in yeast). This, in turn leads to phosphorylation of target substrates in the vicinity of the DSB, thereby creating novel binding platforms for repair proteins. Mre11 itself in conjunction with CtIP (Sae2) initiates break-proximal, short-range 5' strand degradation by an endonucleolytic mechanism (Clerici et al., 2005; Lengsfeld et al., 2007; Sartori et al., 2007). In yeast, this early intermediate serves as template for the

RecQ-family helicase Sgs1 (the *S. cerevisiae* BLM ortholog) and the exonucleases Exo1 and Dna2, which concertedly drive robust, long-range resection (Mimitou and Symington, 2008; Zhu et al., 2008). Interestingly, resection requires Sae2 (CtIP)-phosphorylation by Cdc28 (CDK1) activity and is therefore inhibited in the G1 phase of the cell cycle (Huertas et al., 2008; Huertas and Jackson, 2009; Ira et al., 2004), where in consequence, NHEJ is favored over HR.

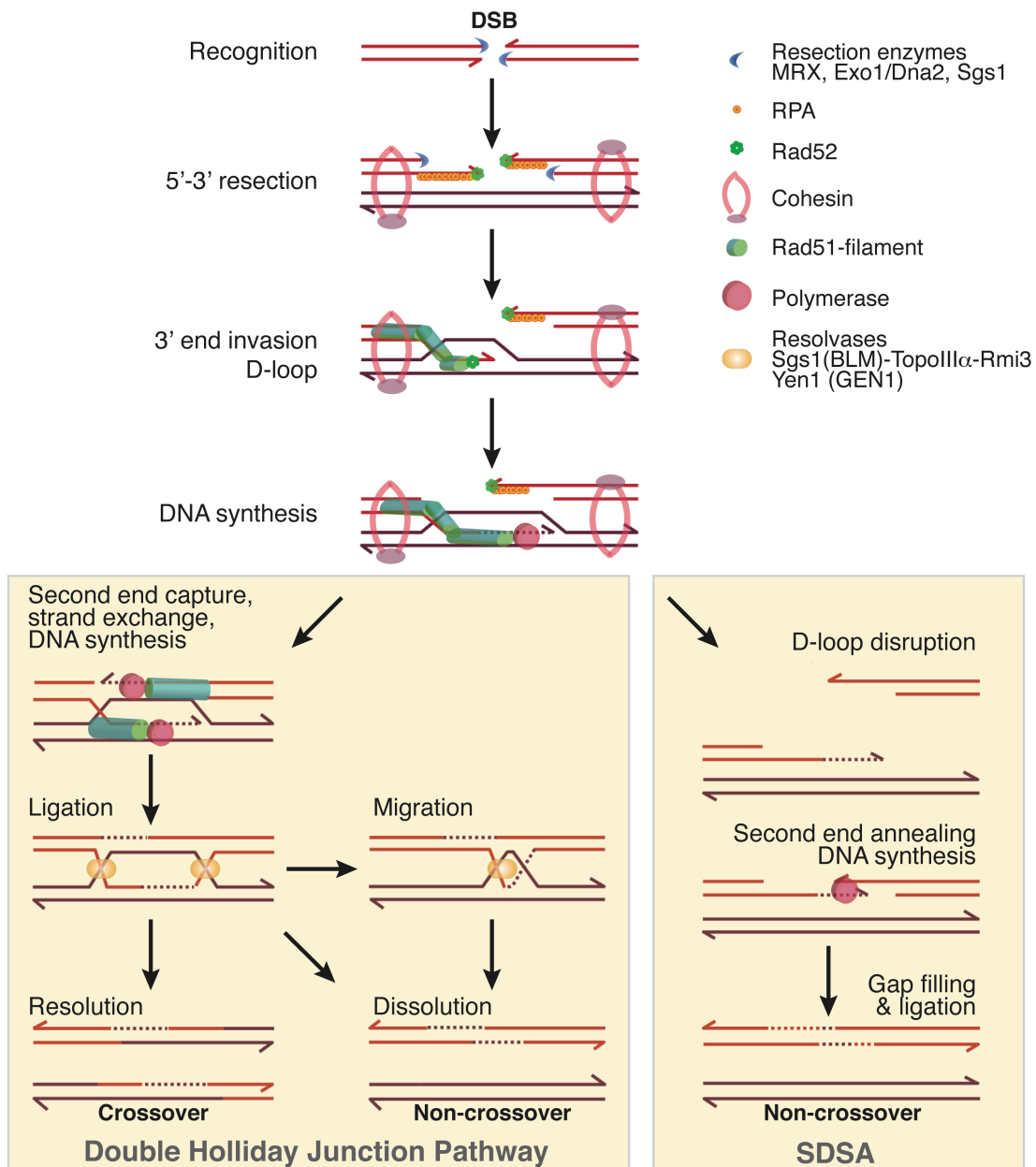


Figure 4. The homologous recombination pathway of DSB repair

5' resection of DSB ends creates 3' single-stranded tails, which are immediately coated by RPA. Cohesins are recruited and cohesion is established *de novo*. With the help of Rad52, RPA is replaced by Rad51, which forms nucleoprotein filaments. In an enigmatic fashion, these search for homology, initiate pairing and catalyze invasion of the homologous duplex DNA. The such-formed D-loop is extended by DNA synthesis. In the SDSA model (right panel), displacement of the invading end disrupts the D-loop, allowing for completion of repair by DNA synthesis. If the second end is captured (left panel), repair proceeds via double Holliday junctions, which can be re- or dissolved to form crossover and non-crossover products (adapted from Hastings et al., 2009).

Next, the ssDNA is rapidly coated by the heterotrimeric RPA (replication protein A)-complex. These RPA-ssDNA complexes serve as crucial triggers and reinforcement cues for the activation of the DNA damage checkpoint. Subsequently, Rad52, an important mediator in HR, replaces RPA for Rad51, the actual recombination catalyst. Rad51 then forms a nucleoprotein filament, which, in a fashion that is still poorly understood, scans the genome for homology. In case of successful homology search, the Rad51 nucleoprotein filament invades the homologous duplex DNA displacing a single-stranded loop, i.e. forming a heteroduplex D-loop structure (Fig. 4). Of note, several eukaryote-specific recombination proteins exist (e.g. Rad59, Rad55/57 and Rad54) which aid or regulate and may give directionality to the recombination reaction. Subsequently, the invading 3' ssDNA break end primes DNA synthesis, which is templated by the homologous donor locus.

In its simplest form, as proposed by the synthesis-dependent strand annealing (SDSA) model, recombination then proceeds by branch migration displacing the newly synthesized strand. Reannealing with the resected, other DSB end is thought to occur without forming crossover structures. Importantly, this results in non-reciprocal transfer of genetic information from the donor locus (gene conversion), which itself remains unedited (Fig. 4, right panel). In an alternative mode of recombination (Szostak et al., 1983), which predominantly occurs in, but is not restricted to, meiosis, the second end is captured to form a stable double Holliday junction. This recombination intermediate can be dissolved by the Sgs1 (BLM)-TopoIII-Rmi1 complex (Ira et al., 2003; Oh et al., 2007; Wu and Hickson, 2003) or resolved by Yen1 (Gen1) (Ip et al., 2008) to yield non-crossover or crossover and non-crossover products, respectively (Fig. 4, left panel).

Two other recombination mechanisms, which will be briefly introduced here, are single-strand annealing (SSA) and break-induced replication (BIR). When a DSB is created within direct repeat sequences, the resected ssDNA repeat regions simply anneal to one another, instead of invading a homologous duplex DNA. This process is termed SSA, is Rad51-independent and results in deletion of one repeat and the repeat-intervening sequence (Fishman-Lobell et al., 1992). Interestingly, the kinetics of SSA correlate best with the length of the sequence separating the direct repeats and the time needed to resect the latter. In fact, first resection speed estimates (5kb/h) come from SSA model systems with differently spaced repeat sequences (Vaze et al., 2002). Another particular case is found with DSBs at telomeres or

broken replication forks, which are single-ended. These are repaired by BIR (McEachern and Haber, 2006), which shares the initial processing steps until D-loop formation with the SDSA model, however results in much longer gene conversion tracks.

1.3.2 The DNA damage checkpoint

The cellular response to DNA damage is coordinated with the cell cycle by a signal transduction cascade termed the DNA damage checkpoint. This pathway arrests cell division until repair has occurred. The DNA damage checkpoint is a multifaceted and highly integrated response, the key players of which can be defined as damage signals, sensor kinases, adaptor proteins and effector kinases. Within this system, a high degree of redundancy and feed forward amplification ensures that even minute levels of damage are detected. Remarkably, in *S. cerevisiae*, a single, unrepaired DSB is sufficient to trigger a prolonged G2/M cell cycle arrest (Lee et al., 1998).

As mentioned above, MRN-complexed break ends and RPA-coated ssDNA are the two fundamental damage indicators within the cell and establish the two pillars of the DDR, ATM and ATR-dependent signaling, respectively. More specifically, the MRN subunit Nbs1 recruits the sensor kinase Tel1 (ATM) whereas the ssDNA/RPA complexes attract Mec1 (ATR) via its recruiting factor Ddc2 (ATRIP) to the site of damage (Paciotti et al., 2000; Rouse and Jackson, 2002; Zou and Elledge, 2003). Despite their apparent homology to the PI3K-family, ATM and ATR are protein kinases. Another indispensable, pivotal factor for checkpoint signaling is the 9-1-1 complex (Rad9, Rad1 and Hus1 in *S. pombe*, and Ddc1, Rad17 and Mec3 in *S. cerevisiae*). Structurally and by sequence identity, it resembles the processivity factor for replication, PCNA, forming a heterotrimeric ring around DNA (Dore et al., 2009; Krishna et al., 1994). Moreover, 9-1-1-loading onto the ssDNA/dsDNA boundaries at DSB sites is accomplished independent of Mec1/Ddc2 by a modified form of the heteropentameric replication factor C (RFC) complex (Kondo et al., 2001), in which the Rfc1 subunit is replaced for Rad24. Again, RPA-coated ssDNA greatly facilitates the 9-1-1 loading reaction. Taken together, it seems that cells generally gauge the amount of damage by assessing the magnitude of RPA covered ssDNA.

The next step in the DNA damage checkpoint is to relay the initial signal onward via the conserved effector kinases Chk1 and Chk2 (Rad53 in yeast). These often necessitate so-called adaptor proteins or mediators, which act as landing pads for the effector kinases at the site of damage. The best understood example of

such a collaborative interplay is represented by Rad53 and Rad9 (53BP1). In response to DNA damage, Mec1 (ATR) phosphorylates Rad9 at multiple SQ/TQ sites (Emili, 1998) in a 9-1-1 – dependent fashion. This triggers relocation to the actual DSB site (Naiki et al., 2004) and oligomerization via the C-terminal BRCT (BRCA1 C-terminal) domain (Soulie and Lowndes, 1999). In addition, Rad9 concentration in the vicinity of DSBs is promoted by γ -H2AX (Celeste et al., 2003; Ward et al., 2003) and via exposed H3K79-trimethylation marks, which are recognized by the Rad9 tudor domain (Huyen et al., 2004; Wysocki et al., 2005). Importantly, patches of phosphorylated Rad9 molecules subsequently serve as landing pads for the major damage effector kinase Rad53, which binds to Rad9 phosphopeptides via a conserved FHA (forkhead associated)-domain. The multivalency of the Rad9-docking module, brings multiple Rad53 molecules into close proximity. This seems to be the crucial trigger for Rad53 kinase activation via a trans-autophosphorylation reaction (Gilbert et al., 2001). Hyperphosphorylated, activated Rad53 gets released from the Rad9 catalytic surface patch, allowing for a new round of activation, quick amplification and downstream signaling. Colocalization of sensor proteins in high concentrations and close proximity to each other indeed seems to be key in the DDR. In support of this notion, it was elegantly demonstrated that artificially colocalizing 9-1-1 and Ddc2/Mec1 on chromosomes is in fact sufficient to trigger a robust activation of the DNA damage checkpoint even in the absence of DSBs or ssDNA (Bonilla et al., 2008).

The final target of the effector kinases Chk1 and Rad53 (Chk2) is the cell cycle machinery itself. Chk1 acts through hyperphosphorylation of the yeast securing ortholog Pds1 (Cohen-Fix and Koshland, 1997; Sanchez et al., 1999). This modification stabilizes the key anaphase inhibitor Pds1 by rendering it resistant to Cdc20/APC-mediated ubiquitylation and subsequent degradation. Next to this Chk1-dependent stabilization mode, the interaction between Cdc20 and Pds1 seems to be counteracted by a parallel, Rad53-dependent mechanism (Agarwal et al., 2003). Inhibition of the mitotic exit network via the polo-like kinase Cdc5 (Sanchez et al., 1999) and a transcriptional response via the Dun1 kinase (Zhao and Rothstein, 2002) are two described modes of Rad53 downstream action. However, falling short of its pivotal role in DSB-induced cell cycle arrest, the full repertoire of Rad53 downstream targets and its mechanism of action remain ill defined.

1.3.3 Adaptation to DNA damage

Whereas multicellular eukaryotes enter senescence or apoptosis if challenged with persistent unreparable DNA damage, the unicellular yeast can escape checkpoint arrest and reenter the cell cycle by a mechanism called adaptation. After expression of HO-endonuclease either continuously or shortly in a repair-deficient background, yeast cells react to the irreparable damage by a prolonged G2/M arrest. However, 15 hours after DSB-induction, the checkpoint is reversed and cell cycle progression is resumed, despite the presence of the persistent DSB (Lee et al., 1998; Toczyski et al., 1997). This invariably leads to genomic instability, as the resulting chromosome fragment is missegregated in the vast majority of cell divisions (Galgoczy and Toczyski, 2001; Kaye et al., 2004). The fact that yeast cells still support this checkpoint escape mechanism implies that for a single-cell organism survival by eventual, slow repair, serendipitous mutation or mating is of higher priority than maintaining genome stability by all means, i.e. at the cost of its own cell death. Genetically, several proteins have been identified to be required for Rad53 inactivation and cell cycle re-entry during adaptation. Many of these factors also direct checkpoint recovery, which allows resumption of cell proliferation if the DNA damage can in fact be repaired. In particular, Ku70/80, Rad51, Srs2, Sae2, as well as the phosphatases Ptc2/3 and the kinases CKII and Cdc5 are required for adaption (Lee et al., 1998; Pellicioli et al., 2001; Toczyski et al., 1997; Vaze et al., 2002). The cellular mechanisms underlying checkpoint adaption remain obscure but most likely involve silencing of the downstream effector kinases, Rad53 and Chk1. Interestingly, the amount of ssDNA formed seems to be a major determinant of whether adaption will ensue, as already two DBSs in one cell or heightened resection rates in Ku-complex mutants preclude checkpoint adaptation (Lee et al., 1998).

1.3.4 DNA repair in the context of chromatin

Much is known about the principle DNA repair pathways and mechanisms. However, in the wake of epigenetics, several concepts had to be revised and repositioned in the context of chromatin, the natural substrate of all DNA repair reactions *in vivo*. Remarkably, research within the past decade has unearthed many important chromatin-based regulatory elements that impact on DNA repair and the DNA damage response. However, a detailed and concise understanding of the intricate crosstalk between epigenetics and DNA repair still has to be obtained in the years to come.

Certainly, a hallmark of the DNA damage response is the ATM/ATR (Tel1/Mec1)-dependent phosphorylation of H2AX (phosphorylated H2A at Ser-129 in *S. cerevisiae*), which occurs already minutes after DSB induction and is considered the earliest known marker of DNA damage. In response to a DSB, phosphorylated H2AX (γ -H2AX) is found in surprisingly large chromatin domains flanking the break site, the spreading ranging from 50-100 kb in *S. cerevisiae* to 1MB in mammals (Rogakou et al., 1999; Shroff et al., 2004). How H2AX is recruited to DSBs is unclear. The current status of research suggests that H2AX is in fact randomly incorporated into chromatin but becomes phosphorylated only around DNA damage sites. Homozygous knockout of H2AX in mice is viable, however causes genome instability, male infertility and defects in the DNA damage response, e.g. less IR-induced foci (Celeste et al., 2002). The crucial event, however seems to be the formation of γ H2AX, as point mutants abrogating phosphorylation by ATM show similar phenotypes as the complete knockout (Celeste et al., 2003).

A major function of γ H2AX seems to be maintaining the activity of the DNA damage checkpoint and recruitment of downstream repair proteins. The key γ H2AX-recognizing factor was shown to be MDC1 (Rad9 in yeast). It binds to the γ H2AX phosphopeptide by C-terminal tandem BRCT-domains and acts as adaptor protein relaying the signal downstream (Stucki et al., 2005). Many other DDR-factors harboring phosphospecific FHA- or BRCT are subsequently recruited to irradiation-induced foci (IRIFs) in a MDC1/ γ H2AX-dependent manner (Stucki and Jackson, 2006). Moreover, Arp4, a shared component of the NuA4 histone acetyltransferase and the Ino80 and Swr1 chromatin remodelers binds directly to γ H2AX, thereby recruiting these multi-subunit protein complexes to DSBs (Bird et al., 2002; Downs et al., 2004; Morrison et al., 2004; van Attikum et al., 2004). Finally, γ H2AX is also the crucial trigger for the post-replicative recruitment of cohesin complexes to DSBs (Strom et al., 2004; Unal et al., 2004).

Besides H2AX phosphorylation, histone ubiquitylation has emerged as another important example of how the DDR harnesses the power of chromatin posttranslational modification to facilitate accumulation and retention of repair- and checkpoint factors at the DSB. A series of very recent publications, have established a regulatory ubiquitylation cascade, involving the chromatin surrounding the DNA lesion. This pathway is controlled by the ubiquitin E3-ligases RNF8 (Huen et al., 2007; Kolas et al., 2007; Mailand et al., 2007) and RNF168 (Doil et al., 2009; Stewart et al., 2009), which sequentially and in conjunction with the E2 conjugating

enzyme Ubc13 mediate ubiquitylation of H2A-type histones (Bergink et al., 2006) and possibly other chromatin substrates (Panier and Durocher, 2009). Ultimately, this series of ubiquitylation results in the recruitment and retention of BRCA1/BARD1 and 53BP1, two essential players in the mammalian DDR. Interestingly, the former is recruited by being associated with the ubiquitin-binding proteins Rap80 and Abraxas (Kim et al., 2007a; Sobhian et al., 2007; Wang et al., 2007), whereas the latter directly binds to di-methylated lysine 20 on histone H4, which seems to become exposed only after histone ubiquitylation (Botuyan et al., 2006). Notably, mutations in RNF168, which abolish its catalytic activity and BRCA1 recruitment to DSBs, were shown to be the genetic cause of RIDDLE syndrome, a human immunodeficiency and radiosensitivity disease (Stewart et al., 2009; Stewart et al., 2007). Intriguingly, BRCA1/BARD1, which are well known for their implication in hereditary predisposition to ovarian and breast cancer, are themselves E3-ubiquitin ligases. However the critical downstream target for ubiquitylation still remains to be identified. In conclusion, ubiquitylation has emerged as a central regulator of the DNA damage response. It will be interesting to decipher the inner workings of this regulation and the full repertoire of substrates in future research.

How chromatin is modified and partially disassembled during the DDR and DSB repair has been studied quite extensively. However much less is known about how chromatin, and its original epigenetic state are restored in the wake of DSB repair. The prevalent γ H2AX signal seems to be eliminated by histone eviction and a phosphatase complex containing Pph3 (Keogh et al., 2006a). Moreover, the histone chaperones CAF-1 and Asf1 aid in the rebuilding of chromatin during recovery from the DNA damage checkpoint (Kim and Haber, 2009). In addition, Asf1-dependent acetylation of histone H3 on lysine 56 by Rtt109 seems to be a critical histone mark fueling chromatin reassembly and checkpoint recovery (Chen et al., 2008). Besides the described histone-deubiquitylation enzymes implicated in transcription (Weake and Workman, 2008), prime candidates for reversing histone ubiquitylation surrounding a DSB are Usp3 and Usp28, which were shown to specifically counteract DSB-induced ubiquitylation events (Nicassio et al., 2007; Zhang et al., 2006). Significant strides have been made but we are still far from understanding the aftermath of the DDR, in particular chromatin restoration and checkpoint reversal.

In summary, there seems to be ample crosstalk between chromatin modifications and the DDR. Particularly γ H2AX and histone ubiquitylation have emerged as integral components of the DNA damage signaling response.

1.4 Nuclear compartmentalization

The cell nucleus is a highly dynamic and complex cellular 'organelle', by far transcending its originally proposed role as mere repository for nucleic acids. Intriguingly, the nucleus itself seems to be compartmentalized, with more and more subnuclear structures being identified. Albeit lacking membranous demarcation, they represent highly specialized domains, concentrating nuclear processes and containing characteristic sets of proteins. For example, the nucleolus harbors rDNA and functions as ribosome biogenesis factory. But also several, smaller nuclear 'bodies' have been identified to date (e.g. PML-, Cajal-, and cleavage bodies as well as stress granules and nuclear speckles; Spector, 2006).

By and large, gene-poor, heterochromatin is enriched at the nuclear periphery, whereas transcriptionally active chromatin is located more centrally (Kosak et al., 2007; Misteli, 2007). Therefore, genomic DNA itself and its epigenetic state still have the biggest impact on nuclear architecture. Despite the lack of condensed chromosome structure in interphase nuclei, the DNA is highly organized. In fact, DNA fluorescence in situ hybridization (FISH) studies revealed that generally, individual chromosomes are confined non-randomly in nuclear volumes termed chromosome territories (Cremer et al., 2006). However, these are still bestowed with sufficient flexibility to allow for interchromosomal interactions.

The double lipid bilayer of the nuclear envelope encompasses the nucleoplasm, being traversed only by nuclear pore complexes which act as gatekeepers of the nucleo-cytoplasmic transport. In metazoans, the inner nuclear membrane is lined by the nuclear lamina, a meshwork of type V intermediate filaments, which are attached to the nuclear membrane by LEM- and SUN-domain containing transmembrane proteins. The nuclear lamina also intimately interacts with the perinuclear heterochromatin and mutations in lamin genes are the cause of muscular dystrophy diseases, the laminopathies (Worman and Bonne, 2007).

Accumulating evidence suggests that the three-dimensional position of a gene locus within the nucleus provides another means of epigenetic regulation (Akhtar and Gasser, 2007; Zhao et al., 2009). For instance, tethering of telomeres to the nuclear periphery was shown to facilitate the so-called telomere positioning effect (TPE), a heritable repression of telomere-proximal genes. However, perinuclear association must not always mean transcriptional repression. Rather on the contrary, several studies have shown that clustering of highly transcribed genes

in the vicinity of nuclear pores ensures a tight and efficient coupling between transcription and subsequent mRNA-export (Rodriguez-Navarro et al., 2004; Taddei et al., 2006). Along these lines, the inducible *GAL* genes were shown to relocate to nuclear pore complexes upon activation (Casolari et al., 2004). Notably, a different study revealed that recently repressed *GAL* genes are retained at non-pore sites on the inner-nuclear membrane to facilitate ‘transcriptional memory’ (Brickner et al., 2007; Brickner, 2009).

In summary, much progress has been made on the description of subnuclear compartments and their functional implications, especially on transcription. However, what regulates recruitment, retention and trafficking of chromosomal loci between the various subnuclear compartments as well as the impact of nuclear positioning on chromatin transactions other than transcription, remains to be elucidated.

2 AIM OF THIS STUDY

At the onset of this thesis work, Mps3, a transmembrane protein of the inner nuclear membrane, seemed an extremely fascinating protein to study. On the one hand, not much was known about the nuclear periphery in general or about Mps3 in particular. First reports on telomere positioning at the nuclear periphery and its impact on transcriptional regulation foreshadowed the tantalizing possibility, that the nuclear envelope could constitute an own subnuclear compartment whose function however remained to be explored. On the other hand, it had been briefly noted in the literature, primarily by high-throughput studies, that both the histone variant H2A.Z as well as the key cohesion establishment protein Eco1 interact with Mps3 (Antoniacci et al., 2004; Uetz et al., 2000). Intriguingly, this presented the possibility of functional links between the nuclear periphery compartment, H2A.Z and sister chromatid cohesion. One aim of this study was therefore, to dissect the functional relevance and to elucidate the connectivity between H2A.Z, chromatin position relative to the nuclear periphery and sister chromatid cohesion.

Repair by homologous recombination had been studied in great detail, however, not particularly in the context of chromatin. Especially the potential impact of histone variants or posttranslational modification thereof remained elusive. The yeast *S. cerevisiae* is special compared to other eukaryotes in that it only harbors a single histone H2A variant, H2A.Z, which in addition is nonessential in this organism. Moreover, most of our knowledge about DSB repair stems from studies conducted in yeast, one of the most highly recombination-proficient species known. A second aim of this thesis was therefore to make use of *S. cerevisiae* as an ideal model organism to discover novel functions for the histone variant H2A.Z and characterize these, especially in respect of DSB repair.

3 RESULTS

3.1 H2A.Z directs DSB processing and DNA damage checkpoint activation

Homologous recombination has been studied in great detail. However, the importance of chromatin structure and histone modifications for DNA double-strand break (DSB) repair and signaling became evident only very recently. In particular, incorporation of the histone H2A variant γ H2A.X seems to be crucial for a full-blown checkpoint response and recruits key DNA repair factors into ionizing radiation-induced foci (IRIF). But also chromatin-remodelers and histone post-translational modification have been implicated to play important regulatory roles in DNA damage processing, signaling and repair.

3.1.1 H2A.Z is implicated in DSB repair

In contrast to higher eukaryotes, the yeast *Saccharomyces cerevisiae* harbors only a single histone H2A variant, H2A.Z. Struck by the importance of histone variants for the mammalian DNA damage response, yeast strains deleted for H2A.Z (also called Htz1) were tested for sensitivity to DSB-inducing chemicals. Strikingly, the *HTZ1* deletion (Δ htz1) was highly sensitive to DSBs, in fact almost as sensitive as strains lacking the major recombination factor Rad51 (Fig. 5). Interestingly, the Δ htz1 sensitivity appears specific for DSBs, as neither the alkylating agent MMS nor UV-irradiation could significantly inhibit growth compared to wild type (data not shown). Together, these findings suggested the histone variant H2A.Z as a new player in DSB repair.

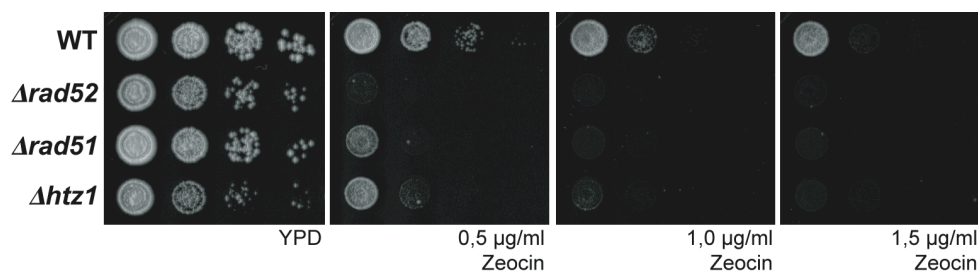


Figure 5. H2A.Z deletion mutants (Δ htz1) are sensitive to DSBs

Equal amounts of cells were spotted onto YPD plates or plates containing the DSB-inducing agent zeocin (pH 7.2). Images were taken after 48h of growth at 30°C.

3.1.2 H2A.Z is required for proper resection of DSB ends

To identify the exact role of H2A.Z in the DNA damage response, the early steps in DSB processing, repair and checkpoint activation, were scrutinized first. To this end, a haploid *S. cerevisiae* strain was used, in which a single genomic DSB at the mating-type (*MAT*) locus can be synchronously created by galactose-inducible expression of HO endonuclease (Fig. 6A). Deletion of the homologous (donor) *HML* and *HMR* loci and the continuous expression of HO endonuclease prevent repair by HR and NHEJ, respectively (Fig. 6B). As repair is impeded in this strain (JKM179, subsequently called donor-deficient), early DSB processing intermediates accumulate and are readily detectable upon DSB-induction.

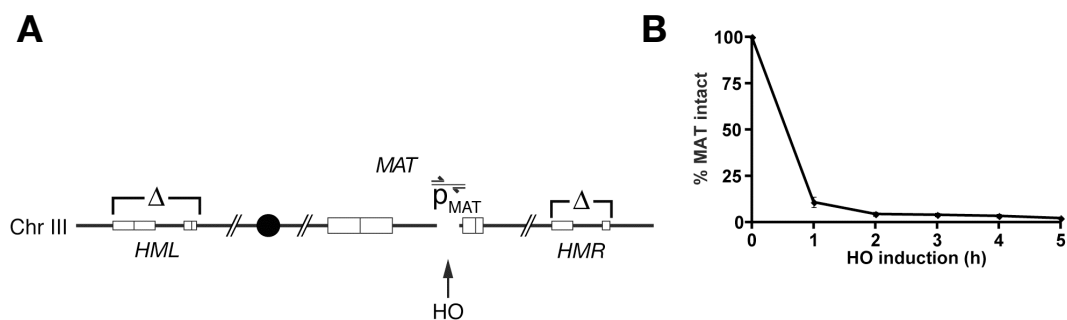


Figure 6. Donor-deficient strain with HO-inducible DSB at *MAT*

(A) Schematic representation of chromosome III. A single DSB (arrow) is induced at the *MAT*-locus by expression of HO endonuclease. Regions of homology are shown as boxes. *HML* and *HMR* loci are deleted in the strain JKM179 (Δ). Position of primer pair P_{MAT} spanning the break site and used for assaying DSB formation in (B) are indicated. A filled circle denotes the relative position of the centromere.

(B) DSB formation determined by quantitative PCR (primer pair P_{MAT}) over time. Continuous expression of HO prevents repair by NHEJ and sister chromatid recombination. Data are shown as mean of 3 independent experiments \pm SEM.

As noted before (Zhu et al., 2008), DNA resection at the HO-induced DSB continues in the donor-deficient wild-type (WT) strain and one can distinguish experimentally initiation of 5'-strand resection at the DSB end from long-range resection. To monitor initiation of resection at the HO cut site, quantitative real-time (RT) PCR was performed with a primer pair amplifying 200 bp proximal to the DSB. Loss of input DNA over time in the vicinity of the DSB is a direct consequence of resection of these regions to ssDNA, resulting in a reduced PCR signal. Therefore, the kinetics of DNA-level reduction at *MAT* can be used as a measure for initiation of resection (Chen et al., 2008). Strikingly, mutants deficient in H2A.Z ($\Delta htz1$) showed a significant delay in the initial formation of ssDNA at the DSB (Fig. 7A). To corroborate this finding further, long-range resection was monitored in Southern blots with an RNA-probe complementary to the 3'-strand 10kb to the left of the HO cut site. As resection progresses, EcoRI, the enzyme used for genomic DNA

digestion, is no longer able to cleave the DSB-proximal regions, which have become single stranded. Therefore, bands corresponding to DNA fragments in Southern blot hybridization diminish over time. Whereas the region 10kb away from the DSB is resected within 6 to 8 hours in WT, it remains double-stranded in cells lacking H2A.Z (Fig 3B). Together these data establish a role for H2A.Z in DSB resection.

To substantiate this finding by an independent assay, the recruitment of the ssDNA-binding RPA complex to the DSB was monitored by chromatin immunoprecipitation (ChIP) analysis directed against the RPA subunit Rfa1 (Fig. 7C).

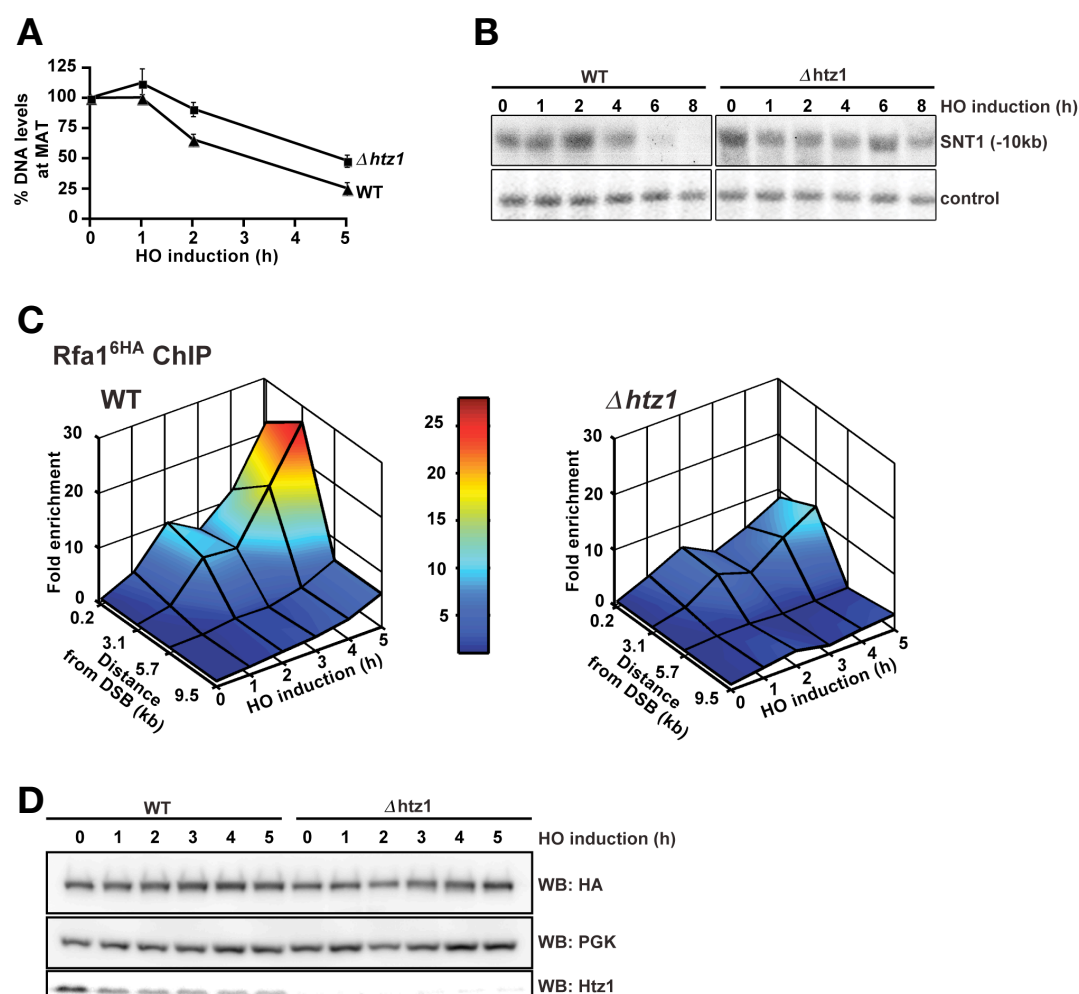


Figure 7. Defects of H2A.Z mutants in DNA resection

(A) Resection measured by RT-PCR as the loss of PCR product (Chen et al., 2008) using primers 0.2 kb from the DSB in WT (triangles) and $\Delta htz1$ (squares). The 0 h time point was set to 100%. Data are shown as mean of 3 independent experiments \pm SEM.

(B) 5'-strand resection measured by Southern blot analysis (Zhu et al., 2008). Genomic DNA prepared from samples taken at the indicated time points was digested with EcoRI and run on an alkaline gel followed by gel blotting and hybridization with 3'-strand-specific ssRNA probes as indicated. The *SNT1* probe binds 10kb to the left of the break; the loading control is a probe against the unaffected *TRA1* locus on chromosome VIII. 5'-strand resection progressively eliminates the EcoRI cut sites around the DSB; therefore, the 5.3 kb *SNT1* fragment disappears in WT after 6-8 hrs.

(C) Rfa1^{6HA}-directed ChIP at the indicated time points after HO induction in WT (left panel) and $\Delta htz1$ (right panel). The heat bar indicates relative enrichments (IP/input).

(D) Western blot analysis of input material for the Rfa1^{6HA}-directed ChIP experiments shown in (C).

In WT, a strong enrichment of RPA at the DSB was detectable and, importantly, it was markedly dependent on both the time of HO induction and the distance from the DSB. In contrast, RPA recruitment in the $\Delta htz1$ mutant was delayed, supporting the finding that this mutant has a resection defect. Importantly, Rfa1 protein levels remained unchanged in the $\Delta htz1$ mutant (Fig. 7D), enervating the possibility of a merely indirect effect of H2A.Z due to its well-documented role in transcription (Zlatanova and Thakar, 2008).

3.1.3 H2A.Z is required for proper DNA damage checkpoint activation

A single DSB, when not repaired, elicits a Mec1-dependent DNA damage checkpoint and cell cycle arrest at the G2/M transition (Harrison and Haber, 2006). The trigger for this signalling cascade is the RPA-coated ssDNA formed as one of the earliest steps in DSB processing. Given the requirement of H2A.Z for proper resection and RPA-recruitment, the question arose whether mutants deficient in H2A.Z would also show a DNA damage checkpoint defect. Indeed, and in accordance with its role in resection, cells lacking either H2A.Z ($\Delta htz1$) or its deposition complex SWR ($\Delta swr1$) show a partial defect in checkpoint activation and cell cycle arrest as monitored by the status of Rad53 phosphorylation (Fig. 8A) and fluorescence-activated cell sorting (FACS)-analysis (Fig. 8B), respectively. Remarkably, full checkpoint activation was only dependent on H2A.Z when in response to a single HO-induced DSB. When cells were challenged with an array of chemically induced DSBs, rapid checkpoint activation occurred even in the absence of H2A.Z (Fig. 8C). These data imply that cells can distinguish single from multiple DSBs and launch a qualitatively different checkpoint response to each stimulus.

Another hallmark of the DNA damage checkpoint is the formation and spreading of phosphorylated H2A (equivalent to mammalian γ H2A.X) around the DSB. Confirming a role for H2A.Z in resection and subsequent checkpoint activation, γ H2A.X formation around the DSB was indeed significantly diminished in $\Delta htz1$ compared to WT (Fig. 8D). Taken together, these data identify H2A.Z as a novel player in DNA resection and single DSB-induced DNA damage checkpoint activation.

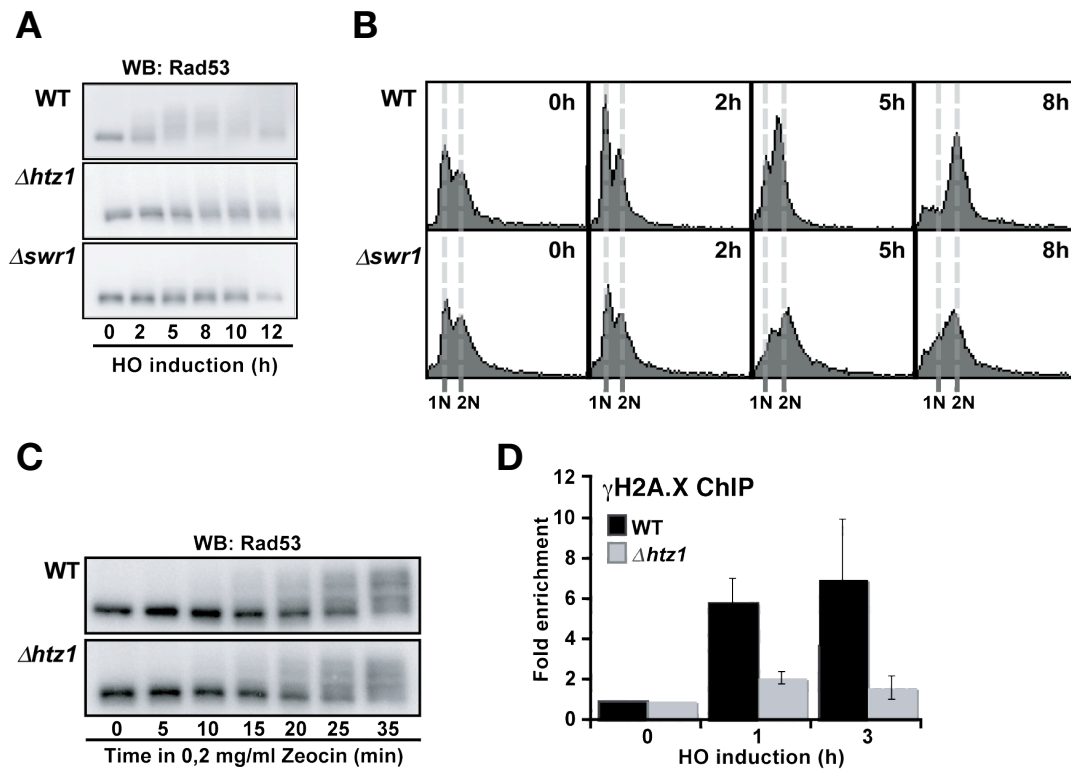


Figure 8. Defects of H2A.Z mutants in DNA damage checkpoint activation

(A) Defective checkpoint activation in response to a single DSB as monitored by Rad53 phosphorylation in $\Delta htz1$ and $\Delta swr1$ compared to WT.

(B) Assessment of cell cycle phase by measuring DNA-content per cell in FACS-analysis. The $\Delta swr1$ strain shows a partial defect in DSB-induced cell cycle arrest at the G2/M stage compared to WT. Samples were taken at the indicated time points after HO induction.

(C) Normal checkpoint activation kinetics in response to chemically induced DSBs. WB as in (A).

(D) Defective checkpoint activation in response to a single DSB as monitored by γ H2A.X (phospho-H2A)-directed ChIP at 9.5 kb from the DSB in WT and $\Delta htz1$. Shown are IP/input signals normalized to 1 for the signal before induction and data are shown as mean of 3 experiments \pm SEM.

3.2 Role of H2A.Z in DSB repair

The striking sensitivity of H2A.Z mutants to DSB-inducing agents (Fig. 5) implied that H2A.Z is indeed functionally linked to DSB repair. To assess H2A.Z's exact role in DSB repair, a donor-proficient strain was used in which a DSB is only shortly induced at *MAT* and subsequently repaired by gene conversion. In this strain, repair involves the homologous *HML α* locus and results in mating type switching from *MAT α* to *MAT α* . Therefore, the kinetics of repair can be readily followed by PCR or Southern blot with *MAT α* -specific primers or probes, respectively. Indeed, when quantified by RT-PCR, mutants lacking H2A.Z showed a significant delay in mating type switching by gene conversion (Fig. 9A and 9B). However, Southern blot analysis demonstrated that H2A.Z, apart from slightly influencing the kinetics, is definitely proficient in mating type switching *per se* (Fig. 9B and 9C). The switched

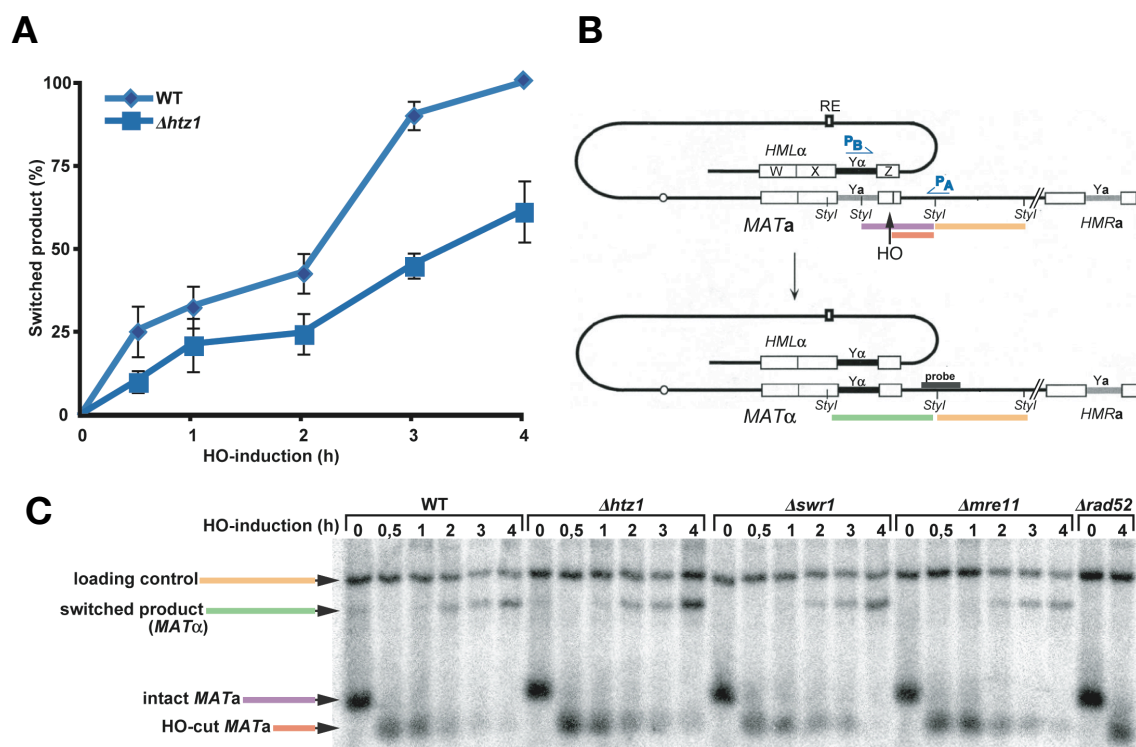


Figure 9. Effect of H2A.Z deletion on DSB repair by gene conversion

(A) RT-PCR with primer pair P_A and P_B as depicted in (B). PCR product formation indicates strand-invasion into the homologous region at HML and mating type switching. Obtained signal intensities were normalized to an unaffected control locus and the WT 4h time point was set to 100%. Data are shown as mean of 3 independent experiments \pm SEM.

(B) Schematic representation of Chromosome III before (top panel) and after (lower panel) mating type switching in the donor proficient strain used to monitor DSB repair by gene conversion in (A) and (C). A single DSB (arrow) is induced at the *MAT*-locus by expression of HO endonuclease. Regions of homology and the recombination enhancer (RE) element are shown as boxes. Position of primer pair P_A and P_B used for assaying mating type switching in (B) are indicated (blue). *StyI* restriction sites, the resulting DNA fragments and the probe used for Southern blot detection in (C) are indicated.

(C) Southern blot analysis of mating type switching. Genomic DNA prepared from samples taken at the indicated time points was digested with *StyI* and run on an alkaline gel followed by gel blotting and hybridization with the *MAT*-specific probe indicated in (B). HO endonuclease cuts the intact *MAT α* fragment (purple, 730 bp) giving rise to a smaller cleavage fragment (red, 508 bp). The switched, *MAT α* product lacks the *StyI* restriction site present within the *MAT α* sequence and is thus larger (green, 1881 bp). The loading control corresponds to the first *StyI* restriction fragment on the right of the *MAT* locus (yellow, 4326 bp), which is not affected by mating type switching.

product restriction fragment appeared in both $\Delta htz1$ and $\Delta swr1$. Of note, yeast mating type switching requires only about 300 bp of DNA to the right of the HO cut site (containing the homology information) to be resected in order for repair to ensue. Thus e.g. mutations in the MRX complex which is required for resection, only delay but do not prevent mating type switching (Ivanov et al., 1994). A stricter requirement for resection can be seen in the single-strand annealing (SSA) pathway, where an induced DSB is repaired by recombination between flanking repeats (Fig. 10A and Vaze et al., 2002). In this assay, galactose-inducible HO expression creates

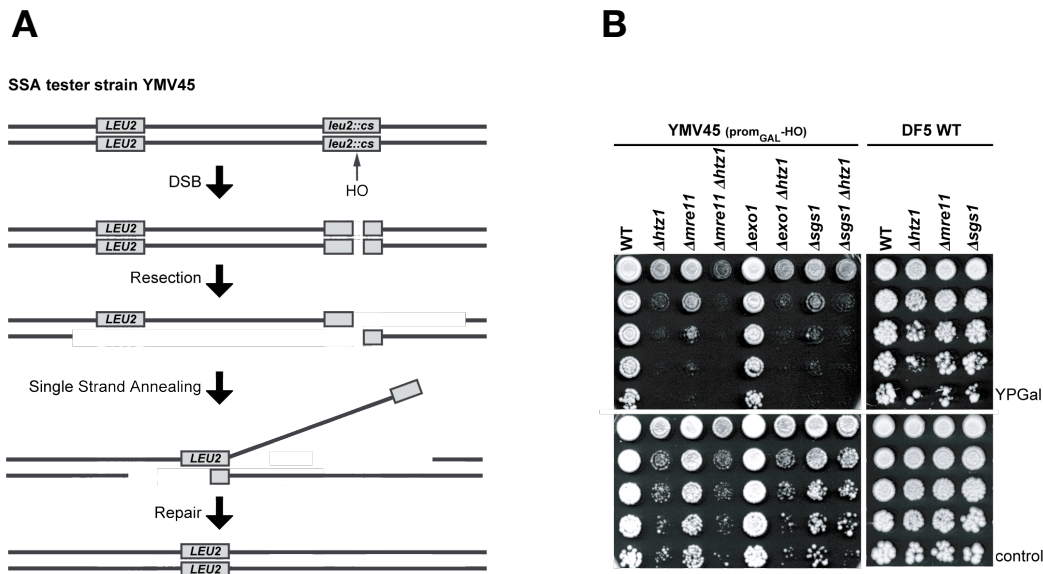


Figure 10. Role of H2A.Z in DSB repair by single strand annealing (SSA)

(A) Schematic representation of DSB repair by SSA in the tester strain YMV45. An HO cut site was introduced into the endogenous *leu2* locus and a second *LEU2* gene copy placed 4.6kb upstream. A single DSB (arrow) is induced at the *leu2*-locus by galactose-induced expression of HO endonuclease. 5'-strand resection needs to proceed for at least 4.6 kb for single strand annealing between the complementary regions to occur. The annealed intermediate is then processed by removal of the overhanging single-stranded tails, gap filling and ligation.

(B) Equal amounts of cells were spotted onto plates containing either galactose (YPGal) or glucose (control) as carbon source. Images were taken after 48h of growth at 30°C.

a DSB within the endogenous *leu2* gene locus. As the second *LEU2* sequence is inserted 4.6 kb downstream, resection of this stretch of DNA is a prerequisite for SSA to occur. To test whether mutants lacking H2A.Z were proficient in SSA, WT and mutant tester strains were spotted onto galactose-containing plates (Fig. 10B). Successful completion of SSA between repeats eliminates the HO cut site, and cells can therefore grow on galactose-containing plates. However, strains incapable of repair by SSA have to continually cope with a persistent DSB and eventually die due to chromosome loss. Similar to known resection mutants like *Δmre11* and *Δsgs1* (Vaze et al., 2002), *Δhtz1* cells are indeed extremely sensitive to HO-expression when productive SSA is required for survival (Fig. 10B). Importantly, *Δhtz1*, which is known to play a role in *GAL*-gene transcription, does not confer galactose sensitivity *per se* as shown by the robust growth in a DF5 WT background (Fig 6B, right panel).

Recent reports have revealed at least two additional pathways that are required for proper resection in the absence of, or in addition to the MRX-complex (Gravel et al., 2008; Mimitou and Symington, 2008; Zhu et al., 2008). While MRX is responsible for the initiation of resection, long-range resection is facilitated in an Sgs1- and Exo1-dependent manner. Interestingly, the effect of *Δhtz1* on SSA was

additive when combined with mutations in Mre11 and Exo1. However, the double mutant $\Delta htz1\Delta sgs1$ showed the same sensitivity as, i.e. was epistatic to, $\Delta htz1$ alone. This suggests that H2A.Z may promote resection in a pathway together with Sgs1 and in parallel to MRX and Exo1.

3.3 A persistent DSB relocates to the nuclear envelope

Although previous studies have established a detailed choreography of events during HR-directed DSB repair, little is known how cells react if no homology is found and the break persists. The observed prolonged DNA resection at the break (Fig. 7B and Zhu et al., 2008) suggested that the HR machinery maintains its activity over several hours even if homologous sequences are not found. This raised the question of how cells cope with broken ends if homology search fails.

3.3.1 DSB movement to the nuclear envelope can be visualized in vivo

To address whether a persistent DSB was positionally stable or would alter its localization within the nucleus, a tandem array of lac repressor binding sites (240 x *lacO*) was integrated adjacent to the HO cut site on chromosome 3 in the donor-deficient strain (Fig. 11A). Expression of a nuclear-targeted GFP-LacI fusion and Nic96^{mars} as a nuclear envelope marker allowed visualization and tracking of DSB movement in live cells and real time.

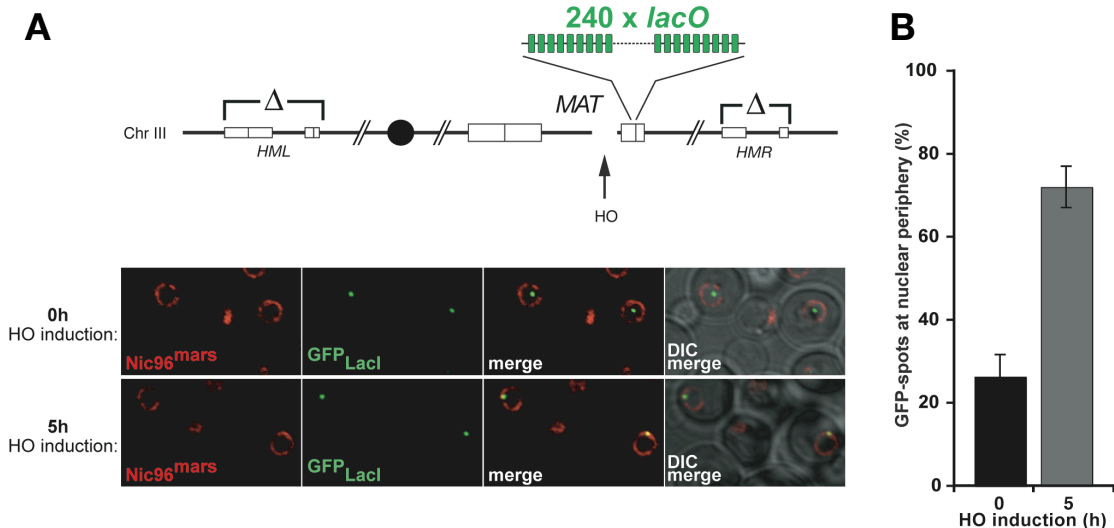


Figure 11. *In vivo* visualization of DSB recruitment to the nuclear periphery

(A) Expression of GFP-LacI fusion marks a 240 x *lacO* array (green) integrated proximal to *MAT*. The nuclear envelope is visualized by Nic96^{mars} (red). A single DSB (arrow) is induced at the *MAT*-locus by expression of HO endonuclease and cells were imaged by live cell microscopy at the indicated time points after HO induction.

(B) Quantification of live-cell microscopy depicted in (A). Shown are means of three independent experiments \pm SEM ($n > 345$).

In this system, the position of the DSB is marked by a single green focus in every nucleus. Prior to induction of the DSB, the *MAT* locus showed a quasi-random distribution with about 30% of the GFP signals touching the nuclear envelope. However, five hours after DSB induction, the labeled DSB relocated to the nuclear periphery as 70% of the GFP-labeled DSBs were found at the periphery at this time (Fig. 11B and 11C). Notably, this value is close to the maximum periphery localization scorable in this experimental setup, as it has been reported that directly tethering the GFP-LacI fusion to the nuclear envelope results in 80% periphery localization (Brickner and Walter, 2004).

3.3.2 Nuclear envelope protein Mps3 binds to the persistent DSB

To verify this interesting phenomenon by an independent assay, nuclear envelope-directed ChIP experiments were performed. Throughout eukarya, attachment of chromosomes to the nuclear periphery and clustering (bouquet formation) is thought to promote homologous chromosome pairing and recombination during meiotic prophase. Mps3, the yeast SUN-protein homolog seems to play a major role in telomere anchoring at the nuclear envelope (Bupp et al., 2007; Conrad et al., 2007; Ding et al., 2007; Penkner et al., 2007; Schober et al., 2009). Supporting the DSB microscopy results (Fig. 11), a robust, time-dependent increase in Mps3 ChIP signal using primers annealing very close to the break site could be observed (Fig. 12).

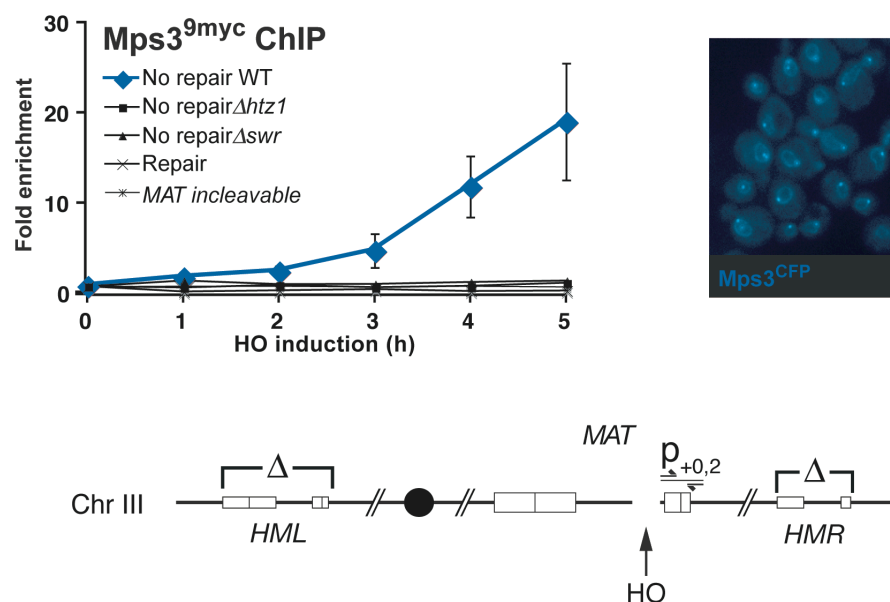


Figure 12. Binding of a persistent DSB to the nuclear envelope protein Mps3
Mps3^{9myc}-directed ChIP at *MAT* after HO induction. Shown are IP/input signals normalized to 1 for the signal before induction. DSB-proximal primers used for quantification are indicated in the schematic below the graph. Inset on right shows localization of endogenous Mps3 to the nuclear envelope and spindle pole bodies. Data are represented as mean \pm SEM.

Remarkably, this binding to the nuclear envelope occurred only at late time points after break induction. Moreover, Mps3 was not recruited to the break site at any time in a mutant bearing a non-cleavable HO site at *MAT* or in a donor proficient strain where the break is repaired by homologous recombination. Together, this strongly suggests that the newly identified response pathway requires a persistent break and homology search failure as crucial trigger for DSB relocation.

3.3.3 DSB tethering requires H2A.Z, Rad51, and the DNA damage checkpoint.

Investigating this novel and interesting phenomenon further, the question emerged, what factors would signal for break relocation to the nuclear envelope. Remarkably, $\Delta rad9 \Delta rad24$ mutants, that are deficient in the DNA damage checkpoint response, completely failed to recruit the break to the nuclear periphery (Fig. 13). To corroborate this finding, a more DSB physiological experimental setup for assessing the checkpoint requirement was conceived. To this end, cells were arrested in the G1 phase of the cell cycle, where NHEJ is favored over HR and, upon endonuclease-induced DSBs, neither resection nor checkpoint activation occur. In line with the aforementioned result, G1-arrested cells are similarly defective in break recruitment to the nuclear periphery (Fig. 14). Taken together, these data indicate that resection and checkpoint activation are required for break relocation to the nuclear periphery. Importantly, this suggested that H2A.Z might be involved in this process as well.

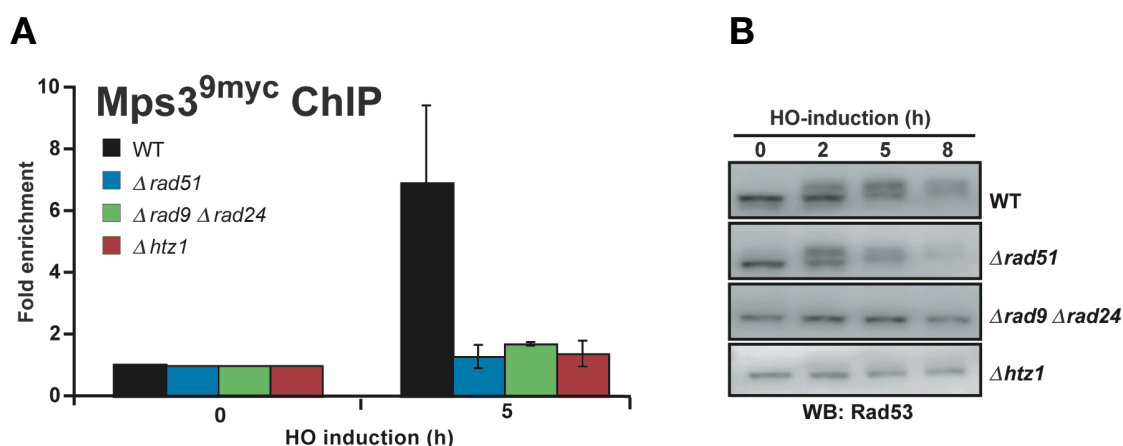


Figure 13. DSB binding to Mps3 requires H2A.Z, Rad51 and the DNA damage checkpoint

(A) Mps3^{9myc}-directed ChIP at *MAT* (0.2 kb from DSB) Shown are IP/input signals normalized to 1 for the signal before induction. Data are represented as mean \pm SEM.

(B) DNA damage checkpoint activation as measured by Rad53 phosphorylation. Western blot analysis of input material used for ChIP experiments shown in (A)

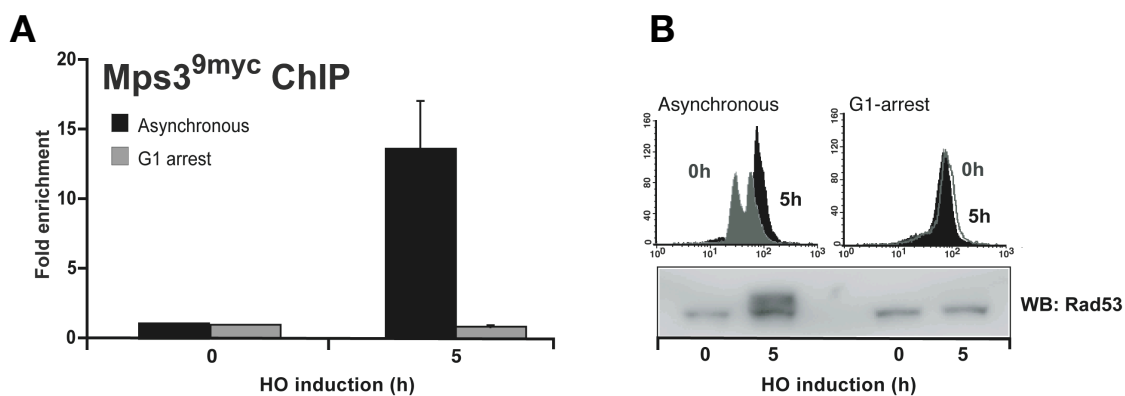


Figure 14. Persistent DSBs fail to relocate to the nuclear periphery in G1

(A) Mps3^{9myc}-directed ChIP at *MAT* (0.2kb from DSB) in either asynchronously growing cultures or cultures arrested in G1 by the addition of 0.5 μ g/ml alpha-factor. Shown are IP/input signals normalized to 1 for the signal before induction. Data are represented as mean \pm SEM.

(B) Cell cycle status as measured by FACS analysis and checkpoint activation as scored by Rad53 phosphorylation for input samples of the ChIP experiment shown in (A).

In accordance with the requirement of H2A.Z for single DSB-induced checkpoint activation (Fig. 8), H2A.Z (Δ *htz1*) deletion mutants as well as *swr1* mutants were indeed defective in Mps3-DSB association (Fig. 12). Interestingly, Δ *rad51* mutants also failed to recruit Mps3 to the DSB (Fig. 13A), demonstrating that Rad51 activity and presumably ongoing homology search is also needed for the relocation process. Interestingly, Rad51 activity seems to be required in addition to the DNA damage checkpoint, as checkpoint activation does occur in the Δ *rad51* mutant (Fig. 13B). In summary, these findings demonstrate that DSB relocation requires both, checkpoint signaling and factors involved in DSB repair. Moreover, H2A.Z seems to guide not only the early resection of DSB ends and subsequent checkpoint activation, but also the final break anchoring to the nuclear envelope.

3.4 H2A.Z SUMOylation is required for DSB relocation

Chromosome behavior and DNA transactions are significantly controlled by protein modifications, specifically on histone tails. Intriguingly, chromatin-associated H2A.Z is modified by the ubiquitin-related protein SUMO on lysine K126 and K133 (Kalocsay, 2010; Kalocsay et al., 2009). To test whether SUMO-modification of H2A.Z is implicated in break relocation to the nuclear periphery, strains were constructed that contained as their only source of H2A.Z the respective non-SUMOylatable mutants (*htz1^{K126R}*, *htz1^{K133R}*, and *htz1^{K126,133R}*). These were subsequently employed in Mps3-directed ChIP (Fig. 15A) and live-cell microscopy (Fig. 15B) experiments. Importantly, although the SUMOylation-defective H2A.Z variants were expressed at normal levels (Fig. 15C), these point mutants showed a prominent defect in break recruitment to the periphery as scored by microscopy and ChIP analysis (Fig. 15A and 15B). These data imply, that besides DNA damage checkpoint, also H2A.Z SUMOylation is specifically required for DSB relocation.

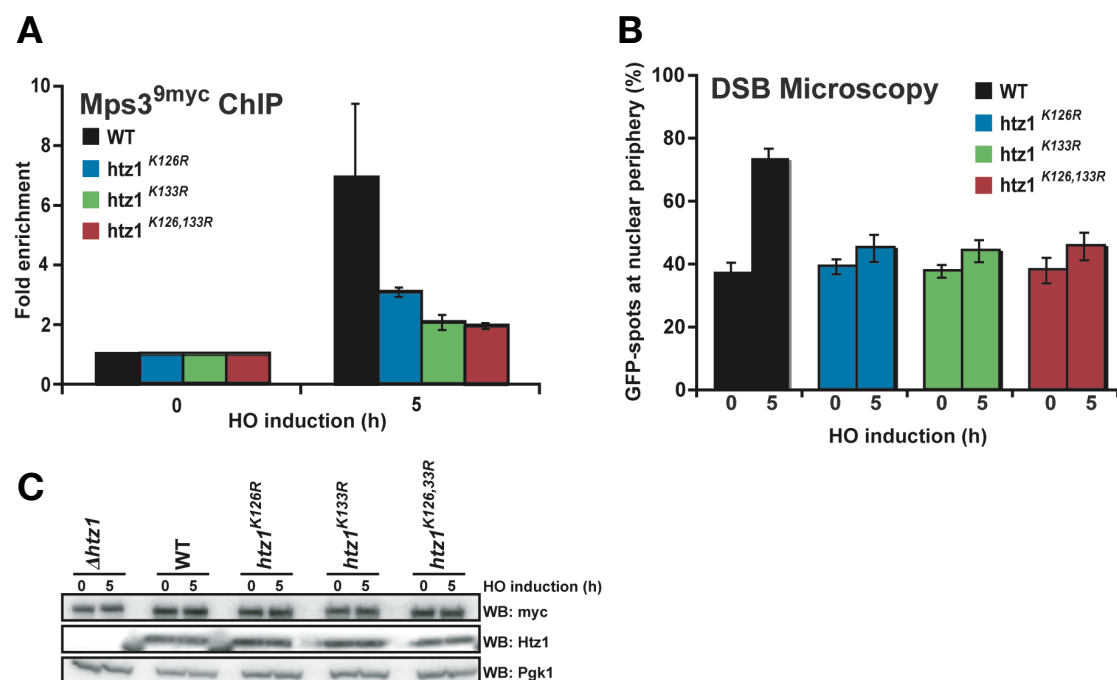


Figure 15. H2A.Z SUMOylation is required for DSB relocation

(A) Mps3^{9myc}-directed ChIP as in Fig. 13A, but in SUMOylation-defective *htz1* point mutants.

(B) Quantification of live-cell microscopy data for DSB relocation to the nuclear envelope (similar setup as that in Fig. 11, n>550). Shown are means of three independent experiments \pm SEM.

(C) SUMOylation-defective *htz1* point mutants are expressed like WT, as seen in input samples for the Mps3^{9myc}-directed ChIP shown in (A).

Surprisingly, however, the SUMOylation-defective H2A.Z variants were not detectably more sensitive to DSB-inducing agents than WT cells (Fig. 16A). In fact, only when preventing repair by HR, e.g. in a $\Delta rad52$ background, H2A.Z SUMOylation could marginally raise the survival rate under DNA damage conditions (Fig. 16B). As the SUMOylation-defective *htz1* mutants still exhibited a normal DNA damage checkpoint response (Fig. 16C), H2A.Z-SUMO and the checkpoint seem to be required independently of each other for the relocation of the unrepaired chromosomal break to the nuclear periphery.

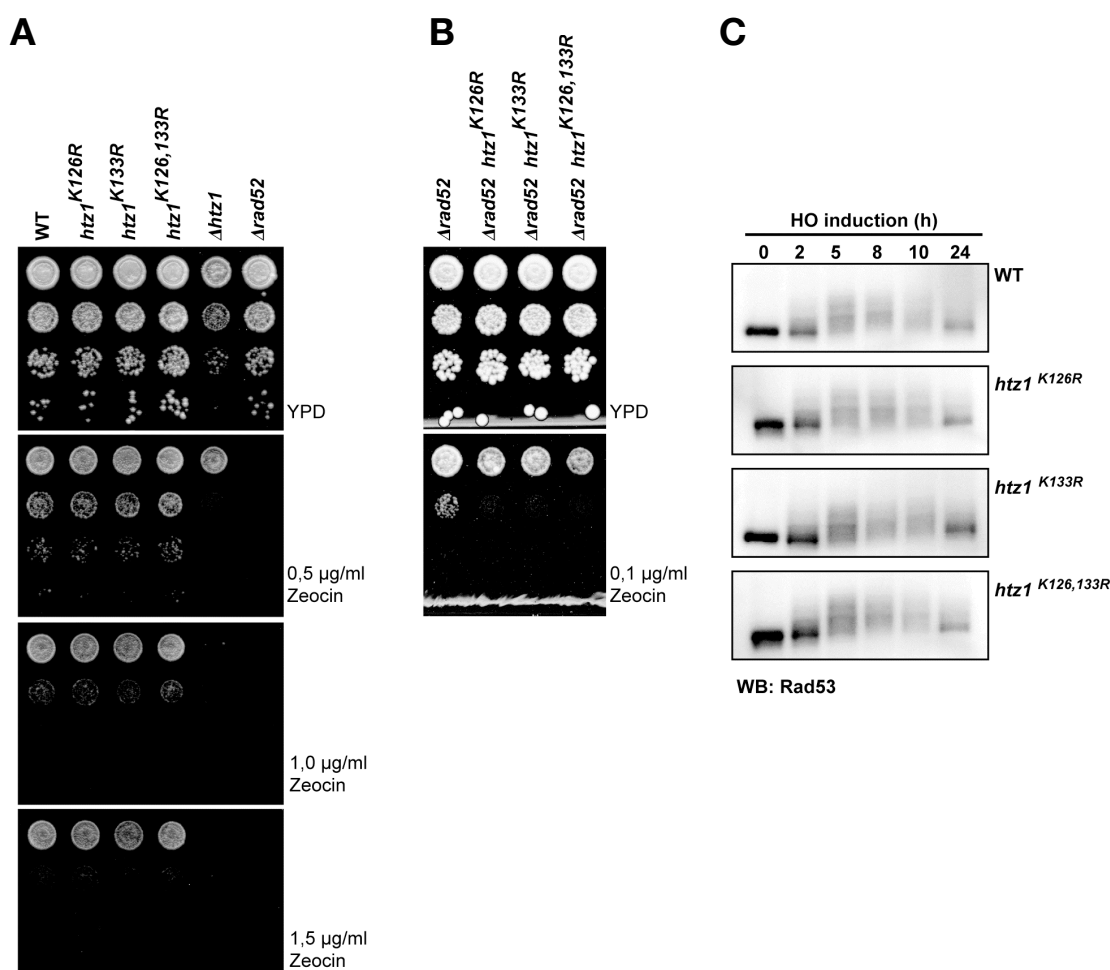


Figure 16. Phenotype of cells expressing the SUMOylation-defective H2A.Z point mutant variants (A, B) Equal amounts of cells were spotted onto YPD plates or plates containing the DSB-inducing agent zeocin (pH 7.2). Images were taken after 48h of growth at 30°C.

(C) H2A.Z lysine mutants show normal DNA damage checkpoint activation in response to a single DSB. Rad53 phosphorylation was monitored in samples taken at the indicated time points after HO induction.

3.5 Interactors of Mps3 at the nuclear envelope

To learn more about what happens to the DSB once it is recruited to the nuclear periphery, a genome-wide, robot-based Y2H screen was performed, using Mps3 as bait. This screen revealed many interesting interactors: intriguingly, H2A.Z, but also polo-like kinase Cdc5, the telomere proteins Ndj1 and Est1, the nuclear envelope protein Prm3, the karyopherin Kap104 as well as the spindle pole body component Nbp1 were identified to physically interact with Mps3.

3.5.1 Mps3 binds to H2A.Z

Of all the identified Mps3 Y2H interactions, the only one that could be confirmed as also strongly co-immunoprecipitating with Mps3 was H2A.Z (Fig. 17A and data not shown). Remarkably, there are strong links between Mps3 and the SUMO-modification machinery. Not only was Mps3 previously identified by SUMO and SUMO-ligase Y2H screens (Hiller, 2006) but it also interacts specifically with the SUMO-interacting motif (SIM) of Fir1 (Fig. 17B), a tool that is useful for identifying SUMOylated or SUMO-interacting proteins (M. Schwarz, unpublished data). As Mps3 itself is not modified by SUMO (data not shown), the question arose which of its interaction partners could constitute the link to the SUMOylation machinery. Interestingly, the only Mps3-interactor to be found modified by SUMO in this study was in fact H2A.Z (Fig. 17C and data not shown). Moreover, the Y2H interaction between Mps3 and the SUMO E2 enzyme Ubc9 was strongly diminished in $\Delta swr1$ mutants (Fig. 17D), indicating that chromatin-associated H2A.Z is likely to be the bridging factor between Mps3 and the SUMO system. Co-localization attempts by live-cell imaging revealed a general distribution of H2A.Z throughout the nucleus, however, showing some overlap with the nuclear envelope staining of Mps3 (Fig. 17E). Together these findings demonstrate a robust interaction between Mps3, H2A.Z and the SUMO-conjugating machinery.

To investigate this interesting link further, the binding site of H2A.Z on the Mps3 nucleoplasmic domain (aa 1-150) was mapped. When being incubated with a synthetic spot-array of overlapping Mps3 peptides (data not shown), recombinant H2A.Z bound strongly to 3 peptide regions on Mps3 (aa 87-93, 100-113, and 126-135). These *in vitro* interaction motifs were subsequently verified by making the respective *mps3* alleles and testing their *in vivo*-H2A.Z binding capabilities in Y2H

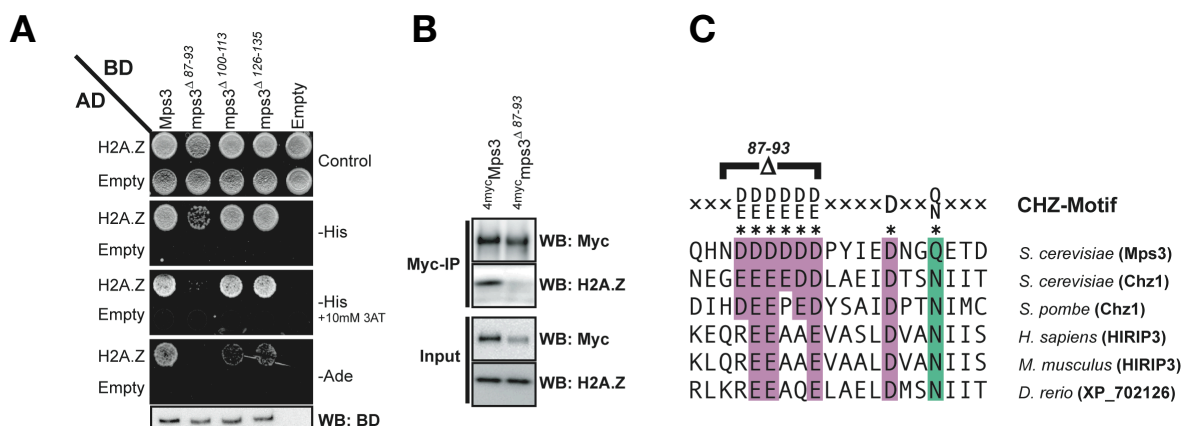


Figure 18. Mps3 binds to H2A.Z via a CHZ-like-Motif.

(A) Mps3 peptide regions binding to recombinant H2A.Z in an *in vitro* peptide array were tested for their *in vivo* binding capabilities in Y2H assays. The respective peptide regions were deleted in Mps3-BD constructs as indicated. Only motif 1, aa 87-93, seems to be required for H2A.Z binding *in vivo*.

(B) Amino acids 87-93 are also essential for the efficient co-IP of H2A.Z with myc-tagged Mps3.

(C) The sequence region around the H2A,Z binding site on Mps3 (aa87-93) shows homology to the CHZ-motif found in the CHZ- (chaperones for Htz1) family of proteins. Alignment of H2A,Z binding regions from *S. cerevisiae* Mps3 and Chz1 and Chz1-homologs from other species as indicated.

other identified *in vitro* binding sites for H2A.Z seemed to be dispensable for the Mps3 H2A.Z interaction *in vivo* (Fig. 18A).

Intriguingly, the sequence motif around the H2A.Z binding site of Mps3 is reminiscent of the so-called CHZ-motif (Fig. 18C), which confers H2A.Z binding specificity to the H2A.Z-selective histone chaperones of the CHZ1-family (Luk et al., 2007; Zhou et al., 2008). In both cases binding is mediated by charge-charge interactions between acidic residues on the H2A.Z-binder presumably contacting the highly basic surface of the histone variant H2A.Z. Luk et al. demonstrated, that within Chz1, especially the conserved residues aspartate (D) 103 and asparagine (N) 106 constitute the key determinants for H2A.Z recognition *in vivo*. Notably, the corresponding residues are conserved in Mps3 with D103 being invariant and N106 being conservatively replaced by a glutamine (Q; Fig. 18C). In summary, the binding site of H2A.Z on Mps3 is constituted by a chaperone-like motif present in the Mps3 nucleoplasmic domain.

3.5.2 Mps3 binds to DSB repair factors

To investigate the function of Mps3 at the DSB, a candidate-approach was embarked upon to search for known DSB repair factors binding to Mps3. Interestingly, both DSB-end binding protein complexes: Ku70/80 as well as the MRX complex could be identified to bind Mps3 in co-IP experiments (Fig 15A and 15B). Remarkably, however, neither interaction was significantly stimulated by DNA damage. In contrast, both the Ku-proteins as well as Mre11 already co-purified with Mps3 in the absence of DSBs (Fig 15). Nevertheless, the strong association of Mps3 with DSB repair proteins clearly suggests a role for this transmembrane protein in DSB processing and repair.

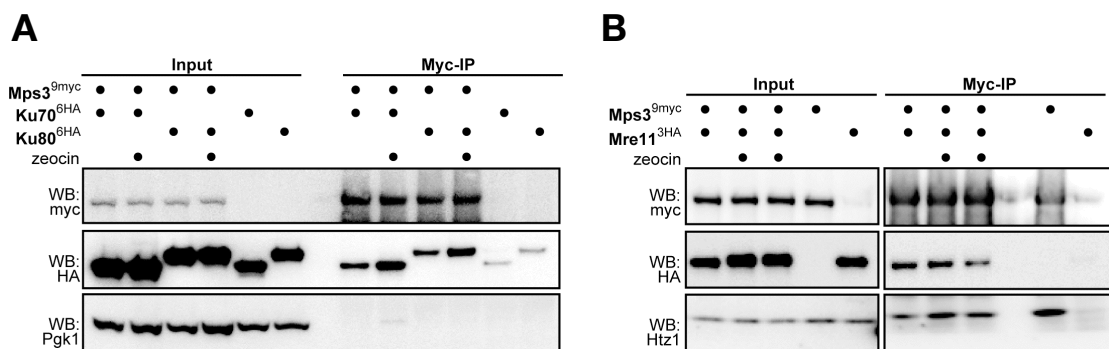


Figure 19. Mps3 binds to DSB repair factors Ku70/80 and Mre11

(A) Mps3 Interaction with Ku70 and Ku80. Co-immunoprecipitations (CoIPs) from doubly tagged strains treated or not treated with 0.2 mg/ml zeocin for 1hr, as indicated. The apparent increase of Ku-proteins in the Myc-IP after zeocin treatment is due to enhanced aspecific binding to the myc-beads and not because of binding to Mps3 (data not shown).

(B) Mps3 interaction with Mre11. Co-IPs were performed as in (A).

3.5.3 Dissecting the function of the Mps3 nucleoplasmic domain

Indicative of its great significance for the cell, Mps3 is essential for yeast viability. To understand which domains within the protein fulfill its essential function, a number of *mps3* truncation alleles were generated and tested for their ability to support viability in an *mps3* deletion strain (Fig. 20A). Being a single pass transmembrane protein of the inner nuclear membrane, the Mps3 N-terminal domain faces the nucleoplasm whereas the C-terminus protrudes into the intermembrane space. Strikingly, the SUN domain (for Mps3 domain composition please see Fig. 20B) as well as the nucleoplasmic domain is required for full viability (Fig 16A).

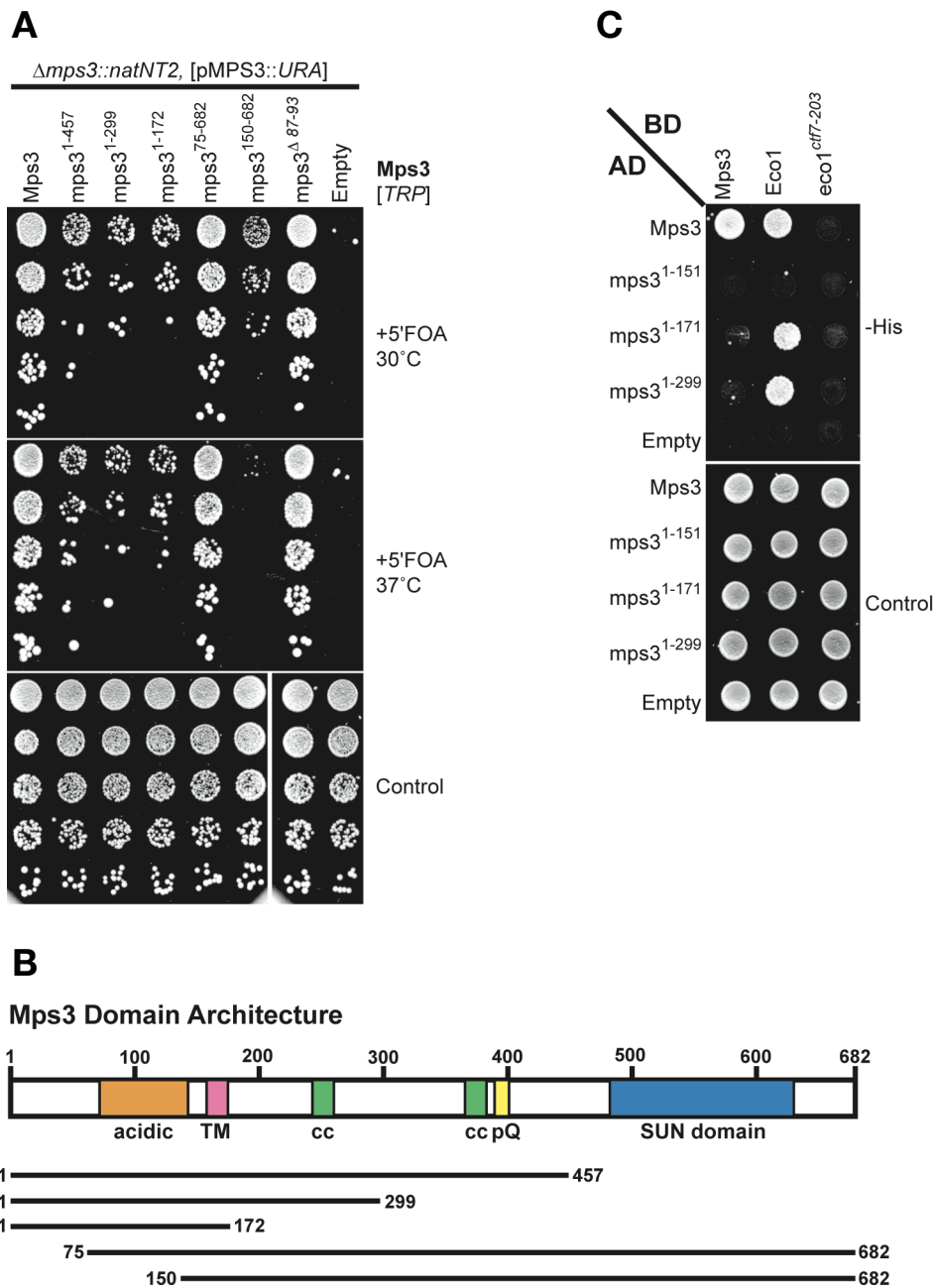


Figure 20. Mps3 nuclear- and SUN-domain are needed for full viability in yeast

(A) Viability of several *mps3* truncation mutants was assayed by shuffling out the WT *MPS3* upon plating on 5'FOA-containing medium. Equal amounts of cells were spotted and images were taken after 48h of growth at 30°C.

(B) Schematic representation of the Mps3 domain architecture. The N-terminus faces the nucleoplasm (aa 1-151) whereas the C-terminal part of Mps3 (aa 170-682) protrudes into the intermembrane space. The highly acidic (orange), transmembrane (TM, pink), coiled-coil (cc, green), polyglutamine (pQ, yellow) and SUN domain (blue), as well as constructs used for experiments shown in (A) and (B) are indicated.

(C) Y2H-assays. The SUN domain facilitates Mps3 homodimerization but is not needed for interaction with nuclear binding partners like Eco1. The *eco1* allele *ctf7-203* was used as negative control.

Sun domains are known to either mediate heterotypic interactions with KASH-domain containing proteins or homodimerization via SUN-SUN interactions. Regarding Mps3, the latter seems to be the case as Y2H constructs lacking the SUN domain no longer showed self-interaction (Fig. 20C). Deleting the SUN domain

within Mps3 abrogates its localization to spindle pole bodies (Jaspersen et al., 2006). This is probably the reason for the observed lethality. Interestingly, this SUN-mediated dimerization is apparently not required for interaction with known nuclear binding partners such as the cohesion establishment factor Eco1 (Antoniacci et al., 2004), but also H2A.Z (Fig. 20C and data not shown). This indicates that their interaction takes place outside of spindle pole bodies. However, such interactions still seem to depend on membrane anchoring, as an Mps3 construct lacking the transmembrane domain ($mps3^{1-150}$) failed to interact with e.g. H2A.Z (Fig. 20C and data not shown).

Remarkably, the first 75 aa within the Mps3 N-terminus were dispensable for cell growth (Fig. 20A). Intriguingly, the remaining essential part of the nuclear domain (aa 75-150) contains the H2A.Z binding site. However, when directly testing the H2A.Z-binding defective allele ($mps3^{\Delta 87-93}$), it showed no growth defect under unperturbed growth conditions (Fig. 20A). This implies that the interaction between Mps3 and H2A.Z is in fact not essential during unchallenged cell growth and that there must be another important function executed by this essential domain.

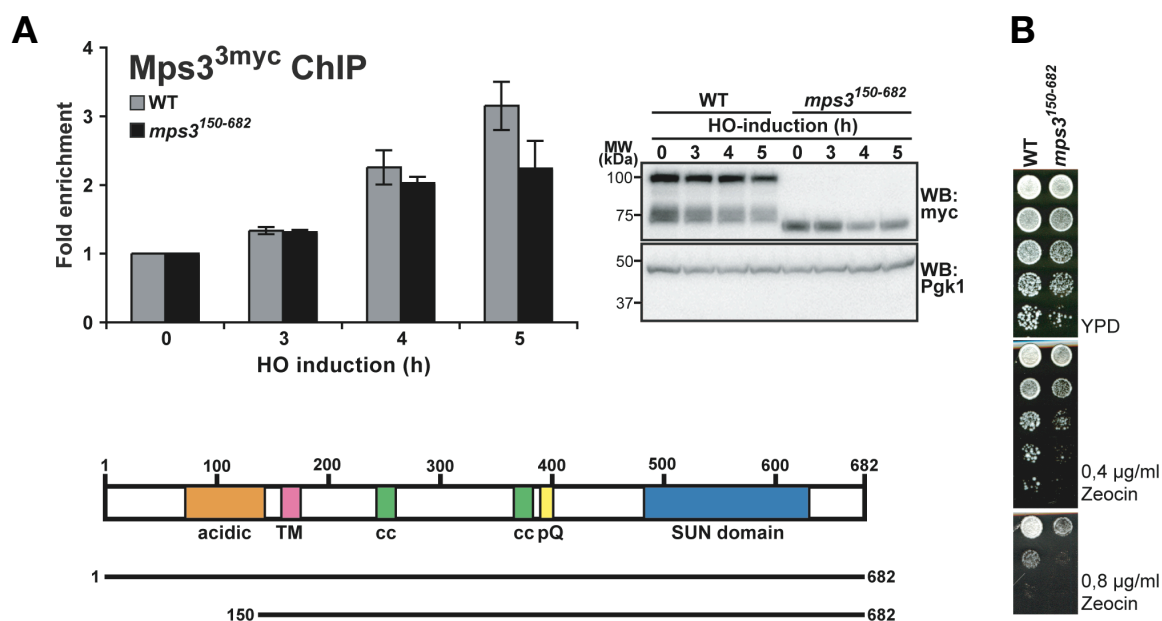


Figure 21. The Mps3 nucleoplasmic domain is hardly required for DSB tethering

(A) $Mps3^{3myc}$ -directed ChIP at *MAT* (0.2kb from DSB) in either WT or a strain lacking the Mps3 nucleoplasmic domain ($mps3^{150-682}$). Shown are IP/input signals normalized to 1 for the signal before induction. Data are represented as mean \pm SEM. Constructs used for ChIP are schematically shown below the graph. Right panel: Western blot of ChIP input samples demonstrating that both WT and truncated Mps3 constructs are expressed normally.

(B) The Mps3 nucleoplasmic domain contributes to resistance to DSBs. Equal amounts of cells were spotted onto YPD plates or plates containing the DSB-inducing agent zeocin (pH 7.2). Images were taken after 48h of growth at 30°C.

Even though interactions identified by ChIP analysis need not necessarily be direct, the fact that Mps3 gets recruited to a persistent DSB (Fig. 12) and co-purifies with DSB repair proteins (Fig. 19) suggested that Mps3 could be the actual anchor for DSB tethering at the nuclear envelope. To test this hypothesis, ChIP assays after DSB induction at *MAT* were performed in a strain lacking the entire Mps3 nucleoplasmic domain (*mps3*¹⁵⁰⁻⁶⁸²). Surprisingly, the Mps3 nucleoplasmic domain was hardly required for DSB tethering (Fig. 21A). However, the Mps3 nucleoplasmic domain still seems to be functionally linked to DSB repair as the truncated construct rendered cells significantly sensitive to DSBs (Fig. 21B).

Given that the absence of the Mps3 nucleoplasmic domain did not significantly hamper recruitment of a persistent break to the periphery, there might be other, possibly redundant DSB-anchoring proteins at the nuclear envelope. To test this idea, ChIP assays with epitope-tagged versions of the nucleoporin Nic96 and the inner nuclear membrane protein Heh2 were performed (Fig. 22). Notably similar to Mps3, these proteins also associated with the persistent break about 3 hours after DSB induction. Intriguingly these results imply, that DSB tethering may not take place exclusively at nuclear pores nor at Mps3 or Heh2, but may involve the nuclear envelope more broadly.

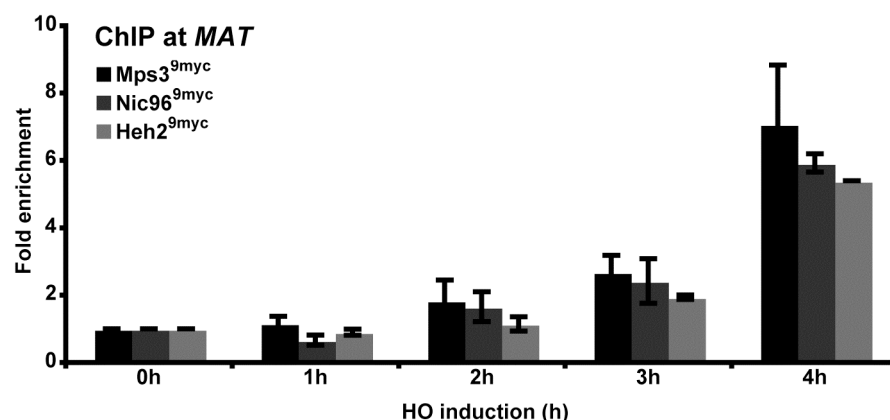


Figure 22. Inner nuclear membrane protein ChIP at *MAT*

The integral nuclear transmembrane proteins Mps3, Heh2, and the nucleoporin Nic96 are enriched at the DSB site 4 h after HO induction, as monitored by ChIP analysis (0.2 kb from DSB). Shown are IP/input signals normalized to 1 for the signal before induction. Data are represented as mean \pm SEM.

3.6 Possible functions of DSB relocation to the nuclear envelope

This study identified a novel DNA damage response pathway elicited by a single persistent chromosomal break. The early steps of this pathway are shared with normal DSB repair, i.e. when homology is present and used for repair by HR. In contrast, the later events involve relocation of the DSB and tethering at the nuclear envelope. Remarkably, this only occurs when no homology is found and the break persists. To identify the function of sequestering an irreparable DSB to the nuclear periphery, several avenues of research were chosen.

3.6.1 The fixed DSB end does not acquire telomere-like features

Intriguingly, at least in yeast, all 16 telomeres are anchored to the nuclear envelope. The function of this fixation on the two-dimensional lattice of the nuclear membrane is still enigmatic. Remarkably, telomeres are in principle also DSBs, however, they are not recognized as such by the DNA damage response and repair machinery and thus do not trigger a checkpoint response. This is because in telomeres, the chromosome-ends are capped with a $(TG)_{1-6}G_{2-3}$ repeat sequence which folds back onto itself to form a T-loop, a protective structure hiding the actual DNA double-strand end (Morin, 1989). In addition, the telomeric repeats recruit telomere-specific protein factors that actively suppress activation of the DNA damage checkpoint (Karlseder, 2003). Similarly, in a process called adaptation to DNA damage, cells revert the DNA damage checkpoint and re-enter the cell cycle if, after more than 15 hours, still no homology was found and the DSB persists. At this stage, and reminiscent of the situation with telomeres, the DSB, although still present, no longer triggers a checkpoint-dependent cell cycle arrest. Remarkably, initiation of adaptation and DSB-tethering at the nuclear envelope timely coincides. Moreover, Mps3, which binds to the persistent DSB at the nuclear envelope was also shown to be involved in telomere anchoring during meiosis (Conrad et al., 2007) and mitosis (Bupp et al., 2007). These apparent analogies raised the question whether the DSB would acquire telomere-like, checkpoint-repressive characteristics once tethered to the nuclear envelope. A first experiment to scrutinize this hypothesis was to monitor whether the relocated DSB would co-localize with telomere-clusters at the nuclear envelope. To this end, telomeres were marked by introducing a fluorescently-tagged Rap1 allele into the strain originally used to track GFP-decorated DSBs in live cells (Fig. 11). Although DSB-relocation again occurred in this strain, the point of DSB

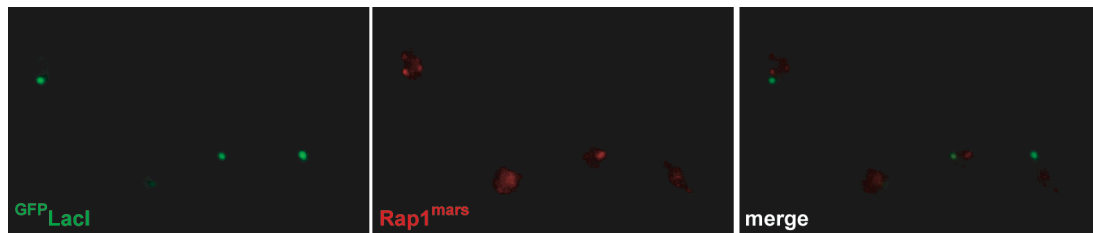


Figure 23. Persistent DSBs at the nuclear periphery do not colocalize with telomere clusters

Expression of GFP-LacI fusion marks a $240\times lacO$ array (green) integrated proximal to *MAT* (similar to setup shown in Fig. 11). Telomeres are visualized by Rap1⁺ (red) and form clusters at the nuclear envelope. A single DSB is induced at the *MAT*-locus by expression of HO endonuclease and cells were imaged by live cell microscopy 5h after HO induction.

fixation 5 h after induction in no case overlapped with telomere clusters (Fig. 23).

Despite being excluded from telomere clusters at the nuclear envelope, the 5'-resected ends of the persistent break could in principal still undergo some sort of processing or capping at the nuclear periphery. To detect possible *de novo* addition of (telomeric) sequences or capping structures at the very break ends during break relocation and fixation at the nuclear envelope, the 3' DSB ends were recovered, cloned by PCR and sequenced in a similar fashion as originally described for sequencing telomeres (Forstemann et al., 2000). By and large, the 3' ends of the persistent DSB were relatively stable (Fig. 24). Even after 24 hours, when resection has degraded up to 80000 bases of the 5'-strand (Zhu et al., 2008), on average only about 25 bases of the 3'-strand are lost. Moreover, hardly any *de novo* addition of nucleotides let alone telomeric sequences could be detected (Fig. 24). Importantly, when performing the same experiment in strains in which relocation to the nuclear periphery was blocked (e.g. *htz1*^{k126,133R}), 3' end stability remained the same. Taken together these findings demonstrate that the 3'-strand at the DSB is surprisingly stable and that this seems to be independent of DSB-relocation to the nuclear periphery.

3.6.2 Mps3, DSB tethering and adaptation

The molecular mechanisms underlying adaptation to a persistent DSB are still enigmatic. Genetic screens in *S. cerevisiae* identified a set of protein factors being required for checkpoint adaptation. These include, but are not limited to: casein kinase II, the phosphatases Ptc2 and Ptc3, the helicase Srs2, the Ku70/80 proteins and the polo-like protein tyrosine kinase Cdc5 (Leroy et al., 2003; Pelliccioli et al., 2001; Toczyski et al., 1997; Vaze et al., 2002). However, their exact role in adaptation and functional connectivity remain to be elucidated. Regarding Cdc5, an allele, *cdc5-ad* (L251W), was identified and shown to be defective in adaptation.

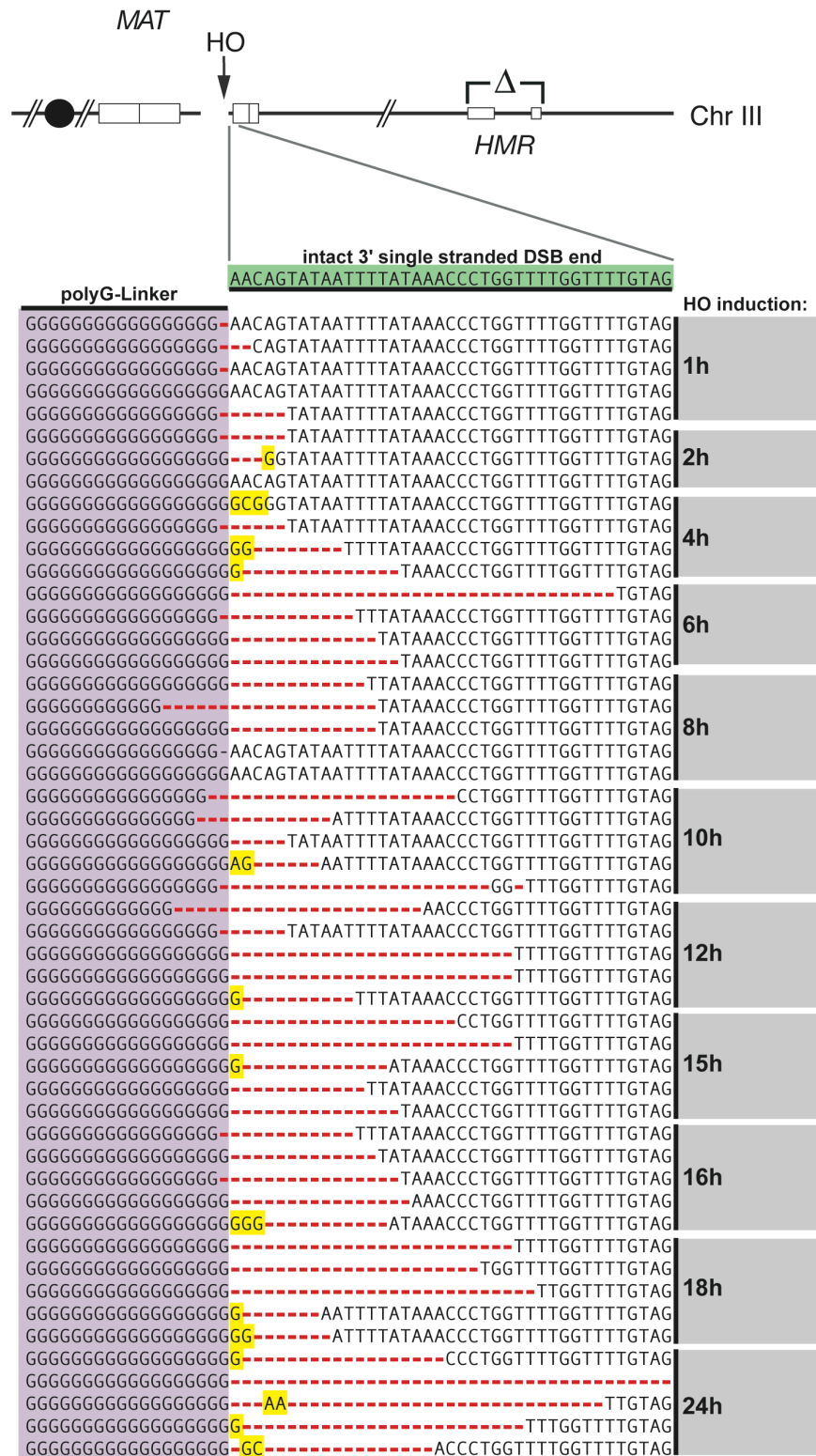


Figure 24. DSB 3' end sequencing

A single DSB (arrow) is induced at the *MAT*-locus by expression of HO endonuclease. In this donor deficient strain, regions of homology are deleted, repair is prevented and the DSB persists. Genomic DNA was isolated, denatured and free 3' ends were tailed with dCTP by terminal deoxynucleotidyl transferase. The DSB 3' sequence was then specifically amplified by PCR with a primer complementary to the dC tail (polyG primer) and a primer specific for a sequence 200 bp distal of the HO cut site at *MAT*. For each time point after HO induction, 5 clones were isolated and sequenced. Original intact 3' end sequence is indicated in green on top of the alignment. Red dashed lines and yellow boxes indicate missing- and *de novo* added nucleotides, respectively.

Interestingly, this study recovered Cdc5 as a strong candidate in a Y2H screen using Mps3 as bait (see section 3.5). The Cdc5-Mps3 interaction could subsequently be verified by *de novo* cloning and directed Y2H-assays (Fig. 25A) as well as co-IP (Fig. 25B). Thus indeed, Cdc5 physically interacts with Mps3. As Mps3 is recruited to a persistent DSB contemporaneously with the initiation of adaptation, the question emerged whether Mps3 might functionally assist Cdc5 in adaptation.

This notion was supported by the discovery that strikingly the *cdc5-ad* allele, although being expressed like WT, could hardly interact with Mps3 as monitored in Y2H assays (Fig. 25A). In contrast, the catalytically inactive *cdc5* mutant (N209A, *cat**), that exhibits general cell cycle defects not related to adaptation, showed a strong binding to Mps3. Moreover, the physical interaction to Mps3 seems to depend on the polo-box domain of Cdc5 (Fig. 25A), an interaction mode common to most reported Polo-like kinase substrates. Together, this indicates that the Mps3-Cdc5 interaction could play a role in adaptation.

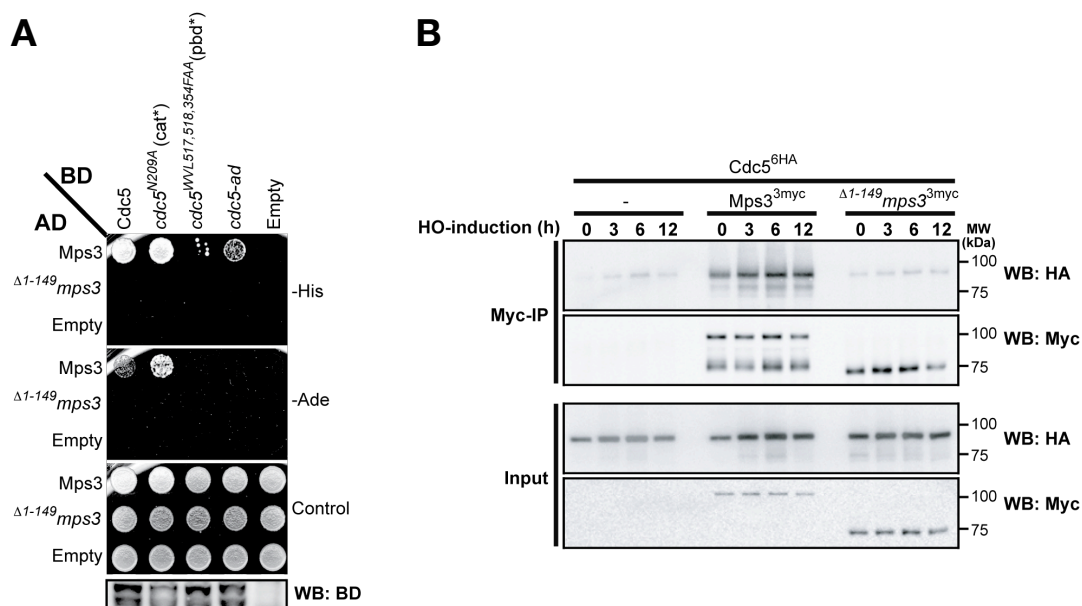


Figure 25. Mps3 binds to Polo-like kinase Cdc5 but not to the adaption-defective allele *cdc5-ad* (A) Y2H assay. Equal amounts of cells were spotted onto selective media as indicated. Positive interactions result in His and Ade prototrophy, the latter of which is a more stringent interaction indicator.

(B) Cdc5^{6HA} co-immunoprecipitates with WT Mps3^{3myc} but not a version lacking the nucleoplasmic domain ($\Delta 1-149$ *m*ps3^{3myc}). This cannot be further stimulated by introduction of a persistent DSB at *MAT*.

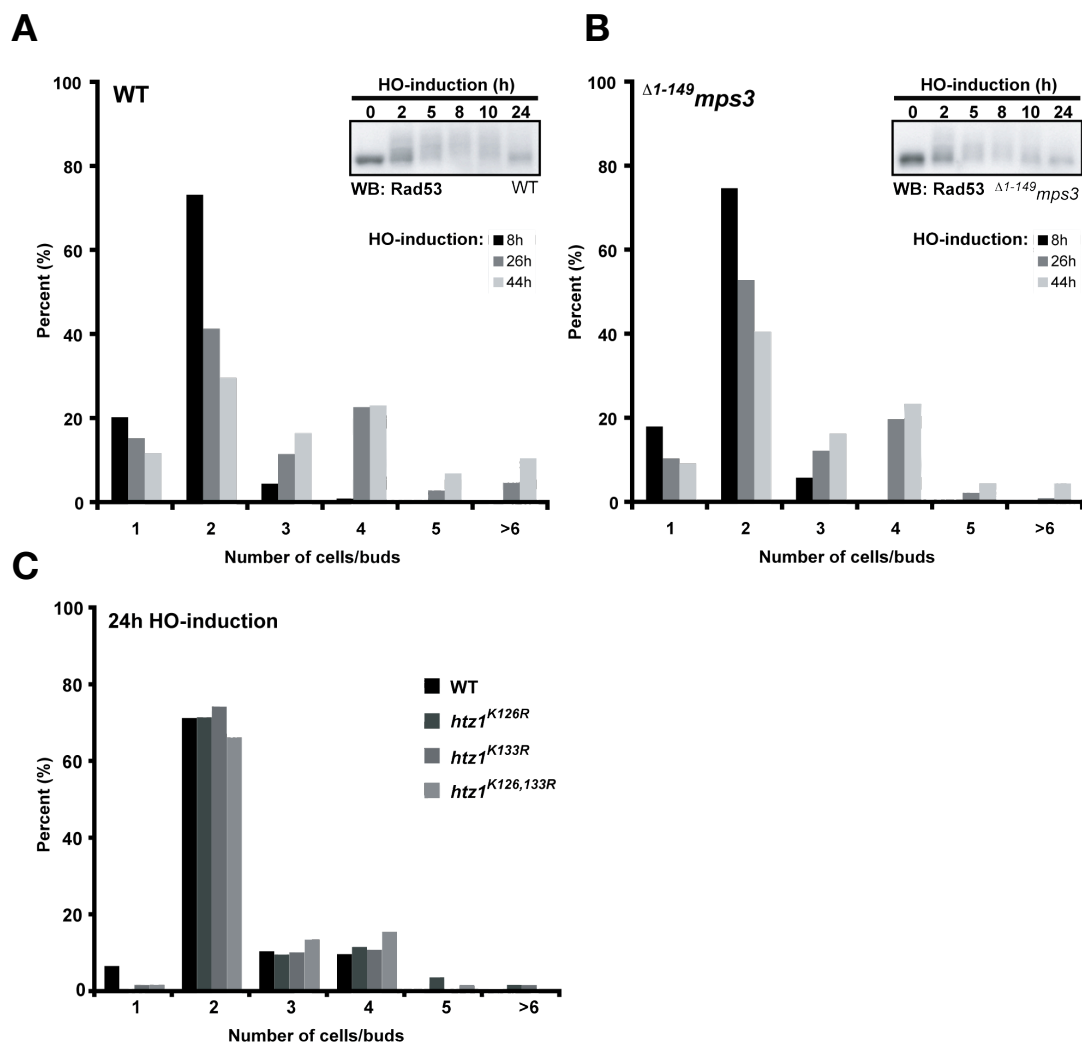


Figure 26. Neither Mps3 nor DSB-tethering seem to be required for checkpoint adaptation

(A) Cell-based adaptation assay. Log-phase cells of a donor deficient strain (same as in Fig. 2) were spread on galactose-containing plates to induce the DSB by HO endonuclease. G1-cells (unbudded) were then micromanipulated under the microscope onto a grid. Arrest morphology, growth and microcolony formation was scored after the indicated time points. The inset on the top right is a W western blot showing checkpoint adaptation after 24 hours as assayed by reversal of Rad53 phosphorylation.

(B) Same setup as in (A), but for $\Delta 1-149$ *mps3* which lacks the entire Mps3 nucleoplasmic domain

(C) Similar setup as in (A), but for the SUMOylation-defective H2A.Z lysine mutants, in which the DSB fails to relocate to the nuclear periphery.

Remarkably, however, the Mps3-Cdc5 interaction was not significantly stimulated by DNA damage. In fact, Cdc5 already co-purified with Mps3 in the absence of DSBs (Fig 21B). Still, the recruitment of Mps3 to the DSB at the onset of adaption together with the marked physical interaction with WT Cdc5, but not with the adaptation-defective variant, strongly suggested a role for Mps3 in adaptation. To test this directly, an allele lacking the entire nucleoplasmic domain ($\Delta 1-149$ *mps3*^{3myc}) of Mps3, and therefore no longer capable of interacting with Cdc5 (Fig, 21B), was employed in cell-based adaptation assays. Surprisingly, this mutant was in fact able

to escape the checkpoint-mediated cell cycle arrest, and re-entered mitosis 24 hours after DSB-induction, just like WT (Fig. 26A and 26B). Remarkably, the same was true for mutants that fail to recruit and tether the DSB to the nuclear periphery such as the SUMO-defective lysine mutants of H2A.Z (Fig. 26C and data not shown). Taken together these findings enervate the hypothesis that Mps3 or DSB fixation at the nuclear envelope might play an important role in adaptation. Nevertheless, DNA damage checkpoint reversal during adaptation might necessitate a highly redundant set of mechanisms for adaptation to occur. This could explain why, albeit being functionally linked, no direct requirement of Mps3 or DSB fixation for adaptation to DSBs could be demonstrated in this study.

3.7 Cohesion establishment in response to DSBs

Research within the past decade has progressively unearthed the importance of sister chromatid cohesion for DNA DSB repair. In fact, today it is widely accepted that besides its essential role in ensuring fidelity of chromosome segregation in mitosis, cohesion also constitutes a key protective means against genotoxic insults such as DSBs. This is because the homologous template needed to guide recombinational repair *in vivo* is in fact predominantly the sister chromatid, if present. By keeping sister chromatids cohesed throughout S/G2, the cell ensures that in the event of damage, the needed homology information will be in direct proximity to the DSB. The importance of cohesion for DSB repair has been underappreciated in part because the majority of systems to study homologous recombination fail to detect sister chromatid recombination. Often, the assays are designed in a way that the readout is exquisitely intra- and interchromosomal recombination or repair via the sister chromatid is prevented by cleaving both sisters (see e.g. experiments described in sections 3.1 – 3.4). Most certainly, in living cells the vast majority of recombinational repair events involves the sister chromatid.

3.7.1 H2A.Z binds Eco1, the key player in cohesion establishment

Cohesin complexes are loaded onto chromosomes in G1 and sister chromatid cohesion must be subsequently established by the activity of the acetyl transferase Eco1 (Ivanov et al., 2002; Skibbens et al., 1999; Toth et al., 1999; Uhlmann and Nasmyth, 1998). Interestingly, this master regulator of cohesion establishment lacks intrinsic DNA-binding capability (Onn et al., 2009). Therefore, Eco1 needs to be recruited to chromosomes by interaction with chromatin-associated recruiting factors. In S-phase this was shown to be via PCNA (Moldovan et al., 2006), the DNA sliding clamp for the replicative polymerase. Eco1 mutants that are defective in PCNA-binding, i.e. when the PIP (PCNA interacting protein)-box of Eco1 is mutated, die due to cohesion defects.

Several recent reports demonstrate a pivotal role for Eco1 in establishing cohesion also outside of S-phase, in particular at DSBs. Notably, in this incident, cohesion establishment and Eco1-recruitment to chromatin is uncoupled from replication and can therefore not be mediated by PCNA (Strom et al., 2007; Unal et al., 2007). This prompted the question which DSB-associated protein could be the substitute-recruiting factor for Eco1.

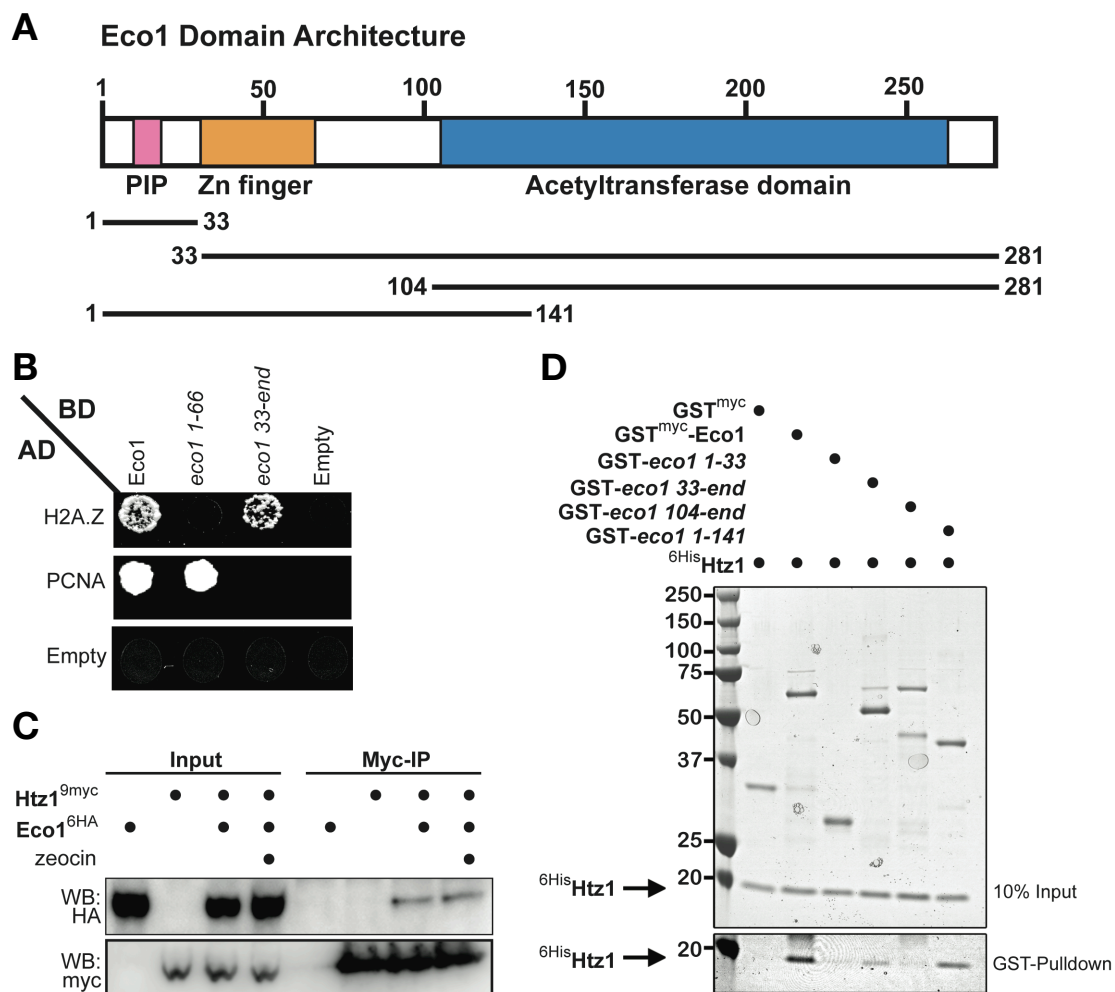


Figure 27. H2A.Z physically interacts with Eco1, the master regulator of cohesion establishment

(A) Scheme depicting Eco1 domain architecture and truncation constructs used in (B) and (D). (B) Y2H assay. H2A.Z physically interacts with Eco1 *in vivo*. The binding sites for H2A.Z and PCNA on Eco1 (PIP box is constituted by amino acids 18-21) do not overlap. (C) Co-IPs from doubly tagged strains treated or not treated with 0.2 mg/ml zeocin for 1hr, as indicated. Endogenous Eco1 co-purifies with Htz1. (D) *In vitro* GST-pulldown assays with recombinant yeast proteins expressed in and purified from *E. coli*. Molecular weight marker is shown and indicated (in kD) on the left.

Interestingly, this thesis could identify H2A.Z as a novel Eco1-interactor in a genome-wide Y2H screen. The interaction seemed specific, as no other histone or protein implicated in the DNA damage response, besides PCNA, was identified in this unbiased screen. Importantly, the interaction could subsequently be reproduced in a directed Y2H assay as well as co-IP experiments (Fig. 27B and 27C). Moreover, the interaction is most likely direct and not mediated by other proteins, as demonstrated by *in vitro* pull-down experiments with *E. coli*-expressed, purified Eco1-glutathione-S-transferase (GST) fusions and purified, recombinant His-tagged H2A.Z (Fig. 27D). To assess the Eco1-H2A.Z interaction in its physiological context, mononucleosomes were purified from yeast chromatin by micrococcal nuclease

(MNase) digestion (Fig. 28A). Interestingly, purified GST-Eco1 was able to pulldown H2A.Z nucleosomes (Fig. 28B, left panel). However, it should be noted, that when incubated with nucleosomes prepared from $\Delta htz1$ chromatin, Eco1 was also capable of pulling down H2A-only containing nucleosomes (Fig. 28B, right panel). The analysis is complicated by the fact that *in vivo*, hybrid H2A and H2A.Z containing nucleosomes seem to be the norm (Tolstorukov et al., 2009; Viens et al., 2006), therefore it is hard to discern whether Eco1 specifically recognizes H2A.Z, H2A or both. However, at least in the initial Y2H-screen, Eco1 showed clear specificity towards H2A.Z. In summary, the observed interaction between Eco1 and H2A.Z together with the fact that H2A.Z is a constitutive component of chromatin, brought forward the hypothesis that H2A.Z might constitute an alternative pathway (besides PCNA) for Eco1 recruitment to DNA.

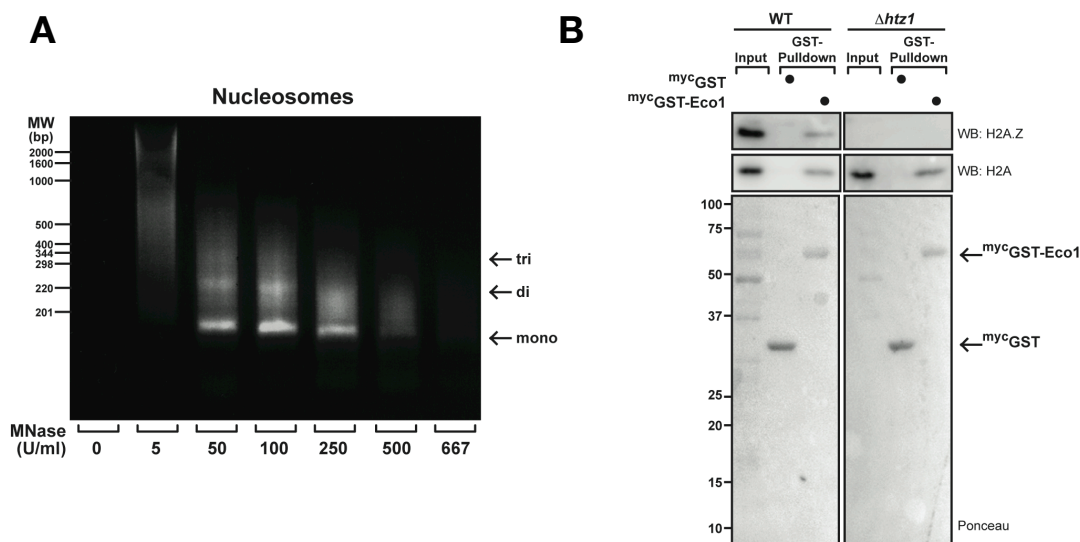


Figure 28. Eco1 interacts with H2A- and H2A.Z-containing nucleosomes

(A) Nucleosomes were obtained by digestion of a highly pure yeast chromatin fraction with MNase. The concentration of MNase was titrated so as to obtain mainly mononucleosomes.

(B) Soluble mononucleosomes (still contaminated with higher molecular weight chromatin proteins, see input) were released from chromatin by digestion with 250 U/ml MNase (A) and used as inputs for pull-downs with $mycGST$ or $mycGST-Eco1$. Samples were run on 12% SDS-PAGE, blotted and probed with antibodies against H2A and H2A.Z respectively.

To characterize the interaction further, truncated constructs of Eco1 were tested for binding to H2A.Z in Y2H in an attempt to map the histone-binding domain on Eco1 (Fig. 29A). Next to the PIP-box, which is constituted by amino acids 18-21 and mediates PCNA binding, Eco1 contains two other described structural motifs (Ivanov et al., 2002), which are both highly conserved throughout evolution. On the C-terminal portion this is the acetyltransferase domain (amino acids 111-266). In addition, the N-terminal part of Eco1 comprises a C_2H_2 -type zinc finger (amino acids

33-57). All of these domains, PIP-box, catalytic activity and zinc finger, are required for cell viability (Moldovan et al., 2006). Whereas the functionally important substrates for Eco1's acetyltransferase activity are known (Ben-Shahar et al., 2008; Rowland et al., 2009; Unal et al., 2008; Zhang et al., 2008), the function of the zinc finger or respective binding partners thereof have remained completely elusive. Zinc fingers are one of the most ubiquitous and structurally conserved folds (Krishna et al., 2003). They have been implicated especially in mediating protein-DNA but also protein-protein interactions (Brayer and Segal, 2008; Wolfe et al., 2000). Strikingly, the self-contained globular fold is composed only of a single helix and a loop, which coordinate a structurally important Zn^{2+} ion (Fig. 29B). Truncation-analysis by Y2H and GST-pulldowns delineated amino acids 33-141 on Eco1 to be necessary for H2A.Z binding (Fig. 27B and 27D). Importantly, the only conserved part in this region is the zinc finger, which hence made it an ideal candidate for constituting the Eco1-H2A.Z binding interface.

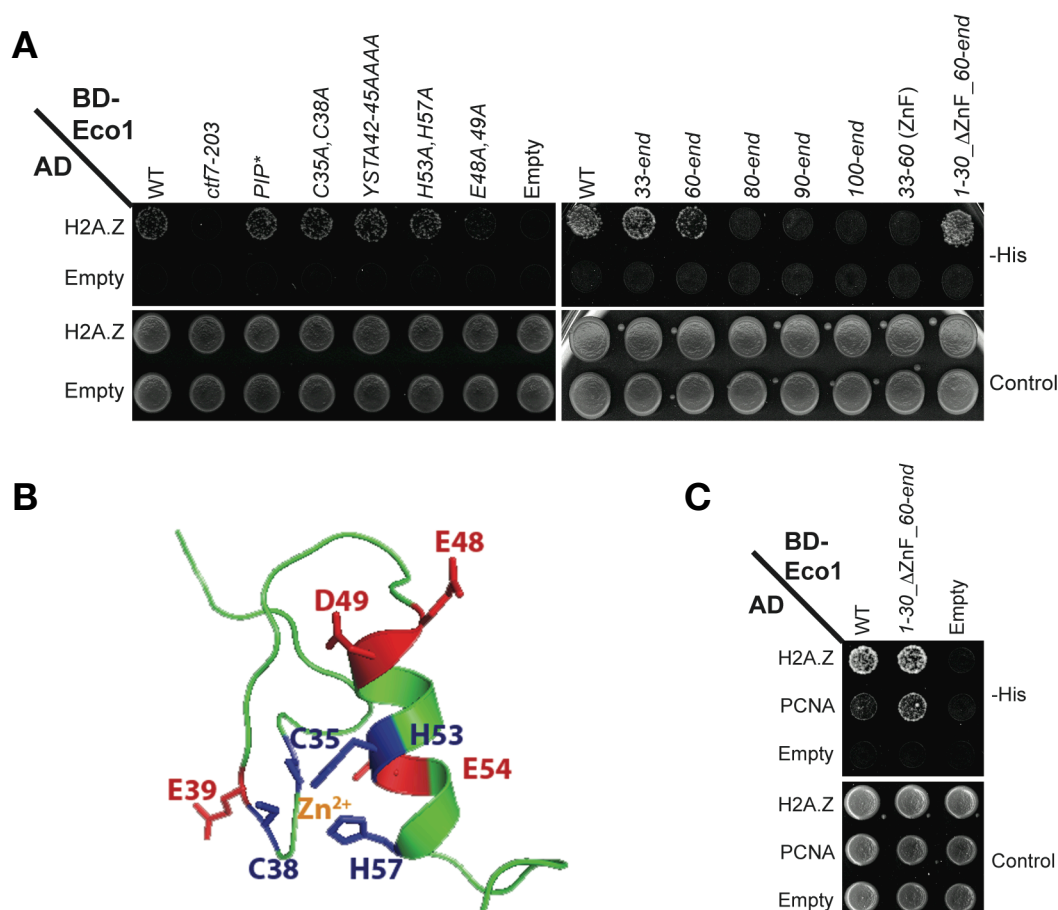


Figure 29. The zinc finger of Eco1 seems to be involved in H2A.Z-binding

(A) Y2H analysis of the interaction of mutant Eco1 proteins with H2A.Z.

(B) Structural model of the Eco1 zinc finger (aa 30-61). Important residues are denoted.

(C) Y2H assay. An Eco1 construct lacking the entire zinc finger (Δ 31-59) binds to H2A.Z like WT, however shows markedly increased interaction with PCNA.

Notably, mutations in the zinc finger directly disrupting Zn-coordination, e.g. C35A, C38A or H53A, H57A had no effect on H2A.Z-binding (Fig. 29A). However, mutation of the evolutionary conserved acidic residues within the zinc finger, glutamate (E) 48 and aspartate (D) 49, significantly reduced binding affinity to H2A.Z (Fig. 29A). Remarkably, the interaction could be even further diminished by additionally mutating acidic residues in the vicinity, such as E39 and E54 (data not shown). Importantly, these constructs are still functional as they are capable of binding PCNA (Moldovan et al., 2006). Of note, despite not being involved in Zn-coordination but rather facing outward of the zinc finger, E48 and D49 are required for cell viability in yeast (Moldovan et al., 2006).

Curiously, Eco1 constructs lacking the first 60 amino acids or deleted for the Zn-finger, still bind H2A.Z (Fig. 29A, right panel) in Y2H. However, surgical excision of the Eco1 Zn-finger, seems to increase Eco1 interaction capabilities in Y2H generally, as e.g. the interaction to PCNA is strongly enhanced in this mutant (Fig. 25C). Together, the here presented binding studies suggest that the zinc finger and especially E48 and D49 significantly contribute to H2A.Z-binding. However, the interaction seems to be highly dovetailed, with several, probably redundant and cooperative protein-protein contacts making up the binding interface.

3.7.2 H2A.Z-SUMOylation represses cohesion establishment

Interestingly, Eco1 interacts with H2A.Z and PCNA with distinct binding modules. Whereas PCNA-binding is mediated via the Eco1 PIP-box at the N-terminus (Moldovan et al., 2006), an Eco1 construct lacking this motif can still bind H2A.Z in Y2H-assays (Fig. 27B). Moreover, *in vitro* pull-down assays identified the region encompassing amino acids 33-141 on Eco1 to be necessary and sufficient for H2A.Z interaction (Fig. 27D). As PCNA travels with the replication fork, an alternative Eco1 recruitment pathway would make sense when cohesion is to be established elsewhere than at the replication fork, e.g. at DSBs and outside of S-phase. Because H2A.Z can still bind to Eco1 variants that are defective in the PIP-box, a prediction from this model is, that overexpression of H2A.Z might rescue the lethality of *eco1* PIP-box mutants. In fact, this was not the case (Fig. 30A, left panel). However, when overexpressing H2A.Z versions that lacked the SUMOylation site (either by C-terminal truncation or K126R mutation) these now indeed partially rescued the lethality of the PIP-box mutant *eco1*^{QKL18-21AAA} (Fig. 30A, right panel).

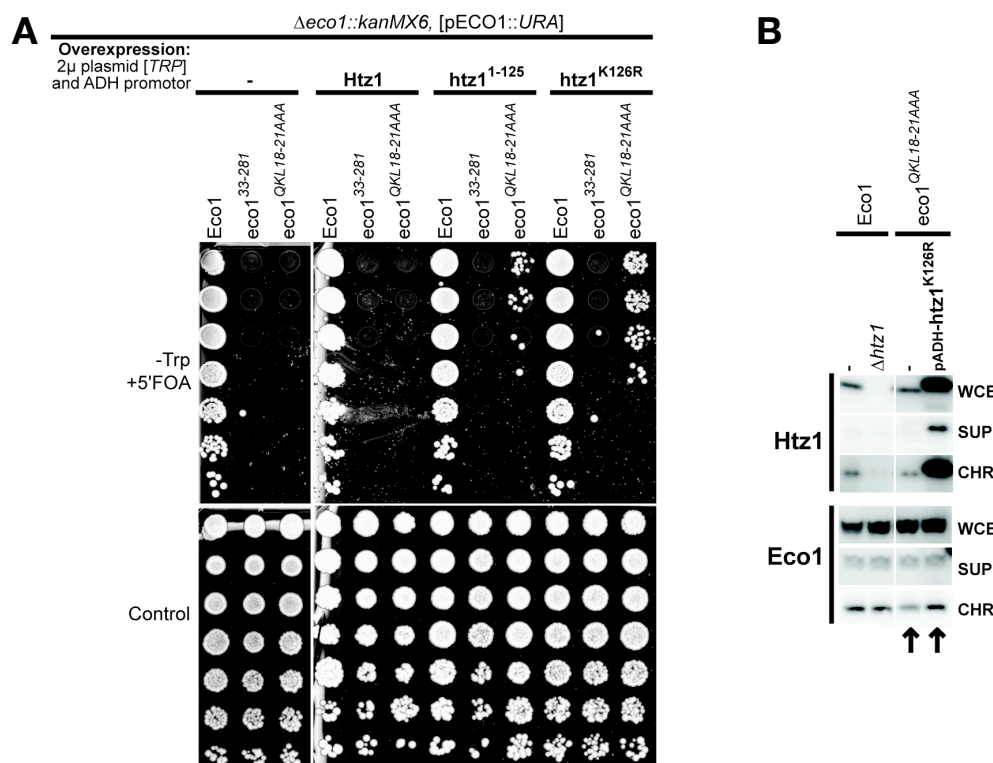


Figure 30. H2A.Z-SUMO-defective mutants can rescue the *eco1* PIP-box mutant

(A) Rescuing effect of overexpression of different H2A.Z constructs on lethality of *eco1* PIP-box mutants was tested by shuffling out the WT *ECO1* upon plating on 5'FOA-containing medium. Equal amounts of cells were spotted and images were taken after 48h of growth at 30°C. The *eco1* PIP-box mutants are inviable. Due to their failure to get recruited to DNA via PCNA, cohesion is not established. Only overexpression of SUMOylation-defective H2A.Z mutants but not of wt H2A.Z can rescue this lethality.

(B) Chromatin binding assay. The *eco1* PIP-box mutant (*QKL18-21AAA*) shows a reduced chromatin (CHR) association, which can be rescued by overexpressing the SUMOylation-defective H2A.Z mutant. (SUP, supernatant; WCE, whole cell extract)

Moreover, chromatin binding assays revealed that indeed, when overexpressing *htz1*^{K126R} the *eco1* PIP-box mutant relocates to the chromatin fraction (Fig. 30B). In conclusion, this supports the notion that the H2A.Z - Eco1 interaction could constitute an alternative recruitment pathway for cohesion establishment, with SUMOylation being a negative regulator of this event.

Intriguingly this is reminiscent of the recruitment pathway involving PCNA. Here, overexpression of PCNA-mutants defective in SUMOylation also rescued *eco1* cohesion mutants (Moldovan et al., 2006), indicating that SUMOylation of the recruitment factor PCNA is inhibitory for cohesion. To test whether a parallel regulation really exists for H2A.Z as well, C-terminal, linear H2A.Z-SUMO fusions were generated (Fig. 31A). As the SUMOylation sites (K126 and K133) lie almost at the very C-terminus of the protein, these fusions are likely to resemble the naturally modified species. Remarkably, overexpression of these constructs was severely toxic to cells (Fig. 31B). Moreover, this dominant negative effect was not observable

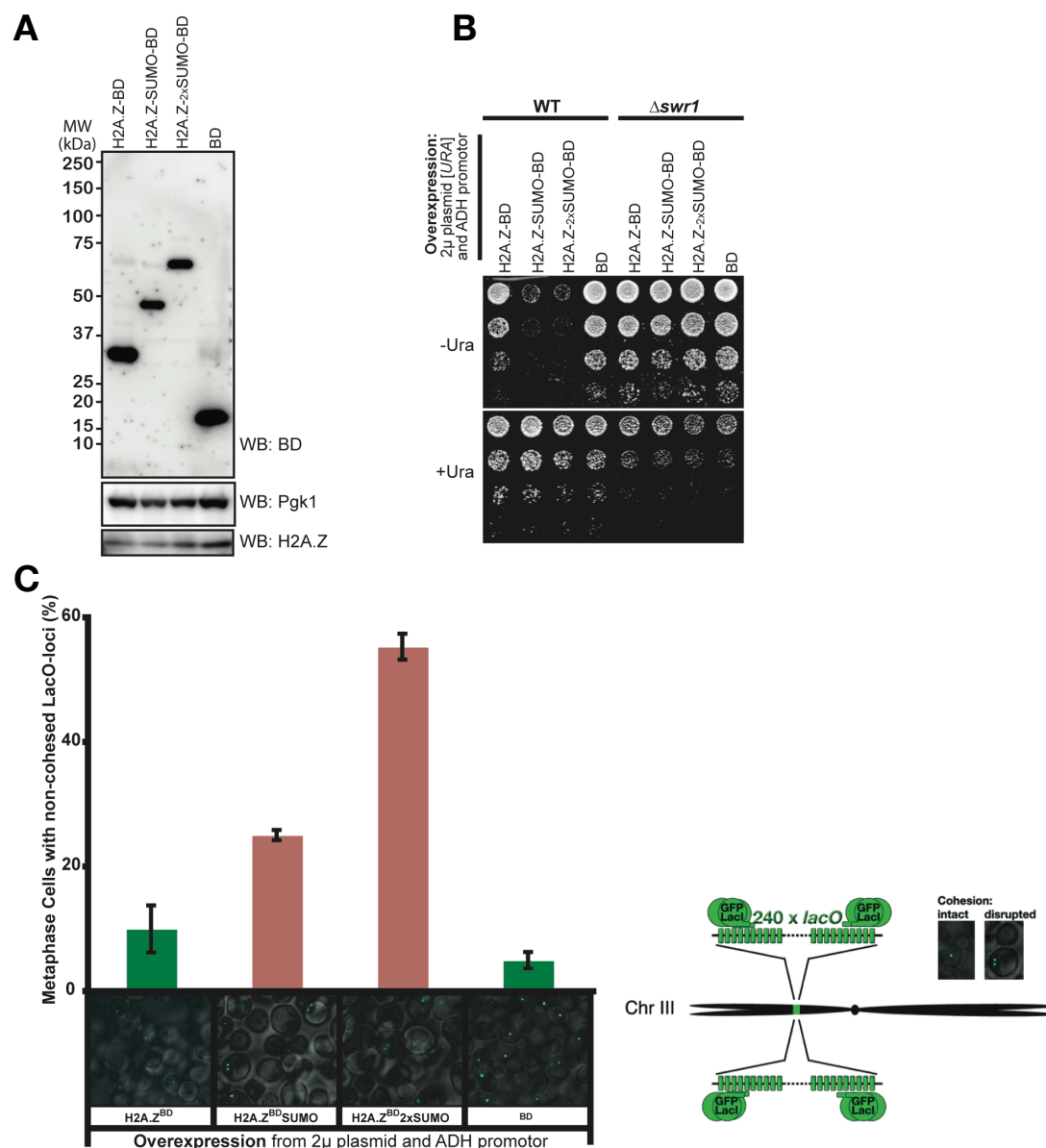


Figure 31. H2A.Z-SUMO represses cohesion establishment

(A) Western blot showing expression of H2A.Z linear fusions.

(B) Overexpression of H2A.Z-SUMO-BD linear fusions is toxic, whereas overexpression of H2A.Z-BD or BD alone does not impair cell growth. This dominant negative effect of the SUMO fusion requires the constructs to be incorporated into chromatin as they lose their toxicity in a $\Delta swr1$ background.

(C) Overexpression of H2A.Z-SUMO fusions leads to cohesion defects. Quantification of cohesion defects in strains GFP-tagged on Chromosome III. Cells were arrested in metaphase and the number of GFP-signal present in each cell was scored, indicating either normal cohesion (one signal) or a cohesion defect (two signals; see examples in micrographs). Data are represented as means of 3 independent experiments ($n > 100$) \pm SEM.

when H2A.Z incorporation into chromatin was impaired, e.g. in $\Delta swr1$, or when domains other than SUMO were linearly fused to the C-terminus of H2A.Z, e.g. the Gal4-BD domain (Fig. 31B).

To test whether the toxicity of the H2A.Z-SUMO fusions correlated or was due to impaired Eco1 function, these constructs were assayed for cohesion defects using cohesion tester strains (Bhalla et al., 2002). These harbor an array of Lac

repressor (LacI) binding sites (LacO) on chromosome IV, which can be made visible by expression of a nuclear-targeted ^{GFP}LacI fusion protein. Is cohesion established properly, the two sister chromatids present in G2 cells will be in close proximity to each other and thus only one GFP focus is observable. However, when cohesion is faulty or lacking, sister chromatids will move away from each other, thereby splitting the GFP signal in two. This system provides a straightforward and accurate means for quantification of cohesion efficiency. Strikingly, the expression of the H2A.Z-SUMO fusions led to a drastic increase in cohesion defects, being even further augmented by the addition of a second SUMO moiety to the fusion protein (Fig. 31C). These data correlate well with the effects observed on cell viability (Fig. 31B) and imply that H2A.Z SUMOylation counteracts cohesion establishment.

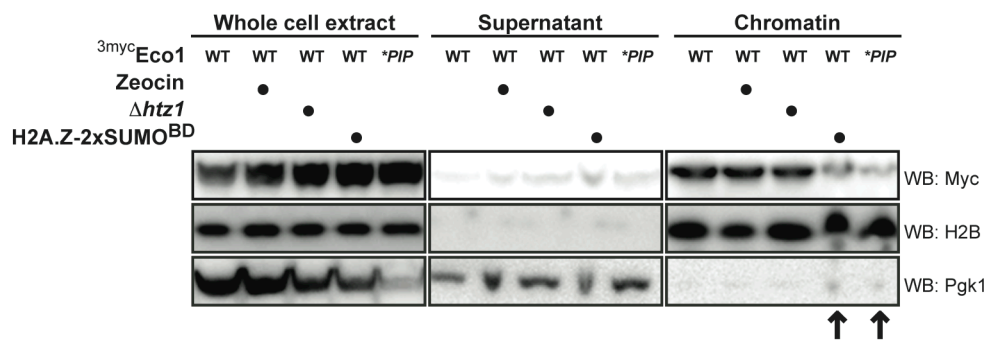


Figure 32. H2A.Z-SUMO represses Eco1-binding to chromatin.

Chromatin binding assay showing that overexpression of H2A.Z-SUMO-fusions blocks Eco1 binding to chromatin (denoted by arrow), similar as when Eco1 binding capability to PCNA is abrogated (*PIP). In $\Delta htz1$ or after DNA damage, Eco1 chromatin association remains unchanged compared to WT.

A reasonable explanation for the above observed toxicity and cohesion defects when overexpressing the H2A.Z-SUMO fusions is that overloading chromatin with H2A.Z-SUMO will act as an Eco1-repellant at the DNA. Indeed, when assayed for chromatin association, cells overexpressing H2A.Z-SUMO showed a similar reduction in Eco1 chromatin binding as when the PCNA-recruitment pathway is blocked by mutations in the PIP-box (Fig. 32).

Taken together, these findings suggest that modification of H2A.Z by SUMO is detrimental for sister chromatid cohesion, whereas unmodified or unmodifiable H2A.Z seems to be stimulatory. At first sight, these results may appear paradoxical, as H2A.Z is constitutively SUMOylated throughout the cell cycle. However, only a very minor fraction of H2A.Z is in fact modified by SUMO. As cohesion appears not to be uniformly distributed throughout the genome (Lengronne et al., 2004), H2A.Z-SUMO might in fact be needed to keep certain chromosomal regions free of cohesion.

3.7.3 H2A.Z is required for Eco1-mediated cohesion at DSBs

In unchallenged cells, the predominant Eco1-recruitment pathway via PCNA is active. Therefore, H2A.Z in chromatin is not required for proper cohesion establishment in this context (compare left-most bars in Fig. 33C and 33D). However, when assaying $\Delta swr1$ cells for cohesion establishment specifically in response to DSBs in G2, a prominent defect was observable (compare right-most bars in Fig. 33C and 33D). More expressly, this demonstrates that H2A.Z is indeed required for Eco1-mediated cohesion at the DSB.

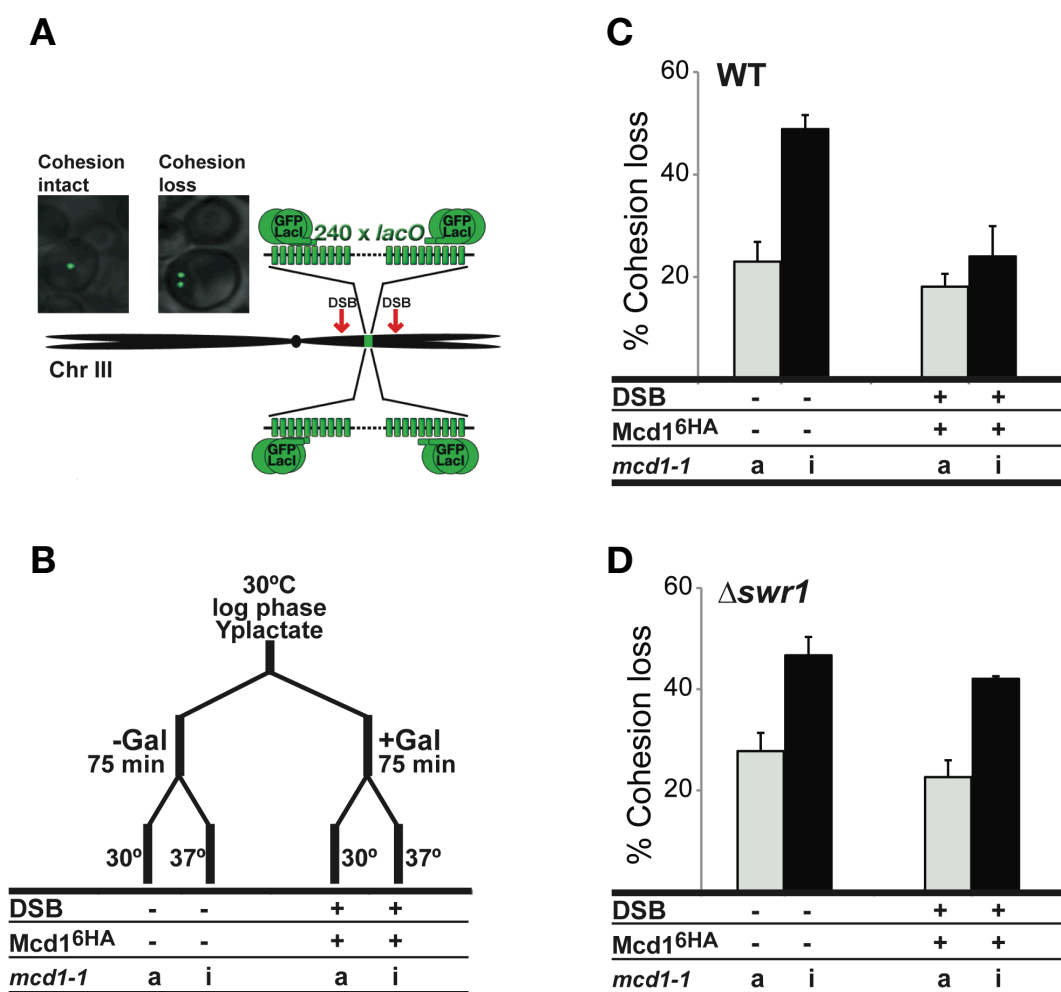


Figure 33. Incorporation of H2A.Z into chromatin is required for DSB-induced cohesion

Assay for DSB-induced cohesion (Unal et al., 2007). Briefly, cells establish cohesion in S-phase using the thermosensitive *mcd1-1* cohesin allele. After G2/M arrest by nocodazole treatment wildtype Mcd1^{6HA} along with the DSB-inducing HO-endonuclease is expressed by the addition of galactose. To test whether the newly expressed, post-DSB-loaded wild type Mcd1^{6HA}-containing cohesin complexes have become cohesive, the S-phase cohesin is specifically deactivated by shifting the cells to the nonpermissive temperature (37°C). Sister Chromatid cohesion is then visualized similar to the assay in Fig. 30C, by GFP-lacI fusion marking a DSB-proximal LacO-array.

In conclusion, the here presented data suggest a model, in which outside of S-phase, Eco1 is recruited to its chromatin template by interaction with nucleosomes, especially such that contain H2A.Z. This seems particularly important at DNA double-strand breaks, where H2A.Z is *de novo* incorporated as an early marker of the break site (Kalocsay, 2010; Kalocsay et al., 2009) and cohesion needs to be established in the absence of PCNA.

4 DISCUSSION

The renaissance of interest in chromatin came from the realization that far transcending its original role in packaging DNA, nucleosomes have evolved as central matchmakers and regulatory hubs in virtually all DNA-linked processes. DNA repair is fundamental to ensure genome stability, and DSBs are particularly toxic as they can lead to translocation-driven tumorigenesis. Ever-more sophisticated techniques to microscopically depict three-dimensional (3D) nuclear structure as well as to study local chromatin composition and dynamics *in vivo* have allowed us to analyze the impact of nuclear positioning and chromatin state on DSB repair.

By monitoring the chromatin composition of a persistent DSB and its position in 3D, this study discovered that cells react by a multifaceted response. In particular this involves the histone variant H2A.Z, which as a novel factor directs early processes such as DSB-resection, DNA damage checkpoint activation and possibly also the establishment of sister chromatid cohesion at the DSB. If no homology is found and the break persists, it later relocates and becomes fixed to the nuclear envelope. Curiously, this process requires the initiation of homology search (Rad51), H2A.Z, the DNA damage checkpoint and independently of the latter also modification of H2A.Z by the small ubiquitin-related modifier SUMO. The here-reported findings and their implications will be discussed in the following sections.

4.1 H2A.Z directs DSB-resection, checkpoint activation & repair

This study identified H2A.Z as a novel and important factor in the DNA damage response. Specifically, it seems to guide resection of the break ends and subsequent checkpoint activation (Fig. 34). Recently, several studies have elucidated the previously enigmatic enzymology of DSB-resection (Clerici et al., 2005; Gravel et al., 2008; Lengsfeld et al., 2007; Mimitou and Symington, 2008; Sartori et al., 2007; Zhu et al., 2008). The current status of research suggests that resection is initiated by the MRX-complex, which, in conjunction with Sae2, produces short, 50-100 bp, single-stranded overhangs. These serve as templates for the so-called long-range resection to ensue. Notably, this process depends on two independent pathways, one mediated by the exonuclease Exo1, the other by the RecQ-type helicase Sgs1 in concert with Dna2, a nuclease previously implicated in Okazaki-fragment processing. This thesis now adds an additional player to the cellular resection arsenal: the histone variant H2A.Z. Monitoring both initial (Fig. 7A) and long range resection (Fig. 7B) revealed, that H2A.Z is in fact involved in both

processes with however the latter displaying a stronger requirement for H2A.Z. Subsequently, genetic, epistasis analysis clearly placed H2A.Z in a pathway together with Sgs1, as it was epistatic to this deletion mutant, but additive with e.g. MRX mutants (Fig. 10). Notably, Sgs1 is the yeast homolog of the bacterial RecQ helicase and the human Bloom's and Werner's syndrome genes, which when mutated strongly predispose to cancer (Hickson, 2003). Intriguingly, H2A.Z is specifically incorporated into nucleosomes exactly at the border where the initial MRX-mediated resection activity passes into the more processive long-range resection. This in fact suggests the tantalizing possibility that H2A.Z might facilitate the relay exchange from MRX to Sgs1/Dna2. Mechanistically this could be brought about by recruiting Sgs1 to its site of action, activating its enzymatic activity at the DSB, or, alternatively, altering the local chromatin structure in a way to facilitate resection.

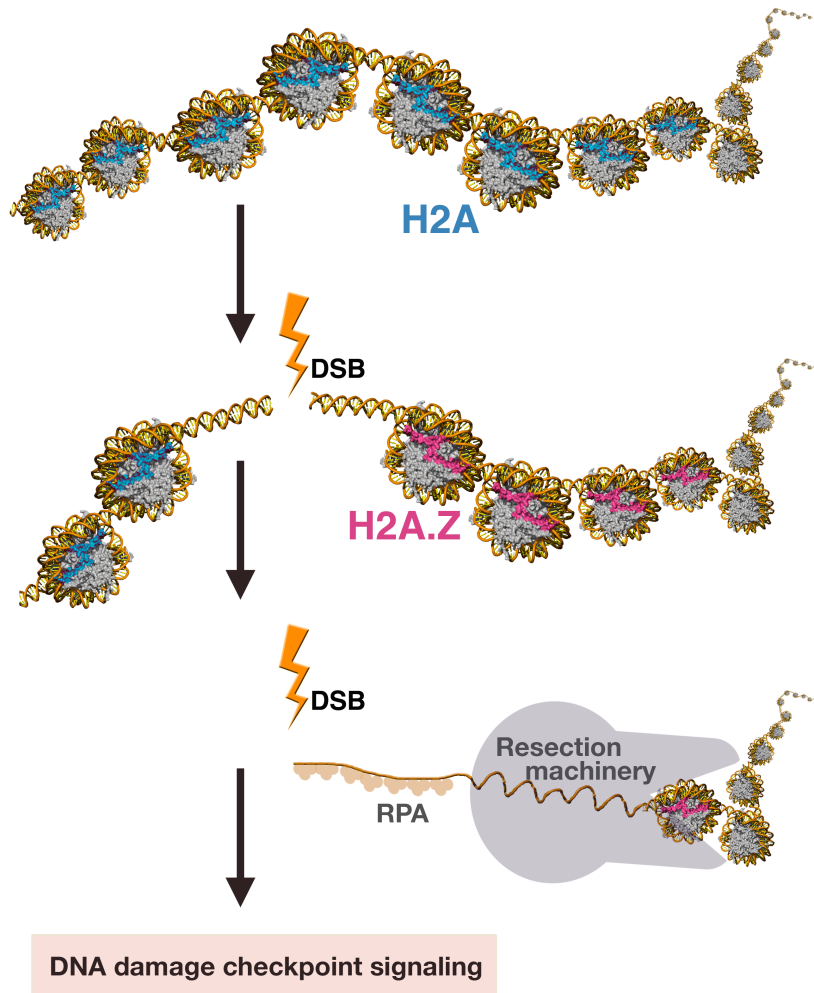


Figure 34. H2A.Z at the DSB guides resection and checkpoint activation

Upon a DSB, H2A.Z is incorporated into break-proximal nucleosomes. This promotes early events such as ssDNA formation, RPA-recruitment and DNA damage checkpoint activation.

Admittedly, the notion that a histone variant is incorporated into a nucleosome specifically to trigger resection, i.e. nucleosome eviction, is perplexing at first thought. However, such a function has been reported before: research on transcriptional regulation has prompted that H2A.Z is apparently incorporated into promotor-nucleosomes during repression of certain genes and poises these promoters to facilitate quick resumption of transcription through nucleosome eviction during a later activation program (Zhang et al., 2005). Moreover, by employing less harsh chromatin preparation protocols, Jin et al. (2009) could in fact show that previously annotated 'nucleosome-free regions', directly preceding open reading frames, are in fact enriched in H3.3 and H2A.Z-containing double-variant nucleosomes. These seem to be metastable, thereby facilitating ready access to the underlying DNA sequences. But also the naturally occurring H2A.Z nucleosome seems to be in a high energy state and therefore prone to nucleosome turnover. The original crystal structure of the intact H2A.Z nucleosome revealed an extended loop in H2A.Z, which was suggested to ensure that nucleosomes would contain either two H2A or two H2A.Z molecules (Suto et al., 2000). The possible existence of 'hybrid' nucleosomes comprising one H2A and one H2A.Z each was rejected as being energetically highly unfavorable due to sterical clashes between the H2A subtypes. However, more recent work has demonstrated, that *in vivo*, hybrid H2A/H2A.Z-containing nucleosomes are in fact the norm (Tolstorukov et al., 2009; Viens et al., 2006), with their inherent metastability being one of the mechanisms by which H2A.Z-depositioning modulates chromatin properties. Assuming that the H2A.Z nucleosomes incorporated at the DSB follow this rule, it is readily conceivable that such hybrid, metastable nucleosomes would alter the local chromatin structure in a way to promote resection and histone loss.

In accordance with the observed impaired resection rates, $\Delta htz1$ mutants are also defective in single DSB-induced checkpoint activation. This is most likely due to the fact that the decreased amount of RPA-covered ssDNA produced in these strains is insufficient to trigger a full-blown DNA damage checkpoint response. Interestingly, this study found H2A.Z to be required for checkpoint activation in response to a single, endonuclease-induced DSB, but not when cells suffer multiple, heterogeneous, e.g. zeocin-induced DSBs. Notably, such a qualitative discrimination concerning the type of DNA-lesion present in the cell has been described in the literature. Specifically, DNA repair pathway choice seems to be dictated not only by the cell cycle stage but also by the type of lesion eliciting the

response (Barlow et al., 2008; Ira et al., 2004; Zierhut and Diffley, 2008). Thus in the G1-phase of the cell cycle, single, endonuclease-induced DSBs are channeled into and processed by the NHEJ-pathway, whereas DSBs inflicted by ionizing radiation are targeted to the homologous recombination machinery regardless of the cell cycle stage (Barlow et al., 2008). This is probably due to the different nature of the break ends, which must somehow be recognized and discerned. H2A.Z might mark “clean” endonuclease-induced breaks and dispatch them for repair by HR. Alternatively, H2A.Z might be involved in gauging the amount of DNA damage, as apparently the response towards single versus multiple DSBs is qualitatively different. Despite checkpoint activation in response to multiple, zeocin-induced DSBs appearing normal in *Δhtz1* cells, they have difficulties surviving these breaks (Fig. 1), which indicates that H2A.Z probably plays an important additional role in the actual repair of DSBs.

Finally, the exact cue for H2A.Z-depositioning into the DSB-proximal nucleosomes remains elusive. Being already deposited at the DSB 30 minutes after HO-induction, H2A.Z incorporation timely coincides with MRX recruitment to the lesion, the most immediate response to a DSB reported thus far. Consequently, it is highly likely, that the SWR-complex, which incorporates H2A.Z, either physically contacts the MRX-complex or alternatively acts itself as a sensor for the DSBs. Moreover, concerning H2A.Z posttranslational modification, technical limitations make it impossible to determine where in the genome H2A.Z SUMOylation takes place. Notably, Pontin, the human homolog of the SWR-complex component Rvb1, was shown to co-purify with Ubc9, the SUMO-conjugating enzyme (Kim et al., 2007b). This raises the intriguing possibility that SUMOylation of H2A.Z might be coupled to its incorporation into chromatin, possibly when targeted to the DSB-proximal nucleosomes. However, since H2A.Z is largely evicted from the break hours before it relocalizes to the periphery in a SUMO-H2A.Z dependent manner, this modification may rather be triggering a signal transduction chain that finally results in chromosome fixation.

4.2 A persistent DSB relocates to the nuclear periphery

Intriguingly, this study identified a novel and unexpected response towards a persistent DSB. The initial steps of the pathway are shared with canonical homologous recombination. However, when homology fails to be found, the DSB relocates and becomes tethered to the two-dimensional scaffold of the nuclear envelope.

4.2.1 Mechanism of break relocation to the nuclear periphery

A parallel study by the laboratory of Susan Gasser proposed that a persistent DSB is specifically targeted to nuclear pores, where the SUMO-dependent ubiquitin-ligase Slx5/Slx8 resides which was suggested to act on the fixed DSB (Nagai et al., 2008). Yet in addition to nucleoporins this thesis work also found non-pore, inner nuclear transmembrane proteins to be associated with the DSB (Fig. 22), suggesting that tethering probably occurs more broadly at the nuclear periphery.

In contrast to nuclear pores, Mps3 seemed an ideal candidate for DSB-tethering at the nuclear periphery. Not only does it associate with the persistent DSB (Fig. 12), but Mps3 also physically interacts with H2A.Z and other DSB-end binding proteins such as the Ku70/80 and MRX complexes (Fig. 18 and Fig. 19). Moreover, Mps3 was already reported to mediate tethering and clustering of meiotic chromosome ends to the nuclear periphery during 'bouquet'-formation (Conrad et al., 2007; Ding et al., 2007; Penkner et al., 2007; Penkner et al., 2009), a process greatly facilitating homologous chromosome pairing and recombination during meiosis. However, mutant strains in which the entire nucleoplasmic domain of Mps3 was deleted showed only a minor sensitivity to DSBs and more importantly, still were capable of recruiting persistent DSBs to the nuclear envelope (Fig. 21). This is in contrast to a recent study, which measured chromatin dynamics during break relocation to the nuclear envelope using chromosome conformation capture (3C). This study claims that Mps3 is indeed the crucial anchor of the persistent DSB to the nuclear periphery (Oza et al., 2009). Taking into additional account the proposed DSB-association with nuclear pores (Nagai et al., 2008) and especially the data presented in this thesis work suggests that there seem to be multiple, possibly redundant DSB tethering mechanisms operating at the nuclear envelope. In the case of telomeres, the paradigm example for chromatin tethering to the nuclear envelope, it was in fact shown that cells have evolved several, redundant mechanisms for chromosome anchoring (Feuerbach et al., 2002; Galy et al., 2000; Hediger et al.,

2002; Tham et al., 2001; Tham and Zakian, 2000). Hence it is readily conceivable that a similar multivalent tethering system acts on the persistent DSB as well.

In another intriguing model, which reconciles the conflicting reports on the nature of the DSB-membrane anchor (Nagai et al., 2008; Oza et al., 2009), the broken chromosome could first be recruited by Mps3 and then passed on to the pore-associated Slx5/8 complex for sustained anchorage and/or processing (as discussed by Gartenberg, 2009). Although such an interaction has yet to be reported in yeast, at least one of the mammalian Mps3 homologs, Sun1, was demonstrated to intimately associate with nuclear pores (Liu et al., 2007). Moreover, in a particular DNA damage response towards eroded telomeres, these were in fact shown to relocate from their original nuclear envelope position to nuclear pores (Khadaroo et al., 2009). Interestingly, Mps3 also interacts in Y2H with the deSUMOylating enzyme Ulp1 and the Slx5/8 complex (Hiller, 2006), which colocalize at nuclear pores.

Intriguingly, DSB-targeting to the nuclear periphery only occurs after homology search has failed and the DSB persists. When monitoring Rad51 occupancy genome-wide in the donor deficient strain, it became apparent that relocation to the nuclear periphery is preceded by extensive 'spreading' of Rad51 along the broken chromosome *in cis*, however notably not affecting other chromosomes *in trans* (Kalocsay, 2010; Kalocsay et al., 2009). Likely, this is the first described snapshot of ongoing homology search *in vivo*. More important for the study at hand is however, that the observed choreography of events: (1) the initial H2A.Z-dependent processing of the DSB being followed by (2) extensive Rad51-mediated homology scanning along the affected chromosome and finally (3) the fixation of the break at the nuclear periphery, suggests the tantalizing possibility that DSB-tethering could be a mere consequence of homology search on the chromosome *in cis* (Fig. 35). More precisely, in this model, DSB-tethering would ensue when the Rad51-coated probing chromosome ends reach telomeric sequences, which in yeast are in fact already tethered to the nuclear envelope throughout most of the cell cycle. This model is supported by the observation that indeed, Rad51 activity is required to target the break to the nuclear periphery (Fig. 13). Moreover, a recent study demonstrated, that intact telomeres (more precisely, a functional telomerase enzyme) are required for DSB relocation to ensue (Oza et al., 2009). In contrast however, the position of the fixated break at the nuclear envelope could not be colocalized with telomere clusters (Fig. 19).

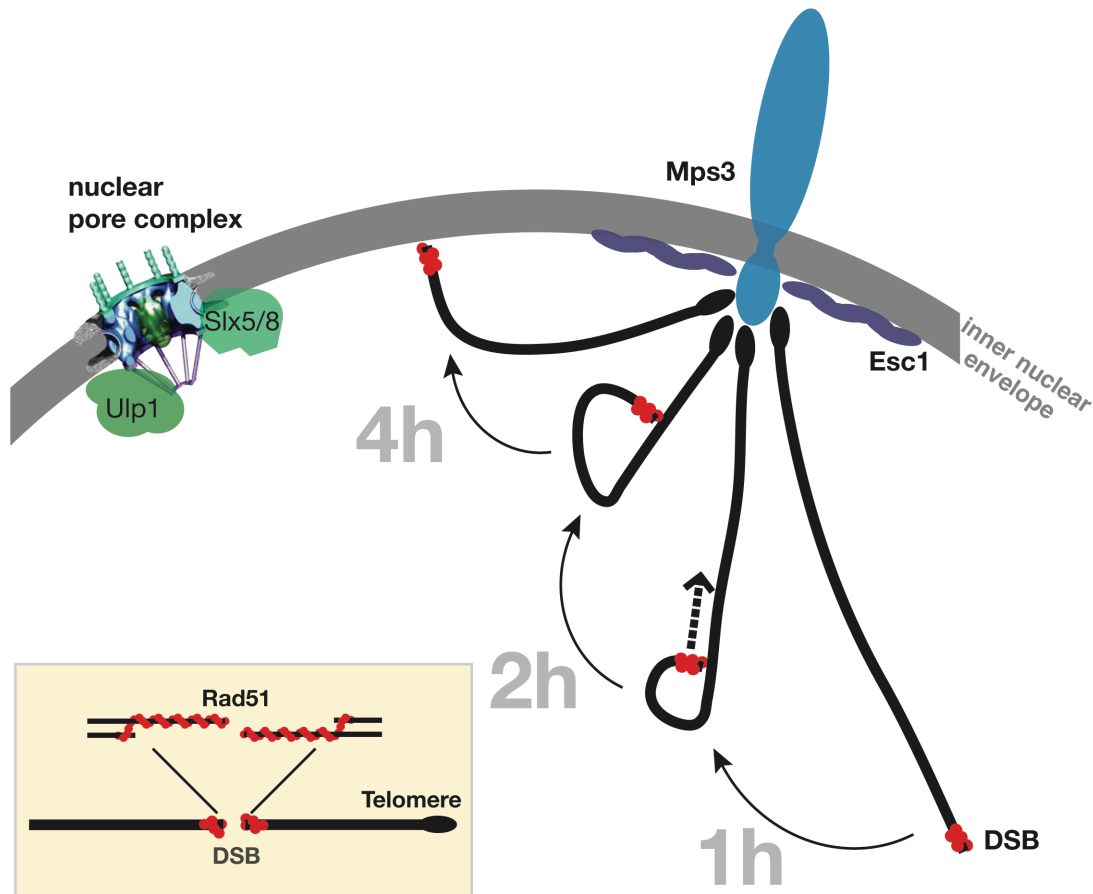


Figure 35. Potential Mechanism of relocation of a persistent DSB to the nuclear envelope

Mps3 and Esc1 serve as telomere anchors at the inner nuclear membrane. In the event of a DSB, the Rad51-coated 3' single-stranded tail scans the genome for homology. Strikingly, in a donor-deficient strain, this happens only on the affected chromosome, *in cis*, and not on other chromosomes *in trans*. In the proposed model, DSB-sequestration at the nuclear periphery occurs when the Rad51-coated DSB end reaches telomeric sequences, which are tethered to the nuclear envelope. Approximate time points post DSB-induction are indicated. The inset shows a detailed view of the Rad51-coated DSB tip. For simplicity, the figure only illustrates the fate of one of the two DSB ends.

Several experiments come to mind to ultimately scrutinize the proposed model. First, mutations that disrupt telomere tethering should also impact on DSB-relocation. Second, the distance separating DSB and telomere could be variegated and correlated with the time needed for the DSB to become tethered at the nuclear envelope. Finally, one could surgically displace the DSB from its usual chromosome environment by e.g. integrating the HO cut site on a plasmid and assaying for relocation of the linearized plasmid within the yeast cell. Along these lines, another elegant experiment would be to introduce a second HO cut site centromere-distal from the DSB, thereby decapping the broken chromosome fragment from its telomere anchor. Following the thus released fragment in microscopy should unequivocally clarify whether telomere attachment is indeed required for DSB-relocalization to the nuclear envelope.

4.2.2 Possible functions of break anchoring at the nuclear periphery

The here reported choreography of events in response to a persistent DSB resembles a multifaceted, however highly ordered and well-orchestrated pathway. As DSB targeting to the nuclear envelope only occurs if no homology is found and the break persists; the function of this novel cellular stress response is probably to enable the cell to cope with hazardous, pertinacious DNA-lesions. Intuitively two possibilities come to mind. Either, DSB relocation after HR-failure functions to activate alternative repair pathways, which might be concentrated at the nuclear periphery to promote chromosome healing. Or alternatively, the nuclear periphery could function as a quarantine compartment, where potentially hazardous irreparable DNA-lesions are sequestered to prevent them from participating in spurious and deleterious recombination events. This might allow the cell to gain time and persevere, until homology is eventually provided by e.g. mating.

Surprisingly, the mutants that were identified in this study to be specifically defective in DSB-targeting to the nuclear envelope (in particular e.g. *htz1*^{K126,133R}) are not detectably more sensitive to DNA damage than wildtype cells. However, typically, yeast cells are highly proficient in homologous recombination. Moreover, homologous sequences are omnipresent, above all of course, on the sister chromatid. Because, cells have powerful repair pathways in check, they can endure and repair relatively high doses of DSBs. Probably, the specific DSB relocation pathway described in this study evolved only for very rare and special cases of DNA-lesions where homology search is hampered for one reason or another. In this case, one would not necessarily expect sensitivity to DNA damage in general, as the vast majority of lesions will be efficiently buffered by the dominant repair pathways. There are in fact cases where homology search can become curtailed *in vivo*, e.g. when *RAD51* or other recombination genes are mutated, which has been reported for several rare cancer-predisposing syndromes (Thacker, 2005). In addition, a very recent publication demonstrated that the persistent DNA damage signal elicited by eroded telomeres drives tetraploidization in human cancers (Davoli et al., 2010). Moreover, in the meantime it has been shown that in instances where recombinational repair is slow, e.g. when the donor sequences for HR are located ectopically or repair by SSA necessitates excessive resection to precede, these more recalcitrant DSBs are also recruited to the nuclear periphery (Oza et al., 2009). Finally, the possibility remains that relocation of DSBs to the nuclear periphery is a

means to preserve genome stability by preventing unwanted repair events such as gross chromosomal rearrangements to ensue.

In contrast to mere sequestration and silencing, steering persistent DSBs to the nuclear periphery might also present a final attempt of the cell to activate alternative DNA repair mechanisms. Surprisingly, studies trying to assess the impact of DSB-tethering on repair pathway choice have yielded highly conflicting results. On the one hand it was reported that artificially tethering a recombination test locus to the nuclear envelope leads to increased gene conversion rates, whereas gross chromosomal rearrangements were suppressed (Nagai et al., 2008). In contrast the second study found exactly the opposite, namely that peripheral localization stimulated GCR and suppressed recombination (Oza et al., 2009). Along these lines, studies on the function of telomere tethering for subtelomeric recombination have also remained inconclusive. Here it was reported that depending on which mutant was used, telomere anchoring either suppressed (Schober et al., 2009) or stimulated (Therizols et al., 2006) subtelomeric DSB repair via homologous recombination. Fortunately this work identified H2A.Z SUMOylation to be a – so far – exclusive mark for break relocalization to the nuclear periphery. This presents a real advance, because the aforementioned studies suffered especially from the fact that the mutants they employed were highly pleiotropic (i.e. nuclear pores are well known to control general nucleocytoplasmic trafficking & transcription; Mps3 is essential for its function in spindle pole body duplication, acts in sister chromatid cohesion and as crucial telomere anchor). Disruption of such broad cellular functions probably masks the effect of disabled DSB-sequestration in their repair assays. Therefore, understanding the hidden repair defects of the here-studied H2A.Z-SUMOylation-defective mutants in detail, and especially also in other, DNA repair mutant backgrounds, will be key to unraveling the still enigmatic function of DSB relocation.

The here-reported notion that a persistent DSB requires independently of DNA damage checkpoint signaling also SUMO-modified H2A.Z to become relocated to the nuclear periphery is highly intriguing. It strikingly parallels the role of SUMOylated Rad52 in relocating broken rDNA out of the nucleolus in order to be repaired (Sacher et al., 2006; Torres-Rosell et al., 2007). The repetitive nature of rDNA, renders it prone to recombination-instigated genome instability. To counteract this inherent predisposition, cells have evolved mechanisms to prevent unwanted recombination within rDNA repeats. Interestingly, besides assembly into silent chromatin, a second means to limit access of the recombination machinery is

the tethering of the rDNA locus to the nuclear periphery (Mekhail et al., 2008). Although this tethering is mediated by yet another set of conserved inner nuclear membrane proteins, Heh1 and Nur1, the underlying concept may well be the same for recruiting a persistent DSB to the nuclear periphery: to prevent recombination reactions with unwanted partners.

Targeting of DNA damage to the nuclear periphery is analogous to another compartmentalized nuclear event involving shuttling of DNA loci to the nuclear envelope: the repression of gene activity (reviewed in Deniaud and Bickmore, 2009; Towbin et al., 2009). Intriguingly, H2A.Z was recently demonstrated to promote the retention of certain inducible genes at the nuclear envelope during repression (Brickner et al., 2007). This gene tethering was proposed to mediate transcriptional memory, as short-term repressed loci at the nuclear periphery were re-activated more rapidly, than long-term repressed loci in the nucleoplasm (Brickner, 2009). Notably, mechanistic insight into the exact role of H2A.Z in this process is still lacking and moreover, the membrane anchor at the periphery remains enigmatic. The here characterized interaction between H2A.Z and Mps3 raise the intriguing possibility that H2A.Z-nucleosomes within promoters of inducible genes would physically interact with Mps3, thereby facilitating the observed retention at the nuclear envelope. Clearly, testing the here-identified H2A.Z-binding deficient Mps3 point mutant (Fig. 18) for its ability to uphold transcriptional memory will be a highly informative experimental approach to dissect the mechanics of gene targeting to the nuclear periphery.

In summary, the nuclear envelope seems to be a compartment on which multiple cellular processes converge. This thesis work added another process, the sequestration and anchorage of persistent DNA damage, into the increasingly complex picture of perinuclear biology. More research is needed to unravel how such diverse processes as DNA repair, telomere maintenance, transcriptional repression and activation and nucleocytoplasmic trafficking are all integrated at the nuclear periphery. It is intriguing to speculate that within the perinuclear compartment there will be subdomains concentrating specialized activities. The results discussed above have probably only given a taste of the high degree of complexity and interdependency inherent to the events taking place at the nuclear periphery.

4.3 H2A.Z and sister chromatid cohesion

Genome stability depends on both, accurate chromosome segregation and high-fidelity DSB repair. Curiously, these two essential processes make use of the same fundamental molecular mechanism, namely sister chromatid cohesion. The importance of the latter for chromosome segregation has been known for a long time. By contrast, the requirement of cohesion for DSB repair has been recognized only within the past decade (Sjogren and Nasmyth, 2001; Strom et al., 2007; Strom et al., 2004; Unal et al., 2007). Signifying the importance of sister chromatid recombination for genomic stability, yeast cells in S and G2 are 10,000 times more resistant to x-rays than in G1 (Brunborg and Williamson, 1978). Cohesion is established by the essential acetyltransferase Eco1, which however, does not bind DNA and therefore needs to be recruited to its chromatin template. In the unchallenged cell cycle, this is achieved by an obligate, PCNA-mediated coupling between Eco1 and the progressing replication fork (Moldovan et al., 2006). Notably, cohesion is also established *de novo* by Eco1 in response to DSBs, however in a PCNA-independent manner (Strom et al., 2007; Unal et al., 2007). How Eco1 is recruited to its chromatin template outside of replication and upon DSBs remained mysterious.

This study reveals and characterizes a novel physical interaction between the histone variant H2A.Z and Eco1 (Fig. 27). Being devoid of enzymatic activity and its specific incorporation at the DSB (Kalocsay, 2010; Kalocsay et al., 2009) make H2A.Z ideally suited to play a role as matchmaker for DSB-related functions. Intriguingly, its interaction with Eco1 suggested a model in which H2A.Z might constitute an alternative recruitment pathway besides the known, PCNA-mediated one (Fig. 36). Although Eco1 also binds purely H2A-containing nucleosomes in GST-pulldown assays (Fig. 28), the interaction with H2A.Z-containing nucleosomes is of particular relevance *in vivo*. Evidencing this, overexpression of certain H2A.Z alleles partially bypassed the requirement for PCNA-mediated Eco1-recruitment to DNA (Fig. 30A). Moreover, chromatin fractionation experiments implied that H2A.Z is capable of binding Eco1 and retaining it on chromatin (Fig. 30B). Finally, mutants devoid of H2A.Z-nucleosomes in chromatin fail to establish sister chromatid cohesion in response to DSBs (Fig. 33). Together these data establish a strong link between H2A.Z and Eco1-mediated cohesion establishment.

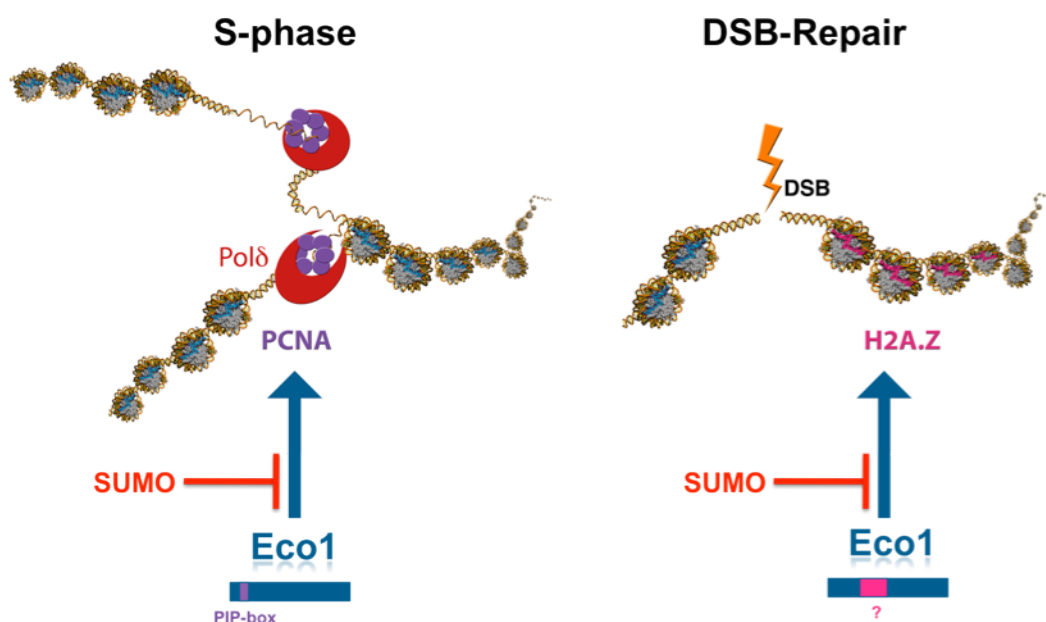


Figure 36. Model of H2A.Z mediating a parallel Eco1-recruitment pathway, besides PCNA

Eco1 is essential for establishing sister chromatid cohesion. Attributing to its lack of inherent DNA-binding capabilities, Eco1 needs to be recruited to chromatin, its site of action. The major recruitment pathway operates in S-phase and necessitates PCNA, which targets Eco1 to the replication fork. In the case of DSBs, cohesion needs to be established *de novo* in the absence of PCNA, for DSB repair to ensue. This study suggests that H2A.Z, which is deposited into the break-proximal nucleosomes, functions as alternative recruitment factor by directly binding to Eco1. Interestingly, in both pathways, SUMO-modification of the recruitment factor acts to repress Eco1 binding and cohesion establishment.

Unfortunately, attempts to map the H2A.Z-binding site on Eco1 were not very straightforward. Although initial truncation analysis in GST-pulldowns suggested a 100 amino acid region encompassing the zinc finger to be required for H2A.Z-binding (Fig. 27D), subsequent mutational analysis in Y2H yielded conflicting results regarding the involvement of the zinc finger (Fig. 29). Of note, the interpretation of the Y2H data is complicated by the fact that Eco1 dimerizes via its acetyltransferase domain, and a second, WT copy is present in the Y2H tester strains. However, the H2A.Z-binding site on Eco1 can clearly not be reduced to a simple linear motif, as was the case for the PIP-box dependent interaction with PCNA. Rather it seems, that the interaction with the H2A.Z-nucleosome is mediated by a wider, three-dimensional binding interface, possibly involving multiple contributing contacts, at least from the Eco1 side. Remarkably, single point mutants at the surface of the Zn-finger (e.g. *eco1 ED 48,49 AA*) hampered binding to H2A.Z, whereas complete excision of the zinc finger had no effect (Fig. 29A). Intriguingly, this raises the possibility that the zinc finger is more indirectly involved, by e.g. stabilizing a protein conformation necessary for H2A.Z binding. Along these lines, it can be conjectured that the Eco1 zinc finger is required to orient and expose a

distinct binding motif, thereby making it accessible to H2A.Z. This indirect, cooperative model would explain, why certain zinc finger residues in the intact protein are necessary for H2A.Z binding, while the zinc finger domain on its own doesn't interact. Further assuming that Eco1 adopts a compact fold with the individual domains tightly packing against each other, the even augmented binding upon excision of the zinc finger domain (Fig. 29C) could be explained by an artifact, in that the thus mutilated protein might expose a novel, or previously less accessible negative surface patch, readily binding to the highly basic histone. In the long run, obtaining a high-resolution three-dimensional structure of Eco1 will be indispensable for the correct interpretation of the here-reported interaction studies.

Interestingly, the inconsistent results regarding the requirement of the Eco1 zinc finger for H2A.Z binding is reminiscent of a different, well characterized protein-protein interaction module involving a Zn-finger-like domain: baculovirus inhibitor of apoptosis repeat (BIR)-domain containing proteins counteract apoptosis by binding and blocking the active site of caspase enzymes. Deletion analysis revealed that fragments comprising the BIR-domain were necessary and sufficient for direct interaction with the caspase active site (Takahashi et al., 1998). Surprisingly however, subsequent obtainment of the crystal structure of the BIR-domain-caspase complex revealed, that in fact a short flanking sequence outside the BIR domain was the only direct contacting element (Chai et al., 2001; Huang et al., 2001; Riedl et al., 2001). This suggested that although necessary for binding, the BIR-domain serves more a regulatory function, providing the structural architecture necessary to position the small linker motif for binding to the caspase active site. Although speculative, it might very well be that a similar principle underlies the Eco1-H2A.Z interaction interface.

Obtaining an H2A.Z binding-deficient Eco1 point mutant is highly desirable. Such a separator-of-function mutation would in principle allow the characterization of Eco1's involvement in DSB-induced cohesion irrespective of its essential role in S-phase. However, the here-described *eco1* mutant, displaying a significantly reduced binding to H2A.Z (*eco1* ED 48,49 AA), already results in a lethal phenotype (Moldovan et al., 2006), despite being competent in the PCNA interaction. Although the reduction in H2A.Z-binding cannot account in full for the observed lethality, it does underscore its general importance.

As evident from the studies on relocation of a persistent DSB to the nuclear periphery and its dependency on H2A.Z-SUMOylation, the repertoire of H2A.Z-

directed nuclear processes is further amplified by posttranslational modification. Importantly, this provides a fast and energetically inexpensive way to regulate protein-protein interactions. A previous report implicated acetylation of H2A.Z on K14 to be specifically important for chromosome transmission fidelity (Keogh et al., 2006b). This however seems to be independent of Eco1 recruitment, as H2A.Z K14R alleles could still interact with Eco1 (data not shown). Strikingly however, this thesis work revealed, that H2A.Z-SUMOylation seems to counteract cohesion establishment, presumably by disrupting the binding to Eco1. This was further supported by the observation that overexpression of linear H2A.Z-SUMO fusions was severely toxic to cells, correlating with drastic cohesion defects and release of Eco1 from chromatin (Fig. 27 and 28). Importantly these effects were entirely dependent on chromatin incorporation, *i.e.* were rescued by $\Delta swr1$. Intriguingly this is reminiscent of the PCNA-mediated Eco1 recruitment pathway, where SUMOylation of PCNA was also shown to act as repellent (Fig. 36 and Moldovan et al., 2006). As H2A.Z is SUMOylated throughout the cell cycle, albeit to a low extent, it might seem counterintuitive, why a mechanism to repress cohesion establishment should be in check constantly. However, only a minute amount of H2A.Z is SUMOylated a given timepoint (Kalocsay, 2010; Kalocsay et al., 2009) and it might be important for certain chromosomal regions to remain free of cohesion or at least sustain dynamic cycles of Eco1-binding and release from chromatin.

Besides its essential role in chromosome transmission during mitosis, cohesion establishment at DSBs is a prerequisite for repair. Importantly, this study demonstrated that H2A.Z nucleosomes, presumably at the DSB, are required for DSB-induced cohesion establishment (Fig. 33). The analysis if this directly involves the H2A.Z-Eco1 interaction is hampered by the fact that Eco1 could so far not be shown to be recruited to DSBs in microscopy or ChIP analysis (data not shown). Therefore, it cannot be excluded that the H2A.Z-mediated effects might be more indirect, for example based on the defective checkpoint activation at DSBs.

Of note, an important difference between yeast and metazoan chromosome biology is the sequential removal of arm and centromeric cohesion during mitosis in higher eukaryotes. Whereas yeast sister chromatids remain cohesed until the onset of anaphase, metazoan arm-cohesion is already removed in prophase (Waizenegger et al., 2000). As centromeric cohesion is apparently sufficient to ensure fidelity of chromosome segregation, arm cohesion could constitute a mere protective means against genotoxic insults, such as DSBs. Along these lines, the prolonged genome-

wide arm cohesion in yeast could in fact account in part for the much higher proficiency in homologous recombination compared to metazoan cells.

The mechanism how cohesins assists in DSB repair is unresolved. Generally, it is assumed that the mere juxtaposition of homologous, potential donor-loci by sister chromatid cohesion will tremendously simplify the Rad51-catalyzed homology-search reaction. However, a (likely additional) direct role for cohesins in guiding homologous recombination cannot be excluded. This idea also stems from the observation that cohesin complexes are actively recruited to DSBs and de novo cohesion establishment at the DSB is required for repair (Strom et al., 2007; Strom et al., 2004; Unal et al., 2004; Unal et al., 2007). Strikingly, the published data on the extensive Rad51-spreading on the broken chromosome in *cis*, notably not affecting any other chromosomes in *trans* (Kalocsay, 2010; Kalocsay et al., 2009), could be an indication that sister chromatid cohesion and Rad51-mediated homology probing are linked. Whether cohesion indeed restricts the Rad51 recombinase activity to the sister chromatid and if in fact cohesion is also a prerequisite for the later relocation to the nuclear periphery, will be an interesting hypothesis to test. Of note in this respect is the published physical interaction between the nuclear envelope transmembrane protein Mps3 and Eco1, which has already linked the nuclear periphery to cohesion establishment activity (Antoniacci et al., 2004).

Taken together, the results of the final part of this thesis work suggest that H2A.Z might constitute the enigmatic recruitment factor, targeting Eco1 activity to DSBs for cohesion establishment to ensue. Above all, this study has evidenced how modifying local chromatin structure by incorporation of the conserved histone variant H2A.Z is a powerful means to initiate such diverse processes as DNA resection, DNA damage checkpoint activation, cohesion establishment and even chromosome movement. Thus H2A.Z seems to act as a hub, integrating various early response pathways at the DSB.

5 MATERIALS AND METHODS

Common chemicals were purchased from Merck (Darmstadt, Germany), Roth (Karlsruhe, Germany), Sigma (Deisenhofen, Germany) or Fluka/Riedel-de Haen (Seelze, Germany), if not otherwise indicated. Enzymes and deoxynucleotide triphosphates (dNTPs) for molecular biology were purchased from NEB (Ipswich, USA). DNA oligonucleotides for cloning were custom-made by Eurofins MWG (Martinsried, Germany). α -factor peptide was synthesized by the MPIB core facility. For all procedures described, sterile flasks, solutions and deionized water was used. Basic microbiological, molecular cloning and biochemical techniques were derived from standard protocols (Ausubel, 1987; Sambrook et al., 1989).

5.1 Microbiology

5.1.1 *Escherichia coli* techniques

E. coli strains

Strain name	Genotype	Source
XL1-Blue	hsd R17 rec A1 end A1 gyrA46 thi-1 sup E44 relA1 lac [F' pro AB lacI ^q Z Δ M15 Tn10 (Tet ^r)]	Stratagene
BL21 (DE3)/RIL	B F ompT hsdS(r _B m _B) dcm+ Tet gal λ (DE3) EndA Hte [argU ileY leuW Cam ^r]	Stratagene
AB1157	F ⁻ thr-1 araC14 leuB6(Am) Δ (gpt-proA)62 lacY1 tsx-33 supE44(AS) galK2(Oc) hisG4(Oc) rfbD1 mgl-51 rpoS396(Am) rpsL31(Str ^R) kdgK51 xylA5 mtl-1 argE3(Oc) thi-1	(Dewitt and Adelberg, 1962)

E. coli vectors

Vector name	Epitope tag	Selection marker	Source
pET28a(+)	6xHis	kanamycin	Novagen
pGEX4T3	GST	ampicillin	Amersham

E. coli plasmids

To obtain 6xHis-tagged Htz1, the open reading frame (ORF) was cloned into pET28a by PCR from yeast genomic DNA. Expression constructs for GST-tagged Eco1 were kindly provided by Lucian Moldovan (Moldovan et al., 2006 and Moldovan, unpublished).

E. coli media & buffers

LB-medium/(plates): 1% Trypton (Difco)
 0,5% yeast extract (Difco)
 1% NaCl
 (1,5% agar) sterilized by autoclaving

Transformation of *E. coli*

Expression- and shuffle vectors were transformed into *E. coli* by electroporation. Strains were made competent by harvesting 1l of log-phase culture by centrifugation (15min, 4000g, 4°C). All subsequent steps were performed as close to 4°C as possible, using pre-chilled, sterile containers and solutions. The cell pellet

was washed once with 250ml and a second time with 125ml ice-cold 10% glycerol. After transfer with 20ml ice-cold 10% glycerol to a 50ml Falcon tube and centrifugation at 3500rpm for 15min at 4°C, the pellet was taken up in a final volume of 2ml ice-cold 10% glycerol. Aliquots were frozen on dry ice and stored at -80°C until further use.

For transformation, competent cells were first thawed on ice. Subsequently, 25µl cells were added on top of 1ul plasmid DNA or completed ligation reaction. This suspension was then electroporated in a pre-chilled cuvette (0,1 cm gap) with a 1.8kV pulse at a resistance of 200Ω in a GenePulser Xcell electroporator (Bio-Rad Laboratories, Hercules, USA). For ampicillin resistance, the transformation mixture was directly plated on selective media. kanamycin resistance required an additional rescue in 1 ml LB at 37°C for 1h prior to plating on selective media.

Recombinant protein expression

For the overexpression of recombinant proteins, competent BL21 (DE3)/RIL cells were transformed with vector DNA, carrying the gene of interest. Inoculation of a single colony was followed by a 12h cultivation at 37°C, shaking in LB-medium containing the appropriate antibiotic (kanamycin at 30µg/ml or ampicillin at 50µg/ml). This preculture was diluted 1:100 and expression was induced by the addition of IPTG at a final concentration of 0.5M, as soon as the culture had reached an OD₆₀₀ of 0.6. After further growth over night at 18°C, cells were harvested by centrifugation at 4°C. Cell pellets were flash-frozen in liquid N₂ and stored at -80°C.

5.1.2 *Saccharomyces cerevisiae* techniques

S. cerevisiae strains

Name	Genotype	Reference
DF5	<i>his3-Δ200, leu2-3,2-112, lys2-801, trp1-1, ura3-52</i>	(Finley et al., 1987)
NHG5-5D	<i>DF5, MATα htz1::natNT2</i>	this study
NHX27-7B	<i>DF5, MATα rad52::kanMX6</i>	this study
NHX26-11D	<i>DF5, MATα rad51::HIS3MX6</i>	this study
NHX29-11C	<i>DF5, MATα mre11::HIS3MX6</i>	this study
Y1271	<i>DF5, MATα sgs1::kanMX6</i>	B. Pfander,
NHT253-7B	<i>DF5, MAT a Htz1-tADH::kanMX6</i>	this study
NHT254-2C	<i>DF5, MAT a htz1-K126R-tADH::kanMX6</i>	this study
NHT255-2D	<i>DF5, MAT a htz1-K133R-tADH::kanMX6</i>	this study
NHT256-3C	<i>DF5, MAT a htz1-K126,133R-tADH::kanMX6</i>	this study
NHX67-6C	<i>DF5, MAT a Htz1-tADH::kanMX6 rad52::HIS3MX6</i>	this study
NHX68-3D	<i>DF5, MATα htz1-K126R-tADH::kanMX6 rad52::HIS3MX6</i>	this study
NHX69-1C	<i>DF5, MATα htz1-K133R-tADH::kanMX6 rad52::HIS3MX6</i>	this study
NHX70-6A	<i>DF5, MATα htz1-K126,133R-tADH::kanMX6 rad52::HIS3MX6</i>	this study
NHT18-9D	<i>DF5, MATα HTZ1^{9myc}::HIS3MX6</i>	this study
NHT18-6B	<i>DF5, MATα Htz1^{9myc}::HIS3MX6 MPS3^{3HA}::KITRP1</i>	this study
NHT19-2C	<i>DF5, MATα CHL1^{9myc}::HIS3MX6</i>	this study
NHT19-13A	<i>DF5, MATα CHL1^{9myc}::HIS3MX6 MPS3^{3HA}::KITRP1</i>	this study
NHT24-7B	<i>DF5, MATα NBP1^{9myc}::HIS3MX6</i>	this study
NHT24-8D	<i>DF5, MATα NBP1^{9myc}::HIS3MX6 MPS3^{3HA}::KITRP1</i>	this study
NHT26-12B	<i>DF5, MATα KAP104^{9myc}::HIS3MX6</i>	this study
NHT26-5C	<i>DF5, MATα KAP104^{9myc}::HIS3MX6 MPS3^{3HA}::KITRP1</i>	this study

Name	Genotype	Reference
NHT27-13C	<i>DF5, MAT a EST1^{9myc}::HIS3MX6</i>	this study
NHT27-13B	<i>DF5, MAT a EST1^{9myc}::HIS3MX6 MPS3^{3HA}::kITRP1</i>	this study
NHT82-3B	<i>DF5, MAT a MPS3^{CFP}::HIS3MX6</i>	this study
NHT83-9B	<i>DF5, MAT a HTZ1^{YFP}::kanMX6</i>	this study
NHX14-3B	<i>DF5, MAT a MPS3^{CFP}::HIS3MX6 HTZ1^{YFP}::kanMX6</i>	this study
NHT7-2C	<i>DF5, MAT a MPS3^{9myc}::HIS3MX6</i>	this study
NHT166-3A	<i>DF5, MAT a KU70^{6HA}::kITRP1</i>	this study
NHT167-1C	<i>DF5, MAT a KU80^{6HA}::kanMX6</i>	this study
NHX44-10C	<i>DF5, MAT a KU70^{6HA}::kITRP1 MPS3^{9myc}::HIS3MX6</i>	this study
NHX45-6C	<i>DF5, MAT a KU80^{6HA}::kanMX6 MPS3^{9myc}::HIS3MX6</i>	this study
NHG17	<i>DF5, MAT a MRE11^{3HA}::kITRP1</i>	S. Bergink,
NHX23-4A	<i>DF5, MAT a MRE11^{3HA}::kITRP1 MPS3^{9myc}::HIS3MX6</i>	this study
NHT125-5C	<i>DF5, MATα mps3::natNT2 YCplac33 MPS3</i>	this study
NHT18-9D	<i>DF5, MATα HTZ1^{9myc}::HIS3MX6</i>	this study
NHT617	<i>DF5, MAT a ECO1^{6HA}::kITRP1</i>	this study
NHX99-3B	<i>DF5, ECO1^{6HA}::kITRP1 HTZ1^{9myc}::HIS3MX6</i>	this study
Y1952	<i>DF5, MATα eco1::kanMX6 YCplac33-ECO1</i>	(Moldovan et al., 2006)
NHT56	<i>DF5, MATα eco1::kanMX6 YCplac33-ECO1 Ylplac128^{myc}ECO1::LEU2</i>	this study
NHT57	<i>DF5, MATα eco1::kanMX6 YCplac33-ECO1 Ylplac128^{myc}eco1^{33-end}::LEU2</i>	this study
NHT58	<i>DF5, MATα eco1::kanMX6 YCplac33-ECO1 Ylplac128^{myc}eco1^{Q18A,K20A,L21A}::LEU2</i>	this study
NHG12	<i>DF5, MATα eco1::kanMX6 YCplac33-ECO1 Ylplac128^{myc}ECO1::LEU2 htz1::natNT2</i>	this study
PJ69-7A	<i>trp-901-, leu2-3,112 ura3-53 his3-200 gal4 gal80 GAL1::HIS GAL2-ADE2 met2::GAL7-lacZ</i>	(James et al., 1996)
NHG57	<i>PJ69-7A, swr1::natNT2</i>	this study
JKM179	<i>Δhml::ADE1 MATα Δhmr::ADE1 ade1-100 leu2-3,112 lys5 trp1::hisG' ura3-52 ade3::GAL::HO</i>	(Lee et al., 1998)
JKM139	<i>Δhml::ADE1 MATa Δhmr::ADE1 ade1-100 leu2-3,112 lys5 trp1::hisG' ura3-52 ade3::GAL::HO</i>	(Lee et al., 1998)
JKM161	<i>HMLα MATa Δhmr::ADE1 ade1-100 leu2-3,112 lys5 trp1::hisG' ura3-52 ade3::GAL::HO</i>	(Sugawara et al., 2003)
MK90	<i>JKM179, RFA1^{6HA}::kITRP1</i>	(Kalocsay, 2010)
NHT394	<i>JKM179, RFA1^{6HA}::kITRP1 htz1::natNT2</i>	this study
NHT71	<i>JKM179, MPS3^{9myc}::kanMX6</i>	this study
NHT72	<i>JKM179, MPS3^{9myc}::kanMX6 htz1::natNT2</i>	this study
NHT73	<i>JKM179, MPS3^{9myc}::kanMX6 swr1::natNT2</i>	this study
NHG48	<i>JKM179, MPS3^{9myc}::kanMX6 MATα-inc</i>	this study
NHT282	<i>JKM179, MPS3^{9myc}::kITRP1 HTZ1-tADH::kanMX6</i>	this study
NHT283	<i>JKM179, MPS3^{9myc}::kITRP1 htz1-K126R-tADH::kanMX6</i>	this study
NHT284	<i>JKM179, MPS3^{9myc}::kITRP1 htz1-K133R-tADH::kanMX6</i>	this study
NHT285	<i>JKM179, MPS3^{9myc}::kITRP1 htz1-K126,133R-tADH::kanMX6</i>	this study
NHT310	<i>JKM179, mps3::natNT2 Ylplac204-MPS3^{3myc}::TRP1</i>	this study
NHT311	<i>JKM179, mps3::natNT2 Ylplac204-mps3 150-682^{3myc}::TRP1</i>	this study
NHT303	<i>JKM179, CDC5^{6HA}::kanMX6</i>	this study
NHT307	<i>JKM179, CDC5^{6HA}::kanMX6 Ylplac204-MPS3^{3myc}::TRP1</i>	this study
NHT308	<i>JKM179, CDC5^{6HA}::kanMX6 Ylplac204-mps3 150-682^{3myc}::TRP1</i>	this study

Name	Genotype	Reference
NHT412	<i>JKM179, MPS3^{9myc}::kanMX6 rad51::hphNT1</i>	this study
NHT417	<i>JKM179, MPS3^{9myc}::kanMX6 rad9::hphNT1 rad24::natNT2</i>	this study
NHT176	<i>JKM179, NIC96^{9myc}::kanMX6</i>	this study
NHT181	<i>JKM179, HEH2^{9myc}::kanMX6</i>	this study
NHT415	<i>JKM139, MPS3^{9myc}::kanMX6 bar1::natNT2</i>	this study
NHT93	<i>JKM161, MPS3^{9myc}::HIS3MX6</i>	this study
NHT345	<i>JKM161, MPS3^{9myc}::HIS3MX6 rad52::hphNT1</i>	this study
NHT427	<i>JKM161, htz1::natNT2</i>	this study
NHT428	<i>JKM161, swr1::natNT2</i>	this study
NHT429	<i>JKM161, mre11::hphNT1</i>	this study
MK97	<i>JKM179, NIC96^{mars}::hphNT1 YCR041W-240xLacO::LEU2, pURA3-GFP-LacI::URA3</i>	(Kalocsay, 2010)
NHT261	<i>MK97, Htz1-tADH::kanMX6</i>	this study
NHT262	<i>MK97, htz1-K126R-tADH::kanMX6</i>	this study
NHT263	<i>MK97, htz1-K133R-tADH::kanMX6</i>	this study
NHT264	<i>MK97, htz1-K126, 133R-tADH::kanMX6</i>	this study
MK92	<i>JKM179, YCR041W-240xLacO::LEU2</i>	(Kalocsay, 2010)
NHT279	<i>JKM179, YCR041W-240xLacO::LEU2, pURA3-GFP-LacI::URA3</i>	this study
NHT280	<i>JKM179, YCR041W-240xLacO::LEU2, pURA3-GFP-LacI::URA3 RAP1^{mars}::kanMX6</i>	this study
YMV45	<i>ho hml::ADE1 mata::hisG hmr::ADE1 leu2::leu2(Asp718-Sall)-URA3-pBR332-MATa ade3::GAL::HO ade1 lys5 ura3-52 trp1::hisG</i>	(Vaze et al., 2002)
NHT480	<i>YMV45, htz1::natNT2</i>	this study
NHT483	<i>YMV45, mre11::natNT2</i>	this study
NHT549	<i>YMV45, mre11::natNT2 htz1::hphNT1</i>	this study
NHT489	<i>YMV45, exo1::natNT2</i>	this study
NHT550	<i>YMV45, exo1::natNT2 htz1::hphNT1</i>	this study
NHT492	<i>YMV45, sgs1::natNT2</i>	this study
NHT551	<i>YMV45, sgs1::natNT2 htz1::hphNT1</i>	this study
AFS173	<i>LacO::LEU2, pCUP1-LacI12-GFP12::HIS3MX6</i>	(Bhalla et al., 2002)
EU3275	<i>MATα Δho Δhml1::ADE1 Δhmr::ADE1 ade1-110 leu2,3-112 lys5 trp1::hisG ura3-52::pGAL:MCD1-6HA::URA3 ade3::GAL10:HO his3::GFP-LacI:KanMX 5'SRD1::2ndHOcs:HYG 5'RIM1::LacO:NAT mcd1-1</i>	(Unal et al., 2007)
NHT615	<i>EU3275, swr1::LEU2</i>	this study

S. cerevisiae vectors

Plasmid type	Name (marker)	Copies/cell	Reference
Integrative	pYIplac211 (URA3)	1	(Gietz and Sugino, 1988)
	pYIplac204 (TRP1)		
	pYIplac128 (LEU2)		
Centromeric	pYCplac33 (URA3)	3-6	(Gietz and Sugino, 1988)
	pYCplac22 (TRP1)		
	pYCplac111 (LEU2)		
2μ	pYEplac195 (URA3)	50-100	(Gietz and Sugino, 1988)
	pYEplac112 (TRP1)		
	pYEplac181 (LEU2)		
Yeast two-hybrid	pGAD-C1-3	50-100	(James et al., 1996)
	pGBD-C1-3		

***S. cerevisiae* plasmids**

Plasmids employed in Y2H assays were derived either from pGAD-C1 (for N-terminal AD-fusions) or pGBD-C1 (for N-terminal BD-fusions). The respective open reading frames were cloned by PCR from yeast genomic DNA. Mutations were introduced by site-directed mutagenesis. Y2H-constructs used, but not generated in this study were as follows: AD-Fir1, AD-Fir1⁶⁰⁹⁻⁷⁷⁰, AD-Fir1⁶⁰⁹⁻⁷⁵⁸, AD-Siz2¹⁻³⁴⁶ (all M. Schwarz, unpublished); AD-Ubc9 (Hoega et al., 2002); BD-Eco1, BD-ctf7-203, BD-eco1 PIP*, BD-eco1 C35A,C38A, BD-eco1 YSTA42-45AAAA, BD-eco1 H53A,H57A, BD-eco1 E48A,E49A, BD-eco1³³⁻²⁸¹, BD-eco1⁶⁰⁻²⁸¹ (Moldovan et al., 2006).

Plasmids to generate mps3 truncation alleles (Fig. 20) are derived from pYIplac204 and contain the endogenous *MPS3* promoter and terminator in addition to an N-terminal 4myc tag. Plasmids for scrutinizing the relevance of the Mps3 nucleoplasmic domain in ChIP assays of the persistent DSB (Fig. 21) are derived from pYIplac204 and contain the endogenous *MPS3* promoter and terminator in addition to a C-terminal 3myc tag.

Plasmids for overexpression of the H2A.Z C-terminal SUMO fusions are based on pYEplac195 and contain an ADH promoter and a C-terminal BD tag. Plasmids to generate the Eco1 WT and mutant shuffle strains were derived from pYIplac128 and generated by L. Moldovan. Plasmids for overexpression of WT Htz1 and the respective SUMO-deficient mutants were provided by M. Kalocsay. They are derived from YEplac112, contain an ADH promoter and a single, C-terminal HA epitope tag.

To monitor the persistent DSB in microscopy, the MAT locus was marked by 240 copies of LacI binding sites (LacO). The plasmid used for this purpose, pMKlacOZ1 (Kalocsay, 2010; Kalocsay et al., 2009), contains a lacO-array which was subcloned from pLAU43 (Lau et al., 2003). As large repetitive arrays are instable in commonly used *rec⁻* *E. coli* strains, pLAU43 and pMKlacOZ1 were propagated at room temperature in the recombination-proficient AB1157 (Dewitt and Adelberg, 1962) strain. The plasmid for ^{GFP}LacI expression, pMKGFP-lacI (Kalocsay, 2010; Kalocsay et al., 2009), was derived from pYIplac111 and constitutive, low expression of the fusion protein is ensured by the presence of a *URA3* promoter.

***S. cerevisiae* media & buffers**

YPD / YPGal (plates)	1% yeast extract (Difco) 2% bacto-peptone (Difco) 2% carbon source (glucose, raffinose or galactose) (2% agar) sterilized by autoclaving
Yp-Lactate	1% yeast extract (Difco) 2% bacto-peptone (Difco) 3% lactic acid adjust pH to 5.5 with NaOH (ca. 12g/L final) sterilized by autoclaving
YPD G418/NAT/Hph plates	After autoclaving, YPD medium with 2% agar was cooled to 50°C, and G418 (geneticine disulphate, PAA Laboratories) to 200mg/l, NAT (nourseothricin, HKI Jena) to 100mg/l or Hph (hygromycin B, PAA Laboratories) to 500mg/l was added.
SC-media (plates)	0.67% yeast nitrogen base (Difco) 0.2% amino acid drop out mix 2% carbon source (glucose, raffinose or galactose)

SC-lactate	(2% agar) sterilized by autoclaving 0.67% yeast nitrogen base (Difco) 0.2% amino acid drop out mix 3% lactic acid adjust pH to 5.5 with NaOH (ca. 12g/L final) sterilized by autoclaving
Amino acid drop out mix:	20mg Ade, Ura, Trp, His 30mg Arg, Tyr, Leu, Lys 50mg Phe 100mg Glu, Asp 150mg Val 200mg Thr 400mg Ser
Sporulation medium:	2% (w/v) potassium acetate, sterilized by autoclaving
Sporulation (plates)	0.25% yeast extract 0.1% glucose 2% potassium acetate 0,168% CSM powder (2% agar) sterilized by autoclaving bring pH to 7 with KOH/Acetic acid
Zymolyase solution	0.9M sorbitol 0.1M Tris-HCl, pH 8. 0.2M EDTA, pH 8.0 50mM DTT 0.5mg/ml zymolyase 20T (Seikagaku Corp., Japan)
SORB:	100mM LiOAc 10mM Tris-HCl, pH 8.0 1mM EDTA, pH 8.0 1M sorbitol sterilized by filtration
PEG:	100mM LiOAc 10mM Tris-HCl, pH 8 1mM EDTA, pH 8.0 40 % (w/v) PEG-3350 sterilized by filtration, stored at 4°C

Cultivation and storage of *S. cerevisiae*

Liquid cultures were inoculated with a single yeast colony from freshly streaked plates and grown overnight. From this preculture the main culture was inoculated to an OD₆₀₀ of 0.1 and incubated in baffle-flasks (size ≥ 5x liquid culture volume) on a shaking platform (150-220 rpm) at 30°C until mid-log phase growth had been reached (equals OD₆₀₀ of 0.6-0.9). The culture density was determined photometrically (OD₆₀₀ of 1 is equal to 1.5x10⁷ cells/ml). Cultures on agar plates were sealed with parafilm and stored at 4°C up to 4 months. For long-term storage, stationary cultures were frozen in 15% (v/v) glycerol solutions at -80°C.

Genetic manipulation of *S. cerevisiae*

Cells were made competent by harvesting 50ml of a mid-log phase culture (500g, 5min, room temperature) and subsequent washing, first with 5ml sterile water and then with 5ml SORB. The pellet was resuspended in 360 μ l SORB + 40 μ l carrier DNA (salmon sperm DNA, 10mg/ml, Invitrogen). Competent cells were stored at -80°C .

For transformation, 0.2 μ g of circular or 2 μ g linearized plasmid DNA or PCR product was incubated for 30min at room temperature with 10 μ l or 50 μ l competent cells, respectively, in 6 volumes of PEG solution. DMSO was added to a final concentration of 10% and transformation mixtures were heat-shocked at 42°C for 15min (for temperature sensitive strains or for transforming JKM179, heat shock was reduced to 7 min). Subsequently, cells were pelleted (at room temperature and 400g for 3min), resuspended in 100 μ l sterile water and plated on the respective SC selection plates. Selection by G418 (*kanMX6*), nourseothricin (*natNT2*) or hygromycin (*hphNT1*) resistance required an additional rescue in 300 μ l YPD at 30°C for 1.5h prior to plating on selective media. Plates were incubated for 2-3 days at 30°C and, if necessary, replica-plated again on selection plates to remove false-positive background.

Deletion mutants (as well as chromosomally tagged strains) were constructed by a PCR-based strategy (Janke et al., 2004; Knop et al., 1999). Briefly, PCR products used for transformation contained the selection marker (and epitope tag) being flanked on both sides by genomic targeting sequences. Stable and correct integration by homologous recombination was subsequently checked by yeast colony PCR. If applicable, successful epitope tagging or gene knockout was additionally confirmed in western blot analysis or microscopy.

For chromosomal, C-terminal RFPmars tagging, a pYM38-mars::hphNT1 plasmid (kindly provided by R. Wedlich-Söldner) was used as PCR template.

All *htz1* mutations were targeted to the endogenous *HTZ1* locus. The PCR products for transformation were obtained by amplifying the ADH terminator and *kanMX6* selection marker (tADH S3: CGTACGCTGCAGGTCGAC; S2: ATCGATGAATTCTCGA GCTCG) from pYM13 (Janke et al., 2004), with the forward primer containing the respective mutations in the Htz1 C-terminus. Correct integration and presence of genomic *htz1* mutation was confirmed by sequencing of the *HTZ1* locus. For *swr1* knockouts with *LEU2* as selection marker, PCR products for transformation were obtained using *LEU2* promoter- and terminator-specific primers (LEU2 S1: AACTGTGGGAATACTCAGGT; LEU2 S2 CCTACCCTATGAACATATTCC and pYlplac128 (Gietz and Sugino, 1988) as template.

The MAT α -inc strain contains a mutated, incleavable HO cut site and was obtained by selecting for JKM179 mutants that were able to grow in the presence of galactose. Mutation of the HO cut site was confirmed by sequencing.

For stable integration of cloned yeast expression constructs, the Ylplac series of vectors was used (Gietz and Sugino, 1988). Before transformation, the vector was linearized with a restriction enzyme cutting within the auxotrophic marker. This ensures integration by HR into the endogenous marker gene locus. Lack of autonomous replication sequences ensures that only stable transformants survive the auxotrophic selection. For Mps3 and Eco1 mutants, single copy integration was verified by quantitative RT-PCR.

Yeast colony PCR

Yeast colony PCR was performed using the Whole Cell Yeast PCR Kit (Bio101, La Jolla, USA) and according to the manufacturer's instructions. Briefly, a minute scoop from the top of a fresh yeast colony was transferred and swirled into a PCR tube containing 1 μ l of 1:4 diluted lysis reagent. 1h incubation at 37°C was followed

by addition of 19 μ l PCR master mix, brief mixing and starting of the PCR cyclers program.

PCR mix		Thermocycler program	
	ul	94°C	3min
10x ThermoPol buffer	2	then 40 cycles	
Primer 1 (10 μ M)	2	94°C	30s
Primer 2 (10 μ M)	2	50°C	30s
dNTPs (10mM each)	0.7	72°C	45s/kb
Taq polymerase	0.5	72°C	10min
H ₂ O	11.8	4°C	∞

Mating, sporulation and tetrad analysis

Freshly streaked haploid yeast strains of opposite mating type (MAT α , MATa) were mixed on a YPD plate and allowed to mate for 10-15h at 30°C. For diploid selection, a patch of cells was restreaked on double-selection plates. Single colonies of thus obtained diploids were inoculated in YPD and grown to saturation (24-48h). For sporulation, 500 μ l were harvested (500g, 5min, room temperature), subsequently washed 4 times with sterile H₂O, resuspended in 4ml sporulation media and incubated for 3-4 days on a shaker at room temperature. In this medium, cells divide a few times before they undergo meiosis as soon as nutrients get limiting. Sporulation efficiency was assessed microscopically.

For tetrad dissection, 10 μ l sporulated culture was incubated with an equal volume of zymolyase solution for 10min at room temperature. Tetrads were dissected with a micromanipulator (Singer MSM Systems). Germination and growth of the spores were carried out on non-selective YPD plates for 2-3 days. Tetrads were analyzed genotypically by replica plating on selection plates and for known phenotypes, if applicable.

Alpha factor arrest (G1)

Treatment of Mata cells with the α -factor pheromone results in cell cycle arrest at the G1 stage. For such cell cycle synchronization, mid-log phase cultures were supplemented with 10 μ M α -factor (stock solution in DMSO) and incubated on a shaker at room temperature. After 3-4h, arrest efficiency was determined microscopically (typically >90%). When ChIP-assays of G1-cells necessitated large-scale cultures, strains were $\Delta bar1$ and arrested in G1 with 0,5 μ g/ml α -factor.

Directed yeast two hybrid (Y2H) assays

PJ69-7a (James et al., 1996), a Y2H tester strain was transformed with pGBD-C1 and pGAD-C1 derivatives coding for the proteins whose interaction should be assessed fused to the Gal4 transcription factor DNA-binding (BD) and the transcriptional activation domain (AD), respectively. Successful protein-protein interaction results in the reconstitution of the Gal4 transcription activator, which then drives the expression of reporter genes under the control of Gal4 (i.e. HIS3, ADE2, leading to growth on the respective selective media). Several colonies of freshly transformed cells were transferred to 1 ml of sterile water. After dilution to OD₆₀₀ = 2, 5 μ l were spotted on the respective selection plates, using a custom-made stamping device where applicable.

High throughput yeast two hybrid screening

For the here mentioned Y2H screens, a spatially ordered array of yeast strains, each expressing one of the ~6000 different yeast ORFs as a Gal4-AD fusion (Cagney *et al.*, 2000; Gera *et al.*, 2002) was used. In this prey array, every protein in the yeast genome is represented only once and always in the form of a full-length construct. A mating strategy is used to introduce the bait protein into the prey array. To this end the bait plasmid was transformed into PJ69-4 α and mated to the Y2H array. This and all subsequent plating steps were performed by a Biomek FX[®] (Beckman Coulter, Brea, USA) automated workstation equipped with robotic 384-pin replicating tools. Diploids expressing both bait and prey constructs were selected by growth on SC -Leu-Trp plates and two hybrid positives were scored by their growth on either SC-Leu-Trp -His or SC-Leu-Trp -Ade plates.

Phenotypic analysis of *S. cerevisiae* mutants, growth & survival assays

Nonessential gene knockout strains and mutants were tested for growth impairments and DNA damage sensitivity by spotting equal amounts of cells, often in serial dilution, onto solid media incubated at 30°C or 37°C or containing DNA damage inducing drugs such as MMS (Sigma) or zeocin (Invitrogen).

For essential genes such as Mps3 or Eco1, 5-fluoroorotic acid (5'FOA) shuffling was used to assess viability of mutants and possibly, their phenotypes. To this end, mutant constructs were integrated into the genome of shuffle strains, which are deleted for the essential gene but surviving due to the presence of a wild type copy on a *URA3*-marked plasmid. Spotting on 5'FOA-containing plates leads to counterselection of the *URA3*-marked WT plasmid, which is 'shuffled out', thereby revealing the (potentially lethal) phenotype of the previously integrated mutants.

For all growth and survival analysis, overnight cultures were harvested and resuspended in 1ml sterile water. After dilution to OD₆₀₀ = 1, six five-fold serial dilutions were prepared and spotted onto the respective plates. Rescue of the *eco1* PIP-box mutants by *htz1 K126R* overexpression was however only seen when overnight cultures in SC-Ura, -Trp were diluted to OD₆₀₀ = 0.1 and grown in YPD until mid-log phase before spotting. For this, 20 OD of cells were harvested, taken up in 1 ml of sterile water and spotted as 1:5 serial dilution on 5' FOA-containing SC-Trp plates.

5.2 Molecular biological techniques

General molecular biology and cloning techniques such as DNA amplification by PCR, restriction digest, ligation or analysis of DNA by agarose gel electrophoresis were performed according to standard (Sambrook *et al.*, 1989) or manufacturer's (New England Biolabs, Ipswich, USA) protocols. Plasmid DNA was propagated in and purified from *E. coli* using the Accuprep[™] plasmid extraction kit (Bioneer Corp., South Korea). To purify DNA-fragments from agarose gels and for PCR-product cleanup, Accuprep[™] gel purification kit (Bioneer Corp., South Korea) and QIAquick PCR purification kits (Qiagen, Hilden, Germany) were used, respectively.

Purification of yeast genomic DNA

Highly pure genomic DNA for Southern blots, PCR applications or DSB-sequencing was isolated by a modified phenol/chloroform extraction protocol (Hoffman and Winston, 1987). 30 OD worth of cells were harvested by centrifugation and transferred to a screw-cap 1 ml tube. Subsequently the pellet was resuspended in 200 μ l TENTS buffer (2% Triton X-100, 1% SDS, 100mM NaCl, 10mM Tris-HCl pH

8.0, 1mM EDTA) and 200 μ l glassbeads (SIGMA, cat. #G8772) as well as 200 μ l phenol:chloroform:isoamylalcohol (25:25:1) were added. After vigorous cell disruption for 5 min in a bead-beater (MM301 from Retsch GmbH, Haan, Germany), 200 μ l TE were added, vortexed briefly, and the suspension was centrifuged for 5min at 14000rpm. The supernatant was carefully recovered and ethanol-precipitated. The pellet was not dried but dissolved in 300 μ l TE and RNA was digested by the addition of 10 μ g RNase (this was made DNase-free by heating RNase stock solution 10min at 99°C).

Determining DNA concentration

Nucleic acid concentration was determined by measuring the absorption at 260nm in an ND1000 spectrophotometer (Nanodrop Technologies), with an OD₂₆₀ unit of 1 corresponding to 50 μ g/ml dsDNA. Purity was assessed by calculating OD₂₆₀/ OD₂₈₀. A ratio below 1.8 indicated residual contamination with phenol, whereas OD₂₆₀/ OD₂₈₀ > 2 indicates RNA contaminants.

Molecular cloning

PCR-primers used for cloning were generally designed to be 20nt complementary to the amplified DNA and containing attached restriction endonuclease cut sites. A typical PCR protocol, using Phusion high-fidelity DNA-polymerase (New England Biolabs, Ipswich, USA) is as follows:

PCR mix		Thermocycler program	
	ul	98°C	30s
10x HF buffer	20	then 30 cycles	
DF5 genomic DNA	2	98°C	10s
Primer 1 (10 μ M)	5	55°C	30s
Primer 2 (10 μ M)	5	72°C	25s/kb
dNTPs (10mM each)	2	72°C	10min
Phusion polymerase	1	4°C	∞
H2O	65		

PCR products were digested with restriction enzymes according to the manufacturer's (New England Biolabs, Ipswich, USA) protocols. Cleaved vector DNA was additionally treated with calf intestinal alkaline phosphatase to prevent self-ligation. Six-fold molar excess of insert DNA was ligated into the corresponding vector by incubation with T4-DNA ligase for 4h at 16°C following the manufacturer's (New England Biolabs, Ipswich, USA) instructions. Before electroporation, the ligation reaction had to be dialyzed against H₂O for 20min to remove excess salt.

DNA sequencing

The MPIB core facility performed all sequencing reactions on an ABI 3730 DNA analyzer (Applied Biosystems Inc., Foster City, USA) using ABI Big Dye 3.1 sequencing chemistry with 300ng plasmid DNA and 5 pmoles primer in a 10 μ l reaction.

Site-directed mutagenesis

Point mutations were introduced into plasmids by following the quick change site-directed mutagenesis approach (Kunkel, 1985). Two complementary primers were designed containing the mutated codon(s) with 15nt wildtype flanking-sequence on each side. For amino acid deletion, primers contained 15nt to the left and to the right of the deleted sequence. A typical quick change PCR protocol for template

plasmids between 3.5 and 7kb, using Pfu turbo DNA-polymerase (Agilent Technologies, Santa Clara, USA) is as follows:

PCR mix		Thermocycler program	
	ul	94°C	3min
10x <i>pfu</i> buffer	2.5	then 19 cycles	
Template plasmid	0.5	94°C	30s
Primer1 (10µM)	0.5	49°C	45s
Primer2 (10µM)	0.5	68°C	16min
dNTPs (10mM each)	0.6	68°C	16min
<i>pfu</i> turbo polymerase	0.5	4°C	∞
H2O	19.9		

Incorporation of the desired mutation and absence of unwanted second-site mutations was confirmed by sequencing of individual clones.

5.3 Biochemistry techniques

5.3.1 Protein methods

General buffers and solutions

IP lysis buffer	50mM Tris base 0.1M NaCl 2mM MgCl ₂ 10% Glycerin 0.1% Triton X-100 adjust pH to 7.5
HU sample buffer	8M Urea 5% SDS 1mM EDTA 1.5% DTT 1% Bromphenolblue 0.2M Tris-HCl pH 6.8
MOPS buffer	50mM MOPS 50mM Tris base 3.5mM SDS 1mM EDTA
Coomassie solution	0.1% Coomassie Brilliant Blue R-250 20% methanol 10% acetic acid
Destaining solution	20% methanol 10% acetic acid
Transfer buffer	0.25M Tris base 1.92M glycine 0.1% SDS 20% methanol

gels; for detection of histones, NuPAGE 12% Bis-Tris gels were used (both from Invitrogen, Carlsbad, USA). Protein samples were prepared in HU buffer, denatured by heating to 65°C for 10min and run at constant voltage of 140V in MOPS buffer. Protein size was determined by comparing to the standard size marker 'Precision Plus Protein All Blue Standard' (Bio-Rad Laboratories GmbH, Hercules, USA).

Coomassie staining

Gels were stained with Coomassie solution for 30min. Background was destained by several washes in 20% methanol, 10% acetic acid.

Western blot analysis

For western blot analysis, proteins separated by PAGE were transferred to polyvinylidene fluoride (PVDF) membranes (Millipore, Billerica, USA) using an electrical tank blotter. This wet blotting was done in transfer buffer at a constant voltage of 75V at 4°C for 60min. Subsequently, membranes were blocked for 20min in TBS-T + 5% milk and incubated over night with primary antibody in TBS-T + 5% milk at 4°C. After 4 washes with TBS-T (5min each), blots were incubated with horse radish peroxidase (HRP)-coupled secondary antibody (Dianova, Hamburg, Germany) for 1h in TBS-T + 5% milk at room temperature. After 4 further washes with TBS-T (5min each) signals were obtained by chemiluminescence reactions using ECL, ECL-Plus or ECL advanced kits (Amersham/GE Healthcare, Little Chalfont, UK) and following the manufacturer's instructions. Signal detection was performed using a LAS-3000 imaging system (Fujifilm Europe GmbH, Düsseldorf, Germany) equipped with a CCD camera.

Primary antibodies used in this study are listed in the following:

Name (cat. no.)	Type	Dilution	Source
anti-HA (sc7392)	mouse monoclonal	1:2000	Santa Cruz Biotechnology Inc.
anti-myc (sc789)	rabbit polyclonal	1:2000	Santa Cruz Biotechnology Inc.
anti-myc (9E10)	mouse monoclonal	1:2000	Sigma-Aldrich
anti-Pgk1 (a6457)	mouse monoclonal	1:15000	Invitrogen - Molecular Probes
anti-Rad53 (yC-19)	goat polyclonal	1:2000	Santa Cruz Biotechnology Inc.
anti-Gal4 BD (sc510)	mouse monoclonal	1:500	Santa Cruz Biotechnology Inc.
anti-Gal4 AD (sc1663)	mouse monoclonal	1:500	Santa Cruz Biotechnology Inc.
anti-H2A (39235)	rabbit polyclonal	1:5000	Active Motif
anti-Smt3	Rabbit polyclonal	1:7500	(Sacher et al., 2006)
anti-Htz1	Rabbit polyclonal	1:500	<i>this study</i>

Secondary antibodies were as follows:

Name	Type	Dilution	Source
goat anti-mouse	HRP-coupled	1:5000	Dianova
goat anti-rabbit	HRP-coupled	1:5000	Dianova
donkey anti-goat	HRP-coupled	1:5000	Dianova

Purification of GST-tagged proteins

Generally, to avoid protein degradation and unfolding, samples were handled as close to 4°C as possible at all times. Cell pellets from 1L of bacterial culture were resuspended in 50ml ice-cold GST lysis buffer complemented with 1mg/ml Pefabloc SC and EDTA-free complete cocktail (Roche), followed by digestion with 1mg/ml lysozyme for 30min at 4°C, rotating. Cell lysis was completed by passage through

an EmulsiFlex C5 cell disruptor (Avestin, Ottawa, Canada). Lysates were cleared by incubation with 1% Triton X-100 for 30min at 4°C, rotating and subsequent pelleting of insoluble material (23000g, 20min, 4°C). The native supernatant was incubated with glutathione sepharose (Amersham/GE Healthcare, Little Chalfont, UK) for 3h at 4°C. The resin was loaded onto a column and washed with 20 column volumes GST wash buffer (WB) A, 30 column volumes GST WB-B and 10 column volumes PBS. Protein was subsequently eluted stepwise with GST elution buffers A and B. Peak fractions were pooled, dialyzed against PBS, 10% glycerol, 1mM DTT and frozen in liquid N₂.

Buffers used in purifications of GST-tagged proteins

Buffer	Composition
PBS	137mM NaCl, 2.7mM KCl, 4.3mM Na ₂ HPO ₄ , 1.47mM KH ₂ PO ₄
GST lysis buffer	PBS, 10% glycerol, 1mM EDTA
GST wash buffer A	PBS, 10% glycerol, 1% Triton X-100, 350mM NaCl
GST wash buffer B	PBS, 10% glycerol, 1% Triton X-100
GST elution buffer A	50mM Tris, 10% glycerol, 0.1% Triton X-100, 10mM glutathione
GST elution buffer B	50mM Tris, 10% glycerol, 0.1% Triton X-100, 30mM glutathione

Purification of ⁶HisHtz1 from inclusion bodies

Htz1 purification was done essentially as described for H2A (Luger et al., 1999). Briefly, 6L of *E. coli* culture were harvested by centrifugation, taken up in 150ml HP-W buffer and lysed by passaging through a cell disruptor for 15min at room temperature. Inclusion bodies were subsequently pelleted (5000g, 30min) and washed twice with HP-W and twice with HP-TW buffer. Inclusion bodies were transferred to a 50ml tube and incubated with 1ml DMSO for 30min, followed by resuspension in 40ml HP-Unfolding buffer. Complete denaturation was allowed by a 1h incubation with head-over-tail rotation at room temperature. Undissolved material was removed by high speed centrifugation (23000g, 10min at room temperature) and the supernatant was applied to a Superdex S200 26/60 gel filtration column (GE Healthcare, Little Chalfont, UK), pre-equilibrated with SAU-1000 buffer. Peak fractions were analyzed by 12% SDS-PAGE, pooled and dialyzed against Ni-NTA buffer B. After loading onto a Ni-NTA agarose (Qiagen, Hilden, Germany) column, the resin was washed with 4 column volumes of Ni-NTA buffer B and 8 column volumes of Ni-NTA wash buffer (WB) C. Highly pure ⁶HisHtz1 protein was subsequently eluted stepwise with Ni-NTA elution buffers D and E. Pooled eluates were dialyzed against 2mM β-mercaptoethanol (ME) and lyophilized (yield: 500mg protein). Before employing ⁶HisHtz1 in binding assays, it was renatured by dialysis in HP refolding buffer.

Buffers used in purification of ⁶HisHtz1

Buffer	Composition
HP-W	50mM Tris pH 7.5, 100mM NaCl, 1mM EDTA, 1mM benzamidine
HP-TW	1% Triton X-100
HP-Unfolding	7M guanidinium HCl, 20mM Tris pH 7.5, 10mM DTT
SAU-1000	7M urea, 1M NaCl, 20mM Na-Acetate, 1mM EDTA, 5mM βME
Ni-NTA buffer B	0.1M NaH ₂ PO ₄ , 10mM Tris, 8M urea, 10mM imidazole, 5mM βME, pH 8.0
Ni-NTA WB-C	0.1M NaH ₂ PO ₄ , 10mM Tris, 8M urea, 10mM imidazole, 5mM βME, pH 6.3
Ni-NTA ElutB-D	0.1M NaH ₂ PO ₄ , 10mM Tris, 8M urea, 0.1M imidazole, 5mM βME, pH 5.9
Ni-NTA ElutB-E	0.1M NaH ₂ PO ₄ , 10mM Tris, 8M urea, 0.1M imidazole, 5mM βME, pH 4.5
HP refolding	2M NaCl, 10mM Tris pH 7.5, 1mM EDTA, 5mM βME

Determining protein concentration

If proteins were pure and contained tryptophane or tyrosine residues, concentration was quantified by measuring the absorption at 280nm in an ND1000 spectrophotometer (Nanodrop Technologies). Alternatively, colorimetric analysis following the Bradford method was performed (Bio-Rad Laboratories GmbH, Hercules, USA), which however required a standard curve with a BSA dilution series of known concentration.

In vitro GST-pulldown (GST-Pd)

20 μ l glutathione sepharose (Amersham/GE Healthcare, Little Chalfont, UK) was incubated with 20 μ g GST-tagged protein for 1h at 4°C in GST-Pd buffer (PBS, 10% glycerol, 1mM EDTA, 5mM MgCl₂, 0.1% Triton X-100) freshly complemented with 1mg/ml Pefabloc SC and EDTA-free complete cocktail (Roche). After two washes with GST-Pd buffer (150g, 2min, 4°C), 60 μ g of bait protein was added and the reaction was incubated in a total volume of 600 μ l for 2h at 4°C. After stringent washing (five times 700 μ l GST-Pd buffer, once with PBS) bound protein complexes were eluted by incubation for 10min at 65°C in 30 μ l HU sample buffer and detected by SDS-PAGE and subsequent coomassie staining. Identity of the ⁶HisHtz1 band in the Eco1 GST-Pd sample was confirmed by mass spectrometry (C. Boulegue, MPIB core facility).

Affinity purification of anti-Htz1 serum

Anti-Htz1 polyclonal antibody was affinity-purified from serum obtained from rabbits immunized with heat-denatured, recombinant ⁶HisHtz1 protein (MPIB animal facility immunization trial on rabbit #1734, using TiterMax Gold, Sigma). For affinity chromatography, purified ⁶HisHtz1 was covalently coupled to CNBr-activated Sepharose 4B (Amersham/GE Healthcare, Little Chalfont, UK) according to the manufacturer's instruction. After blood was received from the animal facility, it was allowed to clot for 1h at 37°C, followed by over night incubation at 4°C and clearing of the serum by high-speed centrifugation. Serum was incubated with 2ml Htz1-affinity matrix over night at 4°C, rotating, and resin-bound antibodies were washed stringently with PBS + 0.5M NaCl. Fractionated acid elution (0.2M acetic acid pH 2.7, 0.5M NaCl) was followed by immediate neutralization with 1M Tris pH 8. Peak fractions, identified by spotting onto nitrocellulose membranes and staining with Ponceau, were pooled, concentrated and dialyzed against PBS. Purified antibody was stored as 40% glycerol solution in aliquots at -20°C.

5.3.2 Chromatin methods

DSB-induction at *MAT* by *HO* endonuclease

All strains isogenic to JKM179, JKM139 or JKM161 (Lee et al., 1998; Sugawara et al., 2003) contain the *HO* gene under the control of a *GAL* promoter. For efficient galactose induction and to avoid glucose repression, cultures were pre-grown in YP-lactate, and when log-phase growth was reached, *HO* expression was induced by the addition of galactose to a final concentration of 2%. DSB-induction at *MAT* could be monitored by real time (RT)-PCR with primers flanking the DSB site (s. below).

Chromatin immunoprecipitation (ChIP)

Time-course experiments and ChIP assays were essentially done as described (Aparicio et al., 2005; Sugawara et al., 2003). For each timepoint, 202ml culture were aliquoted into 1L shake flasks, which had been pre-equilibrated to 30°C. At the exact timepoints post DSB induction, the OD₆₀₀ was measured, a 1OD input sample harvested and the remaining 200ml culture aliquot was fixed by the addition of 5.5ml 37% formaldehyde solution and incubation for exactly 16min, shaking at 23°C. The crosslinking reaction was terminated and quenched by the addition of 30ml 2.5M glycine solution. After a minimum of 20min quenching (shaking at 23°C), a volume worth 160OD of cells was pelleted by centrifugation (5500g, 5min), washed once in PBS and transferred to a 2ml Eppendorf tube. Cell pellets were frozen in liquid N₂ until further use.

For chromatin preparation, 20µl Pefabloc SC (Roche, 100mg/ml) were added directly to the cell pellet. After addition of 800µl FA lysis buffer freshly complemented with 1mg/ml Pefabloc SC and EDTA-free complete cocktail (Roche), zirconia/silica beads (BioSpec Inc., Bartlesville, USA) were added so that only 2mm liquid supernatant remained. Crosslinked cells were lysed on a multitube bead-beater (MM301 from Retsch GmbH, Haan, Germany) for 6 times 3min (frequency = 30/s) with 1min cooling intervals on ice in between. Extracts were transferred (piggyback method) to a 15ml Falcon tube, containing 20µl Pefabloc SC (Roche, 100mg/ml). Chromatin was separated from the soluble fraction by centrifugation in a fresh 2ml tube (20000g, 15min, 4°C). The chromatin pellet was transferred with 2ml ice-cold FA lysis buffer to hard plastic Sumilon 15ml centrifuge tubes (Sumitomo Bakelite Co., Japan) and sheared to an average length of 300-500bp by water bath sonification in a Bioruptor UCD-200 instrument (Diagenode sa, Liège, Belgium) using 30 times 30s cycles with 30s breaks in between at an output of 200W and cooling the water bath compartment by the repeated addition of ice. The solubilized chromatin was purified from cell debris and unbroken cells by centrifugation (20000g, >30min, 4°C). 20µl input sample was taken and 800µl of chromatin solution were incubated with either 50µl anti-HA affinity matrix (Roche Diagnostics GmbH, Mannheim, Germany), 50µl anti-c-MYC agarose conjugate (Sigma-Aldrich, St. Louis, USA) or, in the case of γH2A.X ChIPs, with 50µl pre-swollen Protein A Sepharose CL-4B slurry (Amersham/GE Healthcare, Little Chalfont, UK) and 8µl anti-phospho-H2A^{Ser129} (Upstate/Millipore, no. 07-745) antibody. Precipitations were performed for 2h at 23°C with head-over-tail rotation. Subsequently, the resin was transferred to an Ultrafree-MC centrifugal filter device (Durapore PVDF 5µM, Millipore, Billerica, USA) and washed twice with 380µl FA lysis buffer, once with 380µl FA lysis buffer containing 0.5M NaCl, once with 380µl ChIP wash buffer followed by a final wash with 380µl TE. Beads were dried and transferred with 120µl ChIP elution buffer and using a large orifice tip (Fisher Scientific, Cat no. 02-707-134) to a new tube. Elution of bound precipitated protein-DNA complexes was performed by incubation at 65°C for 15min, shaking at 1000rpm. ChIP sample eluates were recovered by high speed centrifugation through a fresh Ultrafree-MC centrifugal filter device. Input and ChIP samples were subjected to Proteinase K digest (2h at 42°C) and incubation at 65°C for 6h to revert formaldehyde crosslinks. The thus obtained Input and ChIP DNA samples were purified using the QIAquick PCR purification kit (Qiagen, Hilden, Germany), but substituting the kit-provided yellow-colored PBI buffer (which would interfere with subsequent RT-PCR analysis) with the uncolored PB-buffer (Cat. No. 19066, Qiagen, Hilden, Germany). Samples were eluted in 60µl TE and to improve PCR-efficiency, at least two freeze-thaw cycles were performed.

Buffers used in ChIP assays:

Buffer	Composition
FA lysis buffer	50mM Hepes pH 7.5, 150mM NaCl, 1mM EDTA, 1% Triton X-100, 0.1% sodium deoxycholate, 0.1% SDS
ChIP wash buffer	10mM Tris pH 8.0, 250mM LiCl, 1mM EDTA, 0.5% Nonidet P-40, 0.5% sodium deoxycholate,
ChIP elution buffer	50mM Tris pH 7.5, 10mM EDTA, 1%SDS
TE	10mM Tris pH 8.0, 1mM EDTA
Quenching solution	2.5M glycine, sterilize by autoclaving
Galactose 10x stock	20% galactose, sterilize by filtration

Real time PCR quantification

Quantitative, real time (RT)-PCR was performed on a LightCycler 480 System, using the LightCycler 480 SYBR Green I Master hot-start reaction mix (Roche Diagnostics GmbH, Mannheim, Germany). 18µl mastermix containing primers, SYBR Green I Master and H₂O was aliquoted into 384-well LightCycler plates and either 2µl ChIP sample (undiluted) or 2µl input sample (in a 1:10 dilution) was added. Reactions were done in triplicates and pipetting was performed by a CAS-1200 PCR setup robot (Corbett Lifescience/ Qiagen, Hilden, Germany).

Details of the RT-PCR protocol are given in the following.

RT-PCR reaction	ul	Lightcycler program	
		95°C	10min
		then 45 cycles	
SYBR Green I Master Mix	10	95°C	10s
Primer 1 (10µM)	1.2	55°C	10s
Primer 2 (10µM)	1.2	72°C	16s
H2O	5.6	Melting curve analysis	
Sample	2	4°C	∞

Primers used for RT-PCR and ChIP analysis:

Primer name	Sequence	Amplified product
CterYJL112WinNH	GCGTGCCTGGTCACAGGTTTCATACGAC	control locus (Chr. X)
CterYJL112WreNH	TCATACGGCCCAAATATTTACGTCCC	control locus (Chr. X)
HO -100check	GAGCATATTACTCACAGTTTGGCTC	intact <i>MAT</i>
HO +190re	GGATAGCTATACTGACAACATTCAG	intact <i>MAT</i>
HO +0,2 kb in MK	CCTGGTTTTGGTTTTGTAGAGTGG	0.2kb distal of DSB
HO +0,2 kb re MK	GAGCAAGACGATGGGGAGTTTC	0.2kb distal of DSB
HO +1,1 kb in	CAATCTTTTCTATTTTTATTTTCATATC	1.1kb distal of DSB
HO +1,1 kb re	AGGGATAAAAAGTGTGTGATGTGC	1.1kb distal of DSB
HO +3,1 kb in	TAACCAGCAATACCAAGACAGCAC	3.1kb distal of DSB
HO +3,1 kb re	TTTTACCTACCGCACCTTCTAAGC	3.1kb distal of DSB
HO +5,7 kb in	ACCAGCAGTAATAAGTCGTCCTGA	5.7kb distal of DSB
HO +5,7 kb re	CCAAGGAACTAATGATCTAAGCACA	5.7kb distal of DSB
HO +9,5 kb in	GCGGAAAACAATGGCACTCT	9.5kb distal of DSB
HO +9,5 kb re	TGGATCATGGACAAGGTCCTAC	9.5kb distal of DSB
pA (<i>MAT</i> distal)	GCAGCACGGAATATGGGACT	switched <i>MAT</i>
pB (Yα)	ATGTGAACCGCATGGGCAGT	switched <i>MAT</i>

Template DNA concentrations were quantified from the second derivative maximum of the LightCycler PCR amplification curves, using for each primer pair an input

sample dilution series as standard (1:10, 1:20, 1:50, 1:100 and 1:1000). Amplification was followed by a melting curve analysis, which served as quality control that primers were specific and only a single PCR product was amplified per reaction. Most important determinant for RT-PCR performance was quality of primers. Therefore these were aliquoted upon receipt and not refrozen after use.

Normalization of ChIP data

For all RT-PCR experiments on ChIP samples, signals at *MAT* were normalized to an unaffected control locus (*YJL112W/MDV1*) using the formula: Fold-enrichment = [IP(test)/input(test)] / [IP(control)/input(control)]. The efficiency of DSB induction was measured by quantitative PCR with primers spanning the break (Fig. 6). All ChIP data were corrected for cleavage efficiency (van Attikum et al., 2007) as especially *htz1* and *swr1* mutants showed slightly reduced HO cleavage. All signals were finally normalized to 1 for the signal before induction to visualize protein factor recruitment after break induction. In Figure 6B, quantitative PCR with primers spanning the HO-site (P_{MAT} : HO-100 check and HO+190 re) was performed on input DNA samples used for Mps3^{9myc} ChIPs shown in Figure 12. Figure 7A shows input DNA used for ChIP analysis 0.2 kb from the DSB on Chr III (Fig. 7C, 12 and Kalocsay et al., 2009).

Monitoring mating type switching by Southern blot

Southern blot analysis was essentially done as described (Holmes and Haber, 1999; White and Haber, 1990). HO endonuclease expression was allowed for 1h (by galactose induction) and then repressed (by addition of 2% glucose) to allow for repair. Highly pure genomic DNA was prepared (s. above) at 0h, 0.5h, 1h, 2h, 3h and 4h post HO induction. 40µg genomic DNA were digested in a 300µl reaction with 200 units of Styl enzyme (New England Biolabs, Ipswich, USA) at 37°C over night following the manufacturer's instructions. 30µl Na-Acetate (3M) and 3µl EDTA (0.5M) were added and the digested DNA was precipitated with 800µl ice-cold ethanol for several hours at -80°C, and taken up in alkaline loading dye (50mM NaOH, 1mM EDTA, 2.5% Ficoll, 0.025% Bromophenolblue). A 20 x 20 cm, 1.4% agarose gel was prepared and soaked for 45min in alkaline running buffer (50mM NaOH, 1mM EDTA). Samples were run in a horizontal submarine electrophoresis unit (Sigma-Aldrich, St. Louis, USA) at 30V for 10h, and the gel was covered with a glass plate as soon as samples had entered the gel. As the DNA is single-stranded, it is not well stainable with intercalators such as ethidium bromide. Therefore this was omitted. For transfer, the gel was incubated 7min in 0.25M HCl to depurinated DNA, washed briefly in H₂O, followed by a 30min neutralization in 500mM NaOH, 1.5M NaCl. DNA was transferred to a 20 x 20 cm Zeta-Probe GT blotting membrane (Bio-Rad Laboratories, Hercules, USA) by capillary action (Southern blot) over night with 10x SSC (1.5M NaCl, 150mM Na-citrate pH 7.0) according to the manufacturer's instruction. Precut (20 x 20 cm) gel blot paper and 3mm chromatography paper (both Whatman Inc., Maidstone, UK) were used.

A radioactively labeled, *MAT*-specific RNA probe was prepared with the Riboprobe in vitro transcription system (Promega Corp., Madison, USA) according to the manufacturer's standard protocol, using [α -³²P]-CTP (Perkin Elmer, NEG508X), T7 polymerase and 1µg PstI-linearized pJH364 (White and Haber, 1990) as template. To limit radioactive background signal during hybridization, unincorporated nucleotides were removed by size exclusion chromatography using preassembled NucAway Spin Columns (Ambion Inc., Austin, USA). The blot was pre-hybridized with Ultrahyb ultrasensitive hybridization buffer (Ambion Inc., Austin, USA) for 30min at 42°C in appropriately sized glass tubes in a rolling-bottle hybridization oven. The labeled RNA-probe was added and hybridization occurred over night at 42°C,

rolling. The blot was washed twice for 5min in 2xSSC, 0.1% SDS at 42°C and 2x15min in 0.1xSSC, 0.1% SDS at 42°C. If background signal was still too high, a final wash in 0.1xSSC, 0.1% SDS at 68°C was performed. Membranes were covered with plastic wrap, placed in a film cassette with an intensifying screen and exposed to an X-ray film for at least 3h at -80°C or over night.

Monitoring mating type switching by RT-PCR

HO-induced homologous recombination, i.e. mating type switching, was also monitored by RT-PCR, using unique primers pA and pB (for sequence and protocol s. above), which prime distal to *MAT* and within *HML-Y α* (Holmes and Haber, 1999; White and Haber, 1990). RT-PCR was performed on genomic DNA samples as also prepared for Southern blot (s. previous paragraph) and the only difference to the ChIP RT-PCR protocol was the annealing temperature, which was 57°C for the pA, pB primer pair. The signal was normalized to an unaffected control locus on chromosome X (YJL112W) and the WT 4h timepoint was set to 100%.

DSB resection assays

Southern blot analysis of 5'-strand resection was performed as described (Zhu et al., 2008), Genomic DNA samples derived from distinct timepoints after HO induction in a donor deficient strain (isogenic to JKM179) were digested with EcoRI, run on an alkaline 0.8% agarose gel, transferred and hybridized with radioactive 3'-strand-specific RNA probes, as described in the above section for monitoring mating type switching. To be able to generate probes for monitoring resection 10kb centromere-proximal of the DSB and an unaffected control locus, an *SNT1* and an *APA1* locus fragment were amplified by PCR and directly ligated into pGEM-T Easy vectors (Promega Corp., Madison, USA) according to the manufacturer's instruction. For SNT1, insert orientation was checked by sequencing to result after in vitro transcription in a probe complementary to the 3', unresected strand. pGEM-T_SNT1 and pGEM-T_ApaI were linearized with Sall before RNA probe preparation by T7 polymerase with the Riboprobe in vitro transcription system (Promega Corp., Madison, USA).

Sequencing of DSB-ends

DSB ends were cloned and sequenced (including the 3' single stranded tail) using a terminal transferase-mediated PCR method, originally developed for sequencing the single-stranded 3'termini of telomeres (Forstemann et al., 2000). Genomic DNA samples derived from distinct timepoints after HO induction in a donor deficient strain (isogenic to JKM179) were prepared. Terminal transferase (New England Biolabs, Ipswich, USA) was used to tail 3' chromosome- (and DSB-) ends with poly-C oligonucleotides. In a second step a PCR using a *MAT*-specific primer (-190nt in), a poly-G primer and the tailing reaction as template yielded 200 bp DSB-end containing products, which were directly ligated into pGEM-T Easy vectors (Promega Corp., Madison, USA) according to the manufacturer's instruction. The blue/white cloning assay (LB-Amp plates + 0.5mM IPTG + 80µg/ml XGal) allowed quick screening and identification of positive clones, which were subjected to sequencing with a T7 promoter-specific primer.

Chromatin binding assay

The chromatin binding assay used here was adapted from previously published protocols with minor modifications (Liang and Stillman, 1997; Wang et al., 2009). 250D of cells were harvested, resuspended and incubated in 3ml pre-spheroplast buffer for 10min at room temperature. Cells were pelleted by centrifugation (1000g, 5min), resuspended in 2ml spheroplast buffer and cell wall was digested by addition

of 10 μ l zymolyase stock, and incubation at 37°C, shaking for 30-45 min. Spheroplasting was monitored photometrically by measuring 10 μ l reaction aliquots in 1% SDS solution. The OD₆₀₀ should drop by 80% upon efficient spheroplasting. Spheroplasts were pelleted (300g, 1min at 4°C), carefully washed in 1ml wash buffer (cut tip), pelleted again and resuspended in an equal pellet volume of extraction buffer (usually ca. 80 μ l). Lysis was performed by addition of Triton X-100 to 1% final concentration and incubation on ice, with occasional vortexing. A 20 μ l aliquot was dispatched as whole cell extract (WCE) sample. 100 μ l of remaining WCE were carefully applied on top of 50 μ l sucrose cushion and centrifuged for 10min at 20000g and 4°C. 20 μ l supernatant (SUP) were carefully taken from the top, the rest aspirated and the pellet containing the yeast chromatin fraction (CHR) was resuspended in 100 μ l HU buffer. 80 μ l HU buffer was added to the SUP and WCE samples and all were denatured (65°C, 10min, 14000rpm), centrifuged and subjected to SDS-PAGE and western blot analysis.

Buffers used in chromatin binding assays:

Buffer	Composition
Pre-spheroplast buffer	100mM Pipes/KOH pH9.4, 10mM DTT*, 0.1% NaN ₃ *
Spheroplast buffer (SB)	50mM, K ₂ HPO ₄ /KH ₂ PO ₄ pH 7.5, 0.6M Sorbitol, 10mM DTT*
Zymolase stock	20mg/ml Zymolase 100T* (Seikagaku Corp., Japan) in SB
Wash buffer	50mM Hepes/KOG pH 7.5, 100mM KCl, 2.5mM MgCl ₂ , 0.4M Sorbitol
Extraction buffer	Wash buffer supplemented with 1mM DTT*, 1mg/ml Pefabloc SC* and EDTA-free complete cocktail* (Roche)
Sucrose cushion	Extraction buffer, 0.25% Triton X-100, 30% sucrose

* were added freshly only immediately before use.

Preparation of mononucleosomes

To obtain pure yeast mononucleosomes, a chromatin fractionation as described in the previous paragraph, however in large scale, was modified and combined with MNase digest to release mononucleosomes (Lantermann et al., 2009). The above-described chromatin assay was scaled up 12-fold and the extraction buffer was supplemented with 1M NaCl to get rid of chromatin binding proteins. Thus-obtained, high-salt extract was placed in 1ml portions on top of 500 μ l sucrose cushions and centrifuged for 1h at 20000g and 4°C or until firm chromatin pellets was visible. These were thoroughly resuspended in MNase buffer (10mM Tris pH7.4, 10mM KCl, 0.34M Sucrose, 1mM CaCl₂, 0.1% Triton X.100, 10% glycerol, 1mM DTT), supplemented with 1mg/ml Pefabloc SC and EDTA-free complete cocktail (Roche), samples were pooled and digested with 250U MNase/ml for 10min at 37°C, shaking. Reactions were stopped by addition of 2mM EGTA and placed on ice. Solubilized nucleosomes were cleared by centrifugation (20000g, 15min, 4°C) supplemented with fresh Pefabloc, 155mM KCl and 50mM Tris. Quality of mononucleosome preparation was assessed by chloroform/phenol-precipitating a 200 μ l aliquot before and after MNase digest and analyzing DNA length on ethidium bromide-stained 2% agarose gels. The thus obtained mononucleosomes were employed in pulldowns with 40 μ g of GST-tagged Eco1 over night at 4°C. Bound complexes were washed 4 times in wash buffer (50mM Tris, 155mM KCl, 2mM EDTA, 0.5% Triton X-100, 19% glycerol, 1mM DTT 1mg/ml Pefabloc SC and EDTA-free complete cocktail (Roche)), eluted by denaturation in HU-buffer for 10min at 65°C and analyzed by SDS-PAGE and western blot.

5.4 Cell biological techniques

Fluorescence-activated cell sorting (FACS)

FACS analysis was done essentially as described (Pellicoli et al., 2001). A 1ml culture aliquot at the timepoints of interest was harvested by centrifugation, washed in PBS and fixed in 5ml 70% ethanol for 1h on ice. Cells were pelleted, washed in PBS and sonicated briefly (20s in 1ml PBS). RNA was subsequently digested by 1mg/ml RNase for 1h at 37°C. Cells were pelleted, washed in PBS and DNA was stained by incubation with 50µg/ml propidium iodide for 4h at 4°C. DNA amount per cell was subsequently quantified in a FACSCalibur flow cytometer (BD Bioscience, Franklin Lakes, USA) and employing the respective CellQuest Software analysis (BD Bioscience, Franklin Lakes, USA).

Cell-based adaptation assay

To score adaptation (i.e. escape from the DSB-inflicted G2/M cell cycle arrest) single cells and their ability to form microcolonies upon persisting DSBs were monitored microscopically (Lee et al., 1998). Log-phase, YP-lactate cultures of donor deficient strains (isogenic to JKM179) were spread on galactose-containing plates to induce the DSB by HO endonuclease expression. G1-cells (unbudded) were then micromanipulated using a dissection microscope onto a grid. Arrest morphology, growth and microcolony formation was scored at 8h, 24h and 44h post DSB induction.

5.4.1 Live-cell microscopy

To follow the position of an induced DSB by fluorescence microscopy, yeast cells were grown to exponential phase in synthetic lactate medium. Cells were mounted onto Concanavalin A-coated glass bottom dishes (MatTek) and DSBs were induced by adding 2% galactose in SC-lactate. An ANDOR/TiLL iMIC CSU22 spinning disk confocal microscope with a 100x 1.45NA objective lens (Olympus) was used to capture image stacks of 250 nm step-size. For scoring nuclear envelope association, the z-slice with the brightest and most focused GFP-decorated *Lac*-operator array was picked manually. This selection was done irrespective of the nuclear rim staining. Only slices that also showed a clear nuclear rim staining were further analyzed and scored as follows: GFP-LacI spots either touching or coinciding with the Nic96^{mars} nuclear envelope marker were scored as membrane associated; all others were scored as nucleoplasmic.

5.4.2 Cohesion assays

To monitor S-phase cohesion, the AFS173 cohesion tester strain (Bhalla et al., 2002) was arrested by incubation with 15µg/ml nocodazole for 3h at 30°C, shaking. An array of lac repressor binding sites on chromosome IV, made visible by expression of a nuclear-targeted ^{GFP}LacI fusion protein, indicates intact or faulty sister chromatid cohesion (1 versus 2 GFP foci). For this assay, live-cell microscopy was performed.

Quantification of cohesion specifically induced by DSBs was performed exactly as described (Unal et al., 2007) and using the EU3275 strain or derivatives thereof. Briefly, and as schematically depicted in Fig. 33B, a 50ml culture was grown in YP-lactate, 3% glycerol and 0.01mg/ml adenine to OD₆₀₀=0.3 and nocodazole (15µg/ml) was added for 3h at 30°C. The culture was split in two and one was supplemented

with 2% galactose (to induce HO and temperature-resistant, WT cohesion), the other with the respective amount of H₂O. After 1h 13min at 30°C shaking, the cultures were again split in two and one half was shifted to 37°C to inactivate S-phase cohesion. After another 1h 13min incubation on shaking platforms, cells were fixed for microscopy. 1ml culture was pelleted by centrifugation, resuspended in 100µl fixative (4% paraformaldehyde, 3.4% sucrose) and incubated for 17 min at room temperature with occasional vortexing. Cells were washed once in KPS buffer (100mM K₂HPO₄/KH₂PO₄ pH 7.5, 1.2M sorbitol), centrifuged and taken up in 30µl KPS buffer. Thus-prepared fixed cells were stable at 4°C for up to 4 weeks. For microscopy, 3µl of cell suspension was mounted on a coverslip.

Cells were imaged on the spinning disc confocal microscope Marianas SDC (Intelligent Imaging Innovations, Denver, USA), equipped with 488nm and 560nm excitation wavelength lasers and using a 63xoil objective, with a numerical aperture of 1.4 (Carl Zeiss AG, Oberkochen, Germany). Projection images were created using the Slidebook software provided by the manufacturer. For each experimental condition at least 200 cells were scored for GFP spots and mean ± SEM was calculated for three independent experiments.

5.5 Computer-aided analysis

Images obtained by microscopy were processed using ImageJ software (<http://rsbweb.nih.gov/ij/>) and the MBF ImageJ for Microscopy collection of plug-ins (www.macbiophotonics.ca/imagej/).

For sequence search as well as literature review, electronic databases provided by the Saccharomyces Genome Database (www.yeastgenome.org/) and the National Center for Biotechnology Information (www.ncbi.nlm.nih.gov/) were used. Sequence analyses (DNA restriction enzyme maps, DNA sequencing analyses, DNA primer design, protein sequence comparison) were performed using DNA-Star Software (DNA Star Inc.). Contrast of western blot exposures was linearly adjusted using Adobe Photoshop (Adobe Systems Inc.). For the presentation of texts, tables and graphs, the Microsoft Office software package (Microsoft Corp.) was used. Plotting of the here presented Rfa^{6HA} CHIP data into a 3D graph was kindly performed by M. Kalocsay using the Matlab program (www.mathworks.com/products/matlab/).

Figures were labeled and illustrations were created using Adobe Illustrator software (Adobe Systems Inc.).

ClustalW2 (www.ebi.ac.uk/clustalw/) was used to assemble multiple sequence alignments and comparative structural homology modeling of the Eco1 zinc finger was performed with MODELLER (Eswar et al., 2008) using the LMU bioinformatic toolkit available online at <http://toolkit.lmb.uni-muenchen.de/> (Biegert et al., 2006). Protein 3D-coordinates obtained by X-ray crystallography were downloaded from the protein databank (www.pdb.org) and structures were visualized using PyMol calculation (www.pymol.org).

6 REFERENCES

Adam, M., Robert, F., Larochelle, M., and Gaudreau, L. (2001). H2A.Z is required for global chromatin integrity and for recruitment of RNA polymerase II under specific conditions. *Mol Cell Biol* 21, 6270-6279.

Agarwal, R., Tang, Z., Yu, H., and Cohen-Fix, O. (2003). Two distinct pathways for inhibiting pds1 ubiquitination in response to DNA damage. *J Biol Chem* 278, 45027-45033.

Akhtar, A., and Gasser, S.M. (2007). The nuclear envelope and transcriptional control. *Nat Rev Genet* 8, 507-517.

Allis, C.D., Jenuwein, T., and Reinberg, D. (2006). *Epigenetics* (Cold Spring Harbor, N.Y., Cold Spring Harbor Laboratory Press).

Antoniacci, L.M., Kenna, M.A., Uetz, P., Fields, S., and Skibbens, R.V. (2004). The spindle pole body assembly component mps3p/nep98p functions in sister chromatid cohesion. *J Biol Chem* 279, 49542-49550.

Aparicio, O., Geisberg, J.V., Sekinger, E., Yang, A., Moqtaderi, Z., and Struhl, K. (2005). Chromatin immunoprecipitation for determining the association of proteins with specific genomic sequences in vivo. *Curr Protoc Mol Biol*, Unit 21 23.

Ausubel, F.M. (1987). *Current protocols in molecular biology* (New York, Published by Greene Pub. Associates and Wiley- Interscience : J. Wiley).

Barlow, J.H., Lisby, M., and Rothstein, R. (2008). Differential regulation of the cellular response to DNA double-strand breaks in G1. *Mol Cell* 30, 73-85.

Becker, P.B., and Horz, W. (2002). ATP-dependent nucleosome remodeling. *Annu Rev Biochem* 71, 247-273.

Ben-Shahar, T.R., Heeger, S., Lehane, C., East, P., Flynn, H., Skehel, M., and Uhlmann, F. (2008). Eco1-dependent cohesin acetylation during establishment of sister chromatid cohesion. *Science* 321, 563-566.

Berger, S.L. (2007). The complex language of chromatin regulation during transcription. *Nature* 447, 407-412.

Bergink, S., Salomons, F.A., Hoogstraten, D., Groothuis, T.A., de Waard, H., Wu, J., Yuan, L., Citterio, E., Houtsmuller, A.B., Neefjes, J., *et al.* (2006). DNA damage triggers nucleotide excision repair-dependent monoubiquitylation of histone H2A. *Genes Dev* 20, 1343-1352.

Bernstein, C., and Bernstein, H. (1991). *Aging, sex, and DNA repair* (San Diego, Academic Press).

Bhalla, N., Biggins, S., and Murray, A.W. (2002). Mutation of YCS4, a budding yeast condensin subunit, affects mitotic and nonmitotic chromosome behavior. *Mol Biol Cell* 13, 632-645.

References

Biegert, A., Mayer, C., Remmert, M., Soding, J., and Lupas, A.N. (2006). The MPI Bioinformatics Toolkit for protein sequence analysis. *Nucleic Acids Res* *34*, W335-339.

Bird, A.W., Yu, D.Y., Pray-Grant, M.G., Qiu, Q., Harmon, K.E., Megee, P.C., Grant, P.A., Smith, M.M., and Christman, M.F. (2002). Acetylation of histone H4 by Esa1 is required for DNA double-strand break repair. *Nature* *419*, 411-415.

Bonilla, C.Y., Melo, J.A., and Toczyski, D.P. (2008). Colocalization of sensors is sufficient to activate the DNA damage checkpoint in the absence of damage. *Mol Cell* *30*, 267-276.

Botuyan, M.V., Lee, J., Ward, I.M., Kim, J.E., Thompson, J.R., Chen, J., and Mer, G. (2006). Structural basis for the methylation state-specific recognition of histone H4-K20 by 53BP1 and Crb2 in DNA repair. *Cell* *127*, 1361-1373.

Brayer, K.J., and Segal, D.J. (2008). Keep your fingers off my DNA: protein-protein interactions mediated by C2H2 zinc finger domains. *Cell Biochem Biophys* *50*, 111-131.

Brickner, D.G., Cajigas, I., Fondufe-Mittendorf, Y., Ahmed, S., Lee, P.C., Widom, J., and Brickner, J.H. (2007). H2A.Z-mediated localization of genes at the nuclear periphery confers epigenetic memory of previous transcriptional state. *PLoS Biol* *5*, e81.

Brickner, J.H. (2009). Transcriptional memory at the nuclear periphery. *Curr Opin Cell Biol* *21*, 127-133.

Brickner, J.H., and Walter, P. (2004). Gene recruitment of the activated INO1 locus to the nuclear membrane. *PLoS Biol* *2*, e342.

Brunborg, G., and Williamson, D.H. (1978). The relevance of the nuclear division cycle to radiosensitivity in yeast. *Mol Gen Genet* *162*, 277-286.

Bupp, J.M., Martin, A.E., Stensrud, E.S., and Jaspersen, S.L. (2007). Telomere anchoring at the nuclear periphery requires the budding yeast Sad1-UNC-84 domain protein Mps3. *J Cell Biol* *179*, 845-854.

Burma, S., Chen, B.P., Murphy, M., Kurimasa, A., and Chen, D.J. (2001). ATM phosphorylates histone H2AX in response to DNA double-strand breaks. *J Biol Chem* *276*, 42462-42467.

Cagney, G., Uetz, P., and Fields, S. (2000). High-throughput screening for protein-protein interactions using two-hybrid assay. *Methods Enzymol* *328*, 3-14.

Carrozza, M.J., Li, B., Florens, L., Suganuma, T., Swanson, S.K., Lee, K.K., Shia, W.J., Anderson, S., Yates, J., Washburn, M.P., *et al.* (2005). Histone H3 methylation by Set2 directs deacetylation of coding regions by Rpd3S to suppress spurious intragenic transcription. *Cell* *123*, 581-592.

Casolari, J.M., Brown, C.R., Komili, S., West, J., Hieronymus, H., and Silver, P.A. (2004). Genome-wide localization of the nuclear transport machinery couples transcriptional status and nuclear organization. *Cell* *117*, 427-439.

- Celeste, A., Fernandez-Capetillo, O., Kruhlak, M.J., Pilch, D.R., Staudt, D.W., Lee, A., Bonner, R.F., Bonner, W.M., and Nussenzweig, A. (2003). Histone H2AX phosphorylation is dispensable for the initial recognition of DNA breaks. *Nat Cell Biol* 5, 675-679.
- Celeste, A., Petersen, S., Romanienko, P.J., Fernandez-Capetillo, O., Chen, H.T., Sedelnikova, O.A., Reina-San-Martin, B., Coppola, V., Meffre, E., Difilippantonio, M.J., *et al.* (2002). Genomic instability in mice lacking histone H2AX. *Science* 296, 922-927.
- Chadwick, B.P., and Willard, H.F. (2001). A novel chromatin protein, distantly related to histone H2A, is largely excluded from the inactive X chromosome. *J Cell Biol* 152, 375-384.
- Chai, J., Shiozaki, E., Srinivasula, S.M., Wu, Q., Datta, P., Alnemri, E.S., and Shi, Y. (2001). Structural basis of caspase-7 inhibition by XIAP. *Cell* 104, 769-780.
- Chen, C.C., Carson, J.J., Feser, J., Tamburini, B., Zabaronick, S., Linger, J., and Tyler, J.K. (2008). Acetylated lysine 56 on histone H3 drives chromatin assembly after repair and signals for the completion of repair. *Cell* 134, 231-243.
- Chen, M., and Shen, X. (2007). Nuclear actin and actin-related proteins in chromatin dynamics. *Curr Opin Cell Biol* 19, 326-330.
- Choo, J.H., Kim, J.D., Chung, J.H., Stubbs, L., and Kim, J. (2006). Allele-specific deposition of macroH2A1 in imprinting control regions. *Hum Mol Genet* 15, 717-724.
- Clapier, C.R., and Cairns, B.R. (2009). The biology of chromatin remodeling complexes. *Annu Rev Biochem* 78, 273-304.
- Clerici, M., Mantiero, D., Lucchini, G., and Longhese, M.P. (2005). The *Saccharomyces cerevisiae* Sae2 protein promotes resection and bridging of double strand break ends. *J Biol Chem* 280, 38631-38638.
- Cohen-Fix, O., and Koshland, D. (1997). The anaphase inhibitor of *Saccharomyces cerevisiae* Pds1p is a target of the DNA damage checkpoint pathway. *Proc Natl Acad Sci U S A* 94, 14361-14366.
- Conrad, M.N., Lee, C.Y., Wilkerson, J.L., and Dresser, M.E. (2007). MPS3 mediates meiotic bouquet formation in *Saccharomyces cerevisiae*. *Proc Natl Acad Sci U S A* 104, 8863-8868.
- Cortes-Ledesma, F., and Aguilera, A. (2006). Double-strand breaks arising by replication through a nick are repaired by cohesin-dependent sister-chromatid exchange. *EMBO Rep* 7, 919-926.
- Costanzi, C., and Pehrson, J.R. (1998). Histone macroH2A1 is concentrated in the inactive X chromosome of female mammals. *Nature* 393, 599-601.
- Cremer, T., Cremer, M., Dietzel, S., Muller, S., Solovei, I., and Fakan, S. (2006). Chromosome territories--a functional nuclear landscape. *Curr Opin Cell Biol* 18, 307-316.

References

- Davoli, T., Denchi, E.L., and de Lange, T. (2010). Persistent telomere damage induces bypass of mitosis and tetraploidy. *Cell* *141*, 81-93.
- Deniaud, E., and Bickmore, W.A. (2009). Transcription and the nuclear periphery: edge of darkness? *Curr Opin Genet Dev* *19*, 187-191.
- Dewitt, S.K., and Adelberg, E.A. (1962). The Occurrence of a Genetic Transposition in a Strain of Escherichia Coli. *Genetics* *47*, 577-585.
- Dhalluin, C., Carlson, J.E., Zeng, L., He, C., Aggarwal, A.K., and Zhou, M.M. (1999). Structure and ligand of a histone acetyltransferase bromodomain. *Nature* *399*, 491-496.
- Dhillon, N., Oki, M., Szyjka, S.J., Aparicio, O.M., and Kamakaka, R.T. (2006). H2A.Z functions to regulate progression through the cell cycle. *Mol Cell Biol* *26*, 489-501.
- Ding, X., Xu, R., Yu, J., Xu, T., Zhuang, Y., and Han, M. (2007). SUN1 is required for telomere attachment to nuclear envelope and gametogenesis in mice. *Dev Cell* *12*, 863-872.
- Dion, V., Shimada, K., and Gasser, S.M. (2010). Actin-related proteins in the nucleus: life beyond chromatin remodelers. *Curr Opin Cell Biol*.
- Doil, C., Mailand, N., Bekker-Jensen, S., Menard, P., Larsen, D.H., Pepperkok, R., Ellenberg, J., Panier, S., Durocher, D., Bartek, J., *et al.* (2009). RNF168 binds and amplifies ubiquitin conjugates on damaged chromosomes to allow accumulation of repair proteins. *Cell* *136*, 435-446.
- Dore, A.S., Kilkenny, M.L., Rzechorzek, N.J., and Pearl, L.H. (2009). Crystal structure of the rad9-rad1-hus1 DNA damage checkpoint complex--implications for clamp loading and regulation. *Mol Cell* *34*, 735-745.
- Downs, J.A., Allard, S., Jobin-Robitaille, O., Javaheri, A., Auger, A., Bouchard, N., Kron, S.J., Jackson, S.P., and Cote, J. (2004). Binding of chromatin-modifying activities to phosphorylated histone H2A at DNA damage sites. *Mol Cell* *16*, 979-990.
- Eisen, J.A., Sweder, K.S., and Hanawalt, P.C. (1995). Evolution of the SNF2 family of proteins: subfamilies with distinct sequences and functions. *Nucleic Acids Res* *23*, 2715-2723.
- Emili, A. (1998). MEC1-dependent phosphorylation of Rad9p in response to DNA damage. *Mol Cell* *2*, 183-189.
- Eswar, N., Eramian, D., Webb, B., Shen, M.Y., and Sali, A. (2008). Protein structure modeling with MODELLER. *Methods Mol Biol* *426*, 145-159.
- Faast, R., Thonglairoam, V., Schulz, T.C., Beall, J., Wells, J.R., Taylor, H., Matthaei, K., Rathjen, P.D., Tremethick, D.J., and Lyons, I. (2001). Histone variant H2A.Z is required for early mammalian development. *Curr Biol* *11*, 1183-1187.

- Fan, J.Y., Rangasamy, D., Luger, K., and Tremethick, D.J. (2004). H2A.Z alters the nucleosome surface to promote HP1 α -mediated chromatin fiber folding. *Mol Cell* 16, 655-661.
- Feuerbach, F., Galy, V., Trelles-Sticken, E., Fromont-Racine, M., Jacquier, A., Gilson, E., Olivo-Marin, J.C., Scherthan, H., and Nehrbass, U. (2002). Nuclear architecture and spatial positioning help establish transcriptional states of telomeres in yeast. *Nat Cell Biol* 4, 214-221.
- Finley, D., Ozkaynak, E., and Varshavsky, A. (1987). The yeast polyubiquitin gene is essential for resistance to high temperatures, starvation, and other stresses. *Cell* 48, 1035-1046.
- Fishman-Lobell, J., Rudin, N., and Haber, J.E. (1992). Two alternative pathways of double-strand break repair that are kinetically separable and independently modulated. *Mol Cell Biol* 12, 1292-1303.
- Forstemann, K., Hoss, M., and Lingner, J. (2000). Telomerase-dependent repeat divergence at the 3' ends of yeast telomeres. *Nucleic Acids Res* 28, 2690-2694.
- Galgoczy, D.J., and Toczyski, D.P. (2001). Checkpoint adaptation precedes spontaneous and damage-induced genomic instability in yeast. *Mol Cell Biol* 21, 1710-1718.
- Galy, V., Olivo-Marin, J.C., Scherthan, H., Doye, V., Rascalou, N., and Nehrbass, U. (2000). Nuclear pore complexes in the organization of silent telomeric chromatin. *Nature* 403, 108-112.
- Gartenberg, M.R. (2009). Life on the edge: telomeres and persistent DNA breaks converge at the nuclear periphery. *Genes Dev* 23, 1027-1031.
- Gera, J.F., Hazbun, T.R., and Fields, S. (2002). Array-based methods for identifying protein-protein and protein-nucleic acid interactions. *Methods Enzymol* 350, 499-512.
- Gerlich, D., Koch, B., Dupeux, F., Peters, J.M., and Ellenberg, J. (2006). Live-Cell Imaging Reveals a Stable Cohesin-Chromatin Interaction after but Not before DNA Replication. *Curr Biol* 16, 1571-1578.
- Ghaemmaghami, S., Huh, W.K., Bower, K., Howson, R.W., Belle, A., Dephoure, N., O'Shea, E.K., and Weissman, J.S. (2003). Global analysis of protein expression in yeast. *Nature* 425, 737-741.
- Gietz, R.D., and Sugino, A. (1988). New yeast-*Escherichia coli* shuttle vectors constructed with in vitro mutagenized yeast genes lacking six-base pair restriction sites. *Gene* 74, 527-534.
- Gilbert, C.S., Green, C.M., and Lowndes, N.F. (2001). Budding yeast Rad9 is an ATP-dependent Rad53 activating machine. *Mol Cell* 8, 129-136.
- Gravel, S., Chapman, J.R., Magill, C., and Jackson, S.P. (2008). DNA helicases Sgs1 and BLM promote DNA double-strand break resection. *Genes Dev* 22, 2767-2772.

References

- Gruber, S., Haering, C.H., and Nasmyth, K. (2003). Chromosomal cohesin forms a ring. *Cell* *112*, 765-777.
- Guillemette, B., Bataille, A.R., Gevry, N., Adam, M., Blanchette, M., Robert, F., and Gaudreau, L. (2005). Variant histone H2A.Z is globally localized to the promoters of inactive yeast genes and regulates nucleosome positioning. *PLoS Biol* *3*, e384.
- Haering, C.H., Farcas, A.M., Arumugam, P., Metson, J., and Nasmyth, K. (2008). The cohesin ring concatenates sister DNA molecules. *Nature* *454*, 297-301.
- Harrison, J.C., and Haber, J.E. (2006). Surviving the breakup: the DNA damage checkpoint. *Annu Rev Genet* *40*, 209-235.
- Hastings, P.J., Lupski, J.R., Rosenberg, S.M., and Ira, G. (2009). Mechanisms of change in gene copy number. *Nat Rev Genet* *10*, 551-564.
- Hediger, F., Neumann, F.R., Van Houwe, G., Dubrana, K., and Gasser, S.M. (2002). Live imaging of telomeres: yKu and Sir proteins define redundant telomere-anchoring pathways in yeast. *Curr Biol* *12*, 2076-2089.
- Heidinger-Pauli, J.M., Unal, E., Guacci, V., and Koshland, D. (2008). The kleisin subunit of cohesin dictates damage-induced cohesion. *Mol Cell* *31*, 47-56.
- Henikoff, S., and Ahmad, K. (2005). Assembly of variant histones into chromatin. *Annu Rev Cell Dev Biol* *21*, 133-153.
- Hickson, I.D. (2003). RecQ helicases: caretakers of the genome. *Nat Rev Cancer* *3*, 169-178.
- Hiller, N.J. (2006). Studies on SUMO E3-ligases and the search for substrates. Diplomarbeit, Eberhard-Karls-Universität Tübingen: Fakultät für Chemie und Pharmazie.
- Hoegge, C., Pfander, B., Moldovan, G.L., Pyrowolakis, G., and Jentsch, S. (2002). RAD6-dependent DNA repair is linked to modification of PCNA by ubiquitin and SUMO. *Nature* *419*, 135-141.
- Hoffman, C.S., and Winston, F. (1987). A ten-minute DNA preparation from yeast efficiently releases autonomous plasmids for transformation of *Escherichia coli*. *Gene* *57*, 267-272.
- Holmes, A., and Haber, J.E. (1999). Physical monitoring of HO-induced homologous recombination. *Methods Mol Biol* *113*, 403-415.
- Huang, Y., Park, Y.C., Rich, R.L., Segal, D., Myszka, D.G., and Wu, H. (2001). Structural basis of caspase inhibition by XIAP: differential roles of the linker versus the BIR domain. *Cell* *104*, 781-790.
- Huen, M.S., Grant, R., Manke, I., Minn, K., Yu, X., Yaffe, M.B., and Chen, J. (2007). RNF8 transduces the DNA-damage signal via histone ubiquitylation and checkpoint protein assembly. *Cell* *131*, 901-914.

- Huertas, P., Cortes-Ledesma, F., Sartori, A.A., Aguilera, A., and Jackson, S.P. (2008). CDK targets Sae2 to control DNA-end resection and homologous recombination. *Nature* 455, 689-692.
- Huertas, P., and Jackson, S.P. (2009). Human CtIP mediates cell cycle control of DNA end resection and double strand break repair. *J Biol Chem* 284, 9558-9565.
- Huh, W.K., Falvo, J.V., Gerke, L.C., Carroll, A.S., Howson, R.W., Weissman, J.S., and O'Shea, E.K. (2003). Global analysis of protein localization in budding yeast. *Nature* 425, 686-691.
- Huyen, Y., Zgheib, O., Ditullio, R.A., Jr., Gorgoulis, V.G., Zacharatos, P., Petty, T.J., Sheston, E.A., Mellert, H.S., Stavridi, E.S., and Halazonetis, T.D. (2004). Methylated lysine 79 of histone H3 targets 53BP1 to DNA double-strand breaks. *Nature* 432, 406-411.
- Ip, S.C., Rass, U., Blanco, M.G., Flynn, H.R., Skehel, J.M., and West, S.C. (2008). Identification of Holliday junction resolvases from humans and yeast. *Nature* 456, 357-361.
- Ira, G., Malkova, A., Liberi, G., Foiani, M., and Haber, J.E. (2003). Srs2 and Sgs1-Top3 suppress crossovers during double-strand break repair in yeast. *Cell* 115, 401-411.
- Ira, G., Pelliccioli, A., Balijja, A., Wang, X., Fiorani, S., Carotenuto, W., Liberi, G., Bressan, D., Wan, L., Hollingsworth, N.M., *et al.* (2004). DNA end resection, homologous recombination and DNA damage checkpoint activation require CDK1. *Nature* 431, 1011-1017.
- Ivanov, D., Schleiffer, A., Eisenhaber, F., Mechtler, K., Haering, C.H., and Nasmyth, K. (2002). Eco1 is a novel acetyltransferase that can acetylate proteins involved in cohesion. *Curr Biol* 12, 323-328.
- Ivanov, E.L., Sugawara, N., White, C.I., Fabre, F., and Haber, J.E. (1994). Mutations in XRS2 and RAD50 delay but do not prevent mating-type switching in *Saccharomyces cerevisiae*. *Mol Cell Biol* 14, 3414-3425.
- James, P., Halladay, J., and Craig, E.A. (1996). Genomic libraries and a host strain designed for highly efficient two-hybrid selection in yeast. *Genetics* 144, 1425-1436.
- Janke, C., Magiera, M.M., Rathfelder, N., Taxis, C., Reber, S., Maekawa, H., Moreno-Borchart, A., Doenges, G., Schwob, E., Schiebel, E., *et al.* (2004). A versatile toolbox for PCR-based tagging of yeast genes: new fluorescent proteins, more markers and promoter substitution cassettes. *Yeast* 21, 947-962.
- Jaspersen, S.L., Martin, A.E., Glazko, G., Giddings, T.H., Jr., Morgan, G., Mushegian, A., and Winey, M. (2006). The Sad1-UNC-84 homology domain in Mps3 interacts with Mps2 to connect the spindle pole body with the nuclear envelope. *J Cell Biol* 174, 665-675.
- Jha, S., and Dutta, A. (2009). RVB1/RVB2: running rings around molecular biology. *Mol Cell* 34, 521-533.

References

- Jin, C., Zang, C., Wei, G., Cui, K., Peng, W., Zhao, K., and Felsenfeld, G. (2009). H3.3/H2A.Z double variant-containing nucleosomes mark 'nucleosome-free regions' of active promoters and other regulatory regions. *Nat Genet* *41*, 941-945.
- Kalocsay, M. (2010). SUMO-abhängige Reaktionen auf einen persistenten DNA-Doppelstrangbruch. Dissertation, LMU München: Faculty of Biology.
- Kalocsay, M., Hiller, N.J., and Jentsch, S. (2009). Chromosome-wide Rad51 spreading and SUMO-H2A.Z-dependent chromosome fixation in response to a persistent DNA double-strand break. *Mol Cell* *33*, 335-343.
- Kaplan, N., Moore, I.K., Fondufe-Mittendorf, Y., Gossett, A.J., Tillo, D., Field, Y., LeProust, E.M., Hughes, T.R., Lieb, J.D., Widom, J., *et al.* (2009). The DNA-encoded nucleosome organization of a eukaryotic genome. *Nature* *458*, 362-366.
- Karlseder, J. (2003). Telomere repeat binding factors: keeping the ends in check. *Cancer Lett* *194*, 189-197.
- Kaye, J.A., Melo, J.A., Cheung, S.K., Vaze, M.B., Haber, J.E., and Toczyski, D.P. (2004). DNA breaks promote genomic instability by impeding proper chromosome segregation. *Curr Biol* *14*, 2096-2106.
- Keogh, M.C., Kim, J.A., Downey, M., Fillingham, J., Chowdhury, D., Harrison, J.C., Onishi, M., Datta, N., Galicia, S., Emili, A., *et al.* (2006a). A phosphatase complex that dephosphorylates gammaH2AX regulates DNA damage checkpoint recovery. *Nature* *439*, 497-501.
- Keogh, M.C., Mennella, T.A., Sawa, C., Berthelet, S., Krogan, N.J., Wolek, A., Podolny, V., Carpenter, L.R., Greenblatt, J.F., Baetz, K., *et al.* (2006b). The *Saccharomyces cerevisiae* histone H2A variant Htz1 is acetylated by NuA4. *Genes Dev* *20*, 660-665.
- Khadaroo, B., Teixeira, M.T., Luciano, P., Eckert-Boulet, N., Germann, S.M., Simon, M.N., Gallina, I., Abdallah, P., Gilson, E., Geli, V., *et al.* (2009). The DNA damage response at eroded telomeres and tethering to the nuclear pore complex. *Nat Cell Biol* *11*, 980-987.
- Khorasanizadeh, S. (2004). The nucleosome: from genomic organization to genomic regulation. *Cell* *116*, 259-272.
- Kim, H., Chen, J., and Yu, X. (2007a). Ubiquitin-binding protein RAP80 mediates BRCA1-dependent DNA damage response. *Science* *316*, 1202-1205.
- Kim, J.A., and Haber, J.E. (2009). Chromatin assembly factors Asf1 and CAF-1 have overlapping roles in deactivating the DNA damage checkpoint when DNA repair is complete. *Proc Natl Acad Sci U S A* *106*, 1151-1156.
- Kim, J.H., Lee, J.M., Nam, H.J., Choi, H.J., Yang, J.W., Lee, J.S., Kim, M.H., Kim, S.I., Chung, C.H., Kim, K.I., *et al.* (2007b). SUMOylation of pontin chromatin-remodeling complex reveals a signal integration code in prostate cancer cells. *Proc Natl Acad Sci U S A* *104*, 20793-20798.

- Kim, J.S., Krasieva, T.B., LaMorte, V., Taylor, A.M., and Yokomori, K. (2002). Specific recruitment of human cohesin to laser-induced DNA damage. *J Biol Chem* 277, 45149-45153.
- Knop, M., Siegers, K., Pereira, G., Zachariae, W., Winsor, B., Nasmyth, K., and Schiebel, E. (1999). Epitope tagging of yeast genes using a PCR-based strategy: more tags and improved practical routines. *Yeast* 15, 963-972.
- Kobor, M.S., Venkatasubrahmanyam, S., Meneghini, M.D., Gin, J.W., Jennings, J.L., Link, A.J., Madhani, H.D., and Rine, J. (2004). A protein complex containing the conserved Swi2/Snf2-related ATPase Swr1p deposits histone variant H2A.Z into euchromatin. *PLoS Biol* 2, E131.
- Kolas, N.K., Chapman, J.R., Nakada, S., Ylanko, J., Chahwan, R., Sweeney, F.D., Panier, S., Mendez, M., Wildenhain, J., Thomson, T.M., *et al.* (2007). Orchestration of the DNA-damage response by the RNF8 ubiquitin ligase. *Science* 318, 1637-1640.
- Kondo, T., Wakayama, T., Naiki, T., Matsumoto, K., and Sugimoto, K. (2001). Recruitment of Mec1 and Ddc1 checkpoint proteins to double-strand breaks through distinct mechanisms. *Science* 294, 867-870.
- Kornberg, R.D. (1974). Chromatin structure: a repeating unit of histones and DNA. *Science* 184, 868-871.
- Kosak, S.T., Scalzo, D., Alworth, S.V., Li, F., Palmer, S., Enver, T., Lee, J.S., and Groudine, M. (2007). Coordinate gene regulation during hematopoiesis is related to genomic organization. *PLoS Biol* 5, e309.
- Krishna, S.S., Majumdar, I., and Grishin, N.V. (2003). Structural classification of zinc fingers: survey and summary. *Nucleic Acids Res* 31, 532-550.
- Krishna, T.S., Kong, X.P., Gary, S., Burgers, P.M., and Kuriyan, J. (1994). Crystal structure of the eukaryotic DNA polymerase processivity factor PCNA. *Cell* 79, 1233-1243.
- Krogan, N.J., Keogh, M.C., Datta, N., Sawa, C., Ryan, O.W., Ding, H., Haw, R.A., Pootoolal, J., Tong, A., Canadien, V., *et al.* (2003). A Snf2 family ATPase complex required for recruitment of the histone H2A variant Htz1. *Mol Cell* 12, 1565-1576.
- Kunkel, T.A. (1985). Rapid and efficient site-specific mutagenesis without phenotypic selection. *Proc Natl Acad Sci U S A* 82, 488-492.
- Lantermann, A., Stralfors, A., Fagerstrom-Billai, F., Korber, P., and Ekwall, K. (2009). Genome-wide mapping of nucleosome positions in *Schizosaccharomyces pombe*. *Methods* 48, 218-225.
- Lau, I.F., Filipe, S.R., Soballe, B., Okstad, O.A., Barre, F.X., and Sherratt, D.J. (2003). Spatial and temporal organization of replicating *Escherichia coli* chromosomes. *Mol Microbiol* 49, 731-743.
- Lee, S.E., Moore, J.K., Holmes, A., Umezu, K., Kolodner, R.D., and Haber, J.E. (1998). *Saccharomyces Ku70*, *mre11/rad50* and RPA proteins regulate adaptation to G2/M arrest after DNA damage. *Cell* 94, 399-409.

References

- Lengronne, A., Katou, Y., Mori, S., Yokobayashi, S., Kelly, G.P., Itoh, T., Watanabe, Y., Shirahige, K., and Uhlmann, F. (2004). Cohesin relocation from sites of chromosomal loading to places of convergent transcription. *Nature* *430*, 573-578.
- Lengsfeld, B.M., Rattray, A.J., Bhaskara, V., Ghirlando, R., and Paull, T.T. (2007). Sae2 is an endonuclease that processes hairpin DNA cooperatively with the Mre11/Rad50/Xrs2 complex. *Mol Cell* *28*, 638-651.
- Leroy, C., Lee, S.E., Vaze, M.B., Ochsenbien, F., Guerois, R., Haber, J.E., and Marsolier-Kergoat, M.C. (2003). PP2C phosphatases Ptc2 and Ptc3 are required for DNA checkpoint inactivation after a double-strand break. *Mol Cell* *11*, 827-835.
- Li, B., Gogol, M., Carey, M., Lee, D., Seidel, C., and Workman, J.L. (2007). Combined action of PHD and chromo domains directs the Rpd3S HDAC to transcribed chromatin. *Science* *316*, 1050-1054.
- Liang, C., and Stillman, B. (1997). Persistent initiation of DNA replication and chromatin-bound MCM proteins during the cell cycle in *cdc6* mutants. *Genes Dev* *11*, 3375-3386.
- Liu, Q., Pante, N., Misteli, T., Elsagga, M., Crisp, M., Hodzic, D., Burke, B., and Roux, K.J. (2007). Functional association of Sun1 with nuclear pore complexes. *J Cell Biol* *178*, 785-798.
- Luger, K., Mader, A.W., Richmond, R.K., Sargent, D.F., and Richmond, T.J. (1997). Crystal structure of the nucleosome core particle at 2.8 Å resolution. *Nature* *389*, 251-260.
- Luger, K., Rechsteiner, T.J., and Richmond, T.J. (1999). Expression and purification of recombinant histones and nucleosome reconstitution. *Methods Mol Biol* *119*, 1-16.
- Luk, E., Vu, N.D., Patteson, K., Mizuguchi, G., Wu, W.H., Ranjan, A., Backus, J., Sen, S., Lewis, M., Bai, Y., *et al.* (2007). Chz1, a nuclear chaperone for histone H2AZ. *Mol Cell* *25*, 357-368.
- Mailand, N., Bekker-Jensen, S., Faustrup, H., Melander, F., Bartek, J., Lukas, C., and Lukas, J. (2007). RNF8 ubiquitylates histones at DNA double-strand breaks and promotes assembly of repair proteins. *Cell* *131*, 887-900.
- Malik, H.S., and Henikoff, S. (2003). Phylogenomics of the nucleosome. *Nat Struct Biol* *10*, 882-891.
- McEachern, M.J., and Haber, J.E. (2006). Break-induced replication and recombinational telomere elongation in yeast. *Annu Rev Biochem* *75*, 111-135.
- Mekhail, K., Seebacher, J., Gygi, S.P., and Moazed, D. (2008). Role for perinuclear chromosome tethering in maintenance of genome stability. *Nature* *456*, 667-670.
- Meneghini, M.D., Wu, M., and Madhani, H.D. (2003). Conserved histone variant H2A.Z protects euchromatin from the ectopic spread of silent heterochromatin. *Cell* *112*, 725-736.

- Mimitou, E.P., and Symington, L.S. (2008). Sae2, Exo1 and Sgs1 collaborate in DNA double-strand break processing. *Nature* 455, 770-774.
- Misteli, T. (2007). Beyond the sequence: cellular organization of genome function. *Cell* 128, 787-800.
- Mizuguchi, G., Shen, X., Landry, J., Wu, W.H., Sen, S., and Wu, C. (2004). ATP-driven exchange of histone H2AZ variant catalyzed by SWR1 chromatin remodeling complex. *Science* 303, 343-348.
- Moldovan, G.L., Pfander, B., and Jentsch, S. (2006). PCNA controls establishment of sister chromatid cohesion during S phase. *Mol Cell* 23, 723-732.
- Morin, G.B. (1989). The human telomere terminal transferase enzyme is a ribonucleoprotein that synthesizes TTAGGG repeats. *Cell* 59, 521-529.
- Morrison, A.J., Highland, J., Krogan, N.J., Arbel-Eden, A., Greenblatt, J.F., Haber, J.E., and Shen, X. (2004). INO80 and gamma-H2AX interaction links ATP-dependent chromatin remodeling to DNA damage repair. *Cell* 119, 767-775.
- Morrison, A.J., and Shen, X. (2009). Chromatin remodelling beyond transcription: the INO80 and SWR1 complexes. *Nat Rev Mol Cell Biol* 10, 373-384.
- Mossesso, E., and Lima, C.D. (2000). Ulp1-SUMO crystal structure and genetic analysis reveal conserved interactions and a regulatory element essential for cell growth in yeast. *Mol Cell* 5, 865-876.
- Nagai, S., Dubrana, K., Tsai-Pflugfelder, M., Davidson, M.B., Roberts, T.M., Brown, G.W., Varela, E., Hediger, F., Gasser, S.M., and Krogan, N.J. (2008). Functional targeting of DNA damage to a nuclear pore-associated SUMO-dependent ubiquitin ligase. *Science* 322, 597-602.
- Naiki, T., Wakayama, T., Nakada, D., Matsumoto, K., and Sugimoto, K. (2004). Association of Rad9 with double-strand breaks through a Mec1-dependent mechanism. *Mol Cell Biol* 24, 3277-3285.
- Nasmyth, K., and Haering, C.H. (2009). Cohesin: Its Roles and Mechanisms. *Annu Rev Genet*.
- Nicassio, F., Corrado, N., Vissers, J.H., Areces, L.B., Bergink, S., Marteiijn, J.A., Geverts, B., Houtsmuller, A.B., Vermeulen, W., Di Fiore, P.P., *et al.* (2007). Human USP3 is a chromatin modifier required for S phase progression and genome stability. *Curr Biol* 17, 1972-1977.
- Oh, S.D., Lao, J.P., Hwang, P.Y., Taylor, A.F., Smith, G.R., and Hunter, N. (2007). BLM ortholog, Sgs1, prevents aberrant crossing-over by suppressing formation of multichromatid joint molecules. *Cell* 130, 259-272.
- Onn, I., Guacci, V., and Koshland, D.E. (2009). The zinc finger of Eco1 enhances its acetyltransferase activity during sister chromatid cohesion. *Nucleic Acids Res* 37, 6126-6134.

References

Onn, I., Heidinger-Pauli, J.M., Guacci, V., Unal, E., and Koshland, D.E. (2008). Sister chromatid cohesion: a simple concept with a complex reality. *Annu Rev Cell Dev Biol* 24, 105-129.

Oza, P., Jaspersen, S.L., Miele, A., Dekker, J., and Peterson, C.L. (2009). Mechanisms that regulate localization of a DNA double-strand break to the nuclear periphery. *Genes Dev* 23, 912-927.

Paciotti, V., Clerici, M., Lucchini, G., and Longhese, M.P. (2000). The checkpoint protein Ddc2, functionally related to *S. pombe* Rad26, interacts with Mec1 and is regulated by Mec1-dependent phosphorylation in budding yeast. *Genes Dev* 14, 2046-2059.

Panier, S., and Durocher, D. (2009). Regulatory ubiquitylation in response to DNA double-strand breaks. *DNA Repair (Amst)* 8, 436-443.

Pehrson, J.R., and Fried, V.A. (1992). MacroH2A, a core histone containing a large nonhistone region. *Science* 257, 1398-1400.

Pelliccioli, A., Lee, S.E., Lucca, C., Foiani, M., and Haber, J.E. (2001). Regulation of *Saccharomyces* Rad53 checkpoint kinase during adaptation from DNA damage-induced G2/M arrest. *Mol Cell* 7, 293-300.

Penkner, A., Tang, L., Novatchkova, M., Ladurner, M., Fridkin, A., Gruenbaum, Y., Schweizer, D., Loidl, J., and Jantsch, V. (2007). The nuclear envelope protein Matefin/SUN-1 is required for homologous pairing in *C. elegans* meiosis. *Dev Cell* 12, 873-885.

Penkner, A.M., Fridkin, A., Gloggnitzer, J., Baudrimont, A., Machacek, T., Woglar, A., Csaszar, E., Pasierbek, P., Ammerer, G., Gruenbaum, Y., *et al.* (2009). Meiotic chromosome homology search involves modifications of the nuclear envelope protein Matefin/SUN-1. *Cell* 139, 920-933.

Peters, J.M., Tedeschi, A., and Schmitz, J. (2008). The cohesin complex and its roles in chromosome biology. *Genes Dev* 22, 3089-3114.

Raisner, R.M., Hartley, P.D., Meneghini, M.D., Bao, M.Z., Liu, C.L., Schreiber, S.L., Rando, O.J., and Madhani, H.D. (2005). Histone variant H2A.Z marks the 5' ends of both active and inactive genes in euchromatin. *Cell* 123, 233-248.

Raisner, R.M., and Madhani, H.D. (2006). Patterning chromatin: form and function for H2A.Z variant nucleosomes. *Curr Opin Genet Dev* 16, 119-124.

Rangasamy, D., Greaves, I., and Tremethick, D.J. (2004). RNA interference demonstrates a novel role for H2A.Z in chromosome segregation. *Nat Struct Mol Biol* 11, 650-655.

Riedl, S.J., Renatus, M., Schwarzenbacher, R., Zhou, Q., Sun, C., Fesik, S.W., Liddington, R.C., and Salvesen, G.S. (2001). Structural basis for the inhibition of caspase-3 by XIAP. *Cell* 104, 791-800.

Rodriguez-Navarro, S., Fischer, T., Luo, M.J., Antunez, O., Brettschneider, S., Lechner, J., Perez-Ortin, J.E., Reed, R., and Hurt, E. (2004). Sus1, a functional

component of the SAGA histone acetylase complex and the nuclear pore-associated mRNA export machinery. *Cell* 116, 75-86.

Rogakou, E.P., Boon, C., Redon, C., and Bonner, W.M. (1999). Megabase chromatin domains involved in DNA double-strand breaks in vivo. *J Cell Biol* 146, 905-916.

Rouse, J., and Jackson, S.P. (2002). Lcd1p recruits Mec1p to DNA lesions in vitro and in vivo. *Mol Cell* 9, 857-869.

Rowland, B.D., Roig, M.B., Nishino, T., Kurze, A., Uluocak, P., Mishra, A., Beckouet, F., Underwood, P., Metson, J., Imre, R., *et al.* (2009). Building sister chromatid cohesion: smc3 acetylation counteracts an antiestablishment activity. *Mol Cell* 33, 763-774.

Sacher, M., Pfander, B., Hoege, C., and Jentsch, S. (2006). Control of Rad52 recombination activity by double-strand break-induced SUMO modification. *Nat Cell Biol* 8, 1284-1290.

Sambrook, J., Maniatis, T., and Fritsch, E.F. (1989). *Molecular cloning : a laboratory manual*, 2nd edn (Cold Spring Harbor, N.Y., Cold Spring Harbor Laboratory Press).

Sanchez, Y., Bachant, J., Wang, H., Hu, F., Liu, D., Tetzlaff, M., and Elledge, S.J. (1999). Control of the DNA damage checkpoint by chk1 and rad53 protein kinases through distinct mechanisms. *Science* 286, 1166-1171.

Santisteban, M.S., Kalashnikova, T., and Smith, M.M. (2000). Histone H2A.Z regulates transcription and is partially redundant with nucleosome remodeling complexes. *Cell* 103, 411-422.

Sarma, K., and Reinberg, D. (2005). Histone variants meet their match. *Nat Rev Mol Cell Biol* 6, 139-149.

Sartori, A.A., Lukas, C., Coates, J., Mistrik, M., Fu, S., Bartek, J., Baer, R., Lukas, J., and Jackson, S.P. (2007). Human CtIP promotes DNA end resection. *Nature* 450, 509-514.

Schober, H., Ferreira, H., Kalck, V., Gehlen, L.R., and Gasser, S.M. (2009). Yeast telomerase and the SUN domain protein Mps3 anchor telomeres and repress subtelomeric recombination. *Genes Dev* 23, 928-938.

Schule, B., Oviedo, A., Johnston, K., Pai, S., and Francke, U. (2005). Inactivating mutations in ESCO2 cause SC phocomelia and Roberts syndrome: no phenotype-genotype correlation. *Am J Hum Genet* 77, 1117-1128.

Segal, E., Fondufe-Mittendorf, Y., Chen, L., Thastrom, A., Field, Y., Moore, I.K., Wang, J.P., and Widom, J. (2006). A genomic code for nucleosome positioning. *Nature* 442, 772-778.

Segal, E., and Widom, J. (2009). What controls nucleosome positions? *Trends Genet* 25, 335-343.

Shen, X., Ranallo, R., Choi, E., and Wu, C. (2003). Involvement of actin-related proteins in ATP-dependent chromatin remodeling. *Mol Cell* 12, 147-155.

References

Shroff, R., Arbel-Eden, A., Pilch, D., Ira, G., Bonner, W.M., Petrini, J.H., Haber, J.E., and Lichten, M. (2004). Distribution and dynamics of chromatin modification induced by a defined DNA double-strand break. *Curr Biol* 14, 1703-1711.

Sjogren, C., and Nasmyth, K. (2001). Sister chromatid cohesion is required for postreplicative double-strand break repair in *Saccharomyces cerevisiae*. *Curr Biol* 11, 991-995.

Skibbens, R.V., Corson, L.B., Koshland, D., and Hieter, P. (1999). Ctf7p is essential for sister chromatid cohesion and links mitotic chromosome structure to the DNA replication machinery. *Genes Dev* 13, 307-319.

Sobhian, B., Shao, G., Lilli, D.R., Culhane, A.C., Moreau, L.A., Xia, B., Livingston, D.M., and Greenberg, R.A. (2007). RAP80 targets BRCA1 to specific ubiquitin structures at DNA damage sites. *Science* 316, 1198-1202.

Soulier, J., and Lowndes, N.F. (1999). The BRCT domain of the *S. cerevisiae* checkpoint protein Rad9 mediates a Rad9-Rad9 interaction after DNA damage. *Curr Biol* 9, 551-554.

Spector, D.L. (2006). SnapShot: Cellular bodies. *Cell* 127, 1071.

Stewart, G.S., Panier, S., Townsend, K., Al-Hakim, A.K., Kolas, N.K., Miller, E.S., Nakada, S., Ylanko, J., Olivarius, S., Mendez, M., *et al.* (2009). The RIDDLE syndrome protein mediates a ubiquitin-dependent signaling cascade at sites of DNA damage. *Cell* 136, 420-434.

Stewart, G.S., Stankovic, T., Byrd, P.J., Wechsler, T., Miller, E.S., Huissoon, A., Drayson, M.T., West, S.C., Elledge, S.J., and Taylor, A.M. (2007). RIDDLE immunodeficiency syndrome is linked to defects in 53BP1-mediated DNA damage signaling. *Proc Natl Acad Sci U S A* 104, 16910-16915.

Strahl, B.D., and Allis, C.D. (2000). The language of covalent histone modifications. *Nature* 403, 41-45.

Strom, L., Karlsson, C., Lindroos, H.B., Wedahl, S., Katou, Y., Shirahige, K., and Sjogren, C. (2007). Postreplicative formation of cohesion is required for repair and induced by a single DNA break. *Science* 317, 242-245.

Strom, L., Lindroos, H.B., Shirahige, K., and Sjogren, C. (2004). Postreplicative recruitment of cohesin to double-strand breaks is required for DNA repair. *Mol Cell* 16, 1003-1015.

Stucki, M., Clapperton, J.A., Mohammad, D., Yaffe, M.B., Smerdon, S.J., and Jackson, S.P. (2005). MDC1 directly binds phosphorylated histone H2AX to regulate cellular responses to DNA double-strand breaks. *Cell* 123, 1213-1226.

Stucki, M., and Jackson, S.P. (2006). gammaH2AX and MDC1: anchoring the DNA-damage-response machinery to broken chromosomes. *DNA Repair (Amst)* 5, 534-543.

Sugawara, N., Wang, X., and Haber, J.E. (2003). In vivo roles of Rad52, Rad54, and Rad55 proteins in Rad51-mediated recombination. *Mol Cell* 12, 209-219.

- Sutani, T., Kawaguchi, T., Kanno, R., Itoh, T., and Shirahige, K. (2009). Budding yeast Wpl1(Rad61)-Pds5 complex counteracts sister chromatid cohesion-establishing reaction. *Curr Biol* 19, 492-497.
- Suto, R.K., Clarkson, M.J., Tremethick, D.J., and Luger, K. (2000). Crystal structure of a nucleosome core particle containing the variant histone H2A.Z. *Nat Struct Biol* 7, 1121-1124.
- Szostak, J.W., Orr-Weaver, T.L., Rothstein, R.J., and Stahl, F.W. (1983). The double-strand-break repair model for recombination. *Cell* 33, 25-35.
- Taddei, A., Van Houwe, G., Hediger, F., Kalck, V., Cubizolles, F., Schober, H., and Gasser, S.M. (2006). Nuclear pore association confers optimal expression levels for an inducible yeast gene. *Nature* 441, 774-778.
- Takahashi, R., Deveraux, Q., Tamm, I., Welsh, K., Assa-Munt, N., Salvesen, G.S., and Reed, J.C. (1998). A single BIR domain of XIAP sufficient for inhibiting caspases. *J Biol Chem* 273, 7787-7790.
- Talbert, P.B., and Henikoff, S. (2010). Histone variants - ancient wrap artists of the epigenome. *Nat Rev Mol Cell Biol* 11, 264-275.
- Taverna, S.D., Li, H., Ruthenburg, A.J., Allis, C.D., and Patel, D.J. (2007). How chromatin-binding modules interpret histone modifications: lessons from professional pocket pickers. *Nat Struct Mol Biol* 14, 1025-1040.
- Thacker, J. (2005). The RAD51 gene family, genetic instability and cancer. *Cancer Lett* 219, 125-135.
- Tham, W.H., Wyithe, J.S., Ko Ferrigno, P., Silver, P.A., and Zakian, V.A. (2001). Localization of yeast telomeres to the nuclear periphery is separable from transcriptional repression and telomere stability functions. *Mol Cell* 8, 189-199.
- Tham, W.H., and Zakian, V.A. (2000). Telomeric tethers. *Nature* 403, 34-35.
- Therizols, P., Fairhead, C., Cabal, G.G., Genovesio, A., Olivo-Marin, J.C., Dujon, B., and Fabre, E. (2006). Telomere tethering at the nuclear periphery is essential for efficient DNA double strand break repair in subtelomeric region. *J Cell Biol* 172, 189-199.
- Toczyski, D.P., Galgoczy, D.J., and Hartwell, L.H. (1997). CDC5 and CKII control adaptation to the yeast DNA damage checkpoint. *Cell* 90, 1097-1106.
- Tolstorukov, M.Y., Kharchenko, P.V., Goldman, J.A., Kingston, R.E., and Park, P.J. (2009). Comparative analysis of H2A.Z nucleosome organization in the human and yeast genomes. *Genome Res* 19, 967-977.
- Torres-Rosell, J., Sunjevaric, I., De Piccoli, G., Sacher, M., Eckert-Boulet, N., Reid, R., Jentsch, S., Rothstein, R., Aragon, L., and Lisby, M. (2007). The Smc5-Smc6 complex and SUMO modification of Rad52 regulates recombinational repair at the ribosomal gene locus. *Nat Cell Biol* 9, 923-931.
- Toth, A., Ciosk, R., Uhlmann, F., Galova, M., Schleiffer, A., and Nasmyth, K. (1999). Yeast cohesin complex requires a conserved protein, Eco1p(Ctf7), to establish

References

cohesion between sister chromatids during DNA replication. *Genes Dev* 13, 320-333.

Towbin, B.D., Meister, P., and Gasser, S.M. (2009). The nuclear envelope--a scaffold for silencing? *Curr Opin Genet Dev* 19, 180-186.

Uetz, P., Giot, L., Cagney, G., Mansfield, T.A., Judson, R.S., Knight, J.R., Lockshon, D., Narayan, V., Srinivasan, M., Pochart, P., *et al.* (2000). A comprehensive analysis of protein-protein interactions in *Saccharomyces cerevisiae*. *Nature* 403, 623-627.

Uhlmann, F., and Nasmyth, K. (1998). Cohesion between sister chromatids must be established during DNA replication. *Curr Biol* 8, 1095-1101.

Unal, E., Arbel-Eden, A., Sattler, U., Shroff, R., Lichten, M., Haber, J.E., and Koshland, D. (2004). DNA damage response pathway uses histone modification to assemble a double-strand break-specific cohesin domain. *Mol Cell* 16, 991-1002.

Unal, E., Heidinger-Pauli, J.M., Kim, W., Guacci, V., Onn, I., Gygi, S.P., and Koshland, D.E. (2008). A molecular determinant for the establishment of sister chromatid cohesion. *Science* 321, 566-569.

Unal, E., Heidinger-Pauli, J.M., and Koshland, D. (2007). DNA double-strand breaks trigger genome-wide sister-chromatid cohesion through Eco1 (Ctf7). *Science* 317, 245-248.

van Attikum, H., Fritsch, O., and Gasser, S.M. (2007). Distinct roles for SWR1 and INO80 chromatin remodeling complexes at chromosomal double-strand breaks. *Embo J* 26, 4113-4125.

van Attikum, H., Fritsch, O., Hohn, B., and Gasser, S.M. (2004). Recruitment of the INO80 complex by H2A phosphorylation links ATP-dependent chromatin remodeling with DNA double-strand break repair. *Cell* 119, 777-788.

van Vugt, J.J., Raney, M., Campsteijn, C., and Logie, C. (2007). The ins and outs of ATP-dependent chromatin remodeling in budding yeast: biophysical and proteomic perspectives. *Biochim Biophys Acta* 1769, 153-171.

Vaze, M.B., Pellicoli, A., Lee, S.E., Ira, G., Liberi, G., Arbel-Eden, A., Foiani, M., and Haber, J.E. (2002). Recovery from checkpoint-mediated arrest after repair of a double-strand break requires Srs2 helicase. *Mol Cell* 10, 373-385.

Vega, H., Waisfisz, Q., Gordillo, M., Sakai, N., Yanagihara, I., Yamada, M., van Gosliga, D., Kayserili, H., Xu, C., Ozono, K., *et al.* (2005). Roberts syndrome is caused by mutations in ESCO2, a human homolog of yeast ECO1 that is essential for the establishment of sister chromatid cohesion. *Nat Genet* 37, 468-470.

Viens, A., Mechold, U., Brouillard, F., Gilbert, C., Leclerc, P., and Ogryzko, V. (2006). Analysis of human histone H2AZ deposition in vivo argues against its direct role in epigenetic templating mechanisms. *Mol Cell Biol* 26, 5325-5335.

Waizenegger, I.C., Hauf, S., Meinke, A., and Peters, J.M. (2000). Two distinct pathways remove mammalian cohesin from chromosome arms in prophase and from centromeres in anaphase. *Cell* 103, 399-410.

- Wang, A.Y., Schulze, J.M., Skordalakes, E., Gin, J.W., Berger, J.M., Rine, J., and Kobor, M.S. (2009). Asf1-like structure of the conserved Yaf9 YEATS domain and role in H2A.Z deposition and acetylation. *Proc Natl Acad Sci U S A* 106, 21573-21578.
- Wang, B., Matsuoka, S., Ballif, B.A., Zhang, D., Smogorzewska, A., Gygi, S.P., and Elledge, S.J. (2007). Abraxas and RAP80 form a BRCA1 protein complex required for the DNA damage response. *Science* 316, 1194-1198.
- Ward, I.M., and Chen, J. (2001). Histone H2AX is phosphorylated in an ATR-dependent manner in response to replicational stress. *J Biol Chem* 276, 47759-47762.
- Ward, I.M., Minn, K., Jorda, K.G., and Chen, J. (2003). Accumulation of checkpoint protein 53BP1 at DNA breaks involves its binding to phosphorylated histone H2AX. *J Biol Chem* 278, 19579-19582.
- Weake, V.M., and Workman, J.L. (2008). Histone ubiquitination: triggering gene activity. *Mol Cell* 29, 653-663.
- White, C.I., and Haber, J.E. (1990). Intermediates of recombination during mating type switching in *Saccharomyces cerevisiae*. *Embo J* 9, 663-673.
- Witte, G. (2004). Bakterielle Einzelstrang-DNA bindende Proteine und ihre Wechselwirkungen. Dissertation, Leibniz Universität Hannover.
- Wolfe, S.A., Nekludova, L., and Pabo, C.O. (2000). DNA recognition by Cys2His2 zinc finger proteins. *Annu Rev Biophys Biomol Struct* 29, 183-212.
- Worman, H.J., and Bonne, G. (2007). "Laminopathies": a wide spectrum of human diseases. *Exp Cell Res* 313, 2121-2133.
- Wu, L., and Hickson, I.D. (2003). The Bloom's syndrome helicase suppresses crossing over during homologous recombination. *Nature* 426, 870-874.
- Wu, W.H., Alami, S., Luk, E., Wu, C.H., Sen, S., Mizuguchi, G., Wei, D., and Wu, C. (2005). Swc2 is a widely conserved H2AZ-binding module essential for ATP-dependent histone exchange. *Nat Struct Mol Biol* 12, 1064-1071.
- Wysocki, R., Javaheri, A., Allard, S., Sha, F., Cote, J., and Kron, S.J. (2005). Role of Dot1-dependent histone H3 methylation in G1 and S phase DNA damage checkpoint functions of Rad9. *Mol Cell Biol* 25, 8430-8443.
- Zhang, D., Zaugg, K., Mak, T.W., and Elledge, S.J. (2006). A role for the deubiquitinating enzyme USP28 in control of the DNA-damage response. *Cell* 126, 529-542.
- Zhang, H., Roberts, D.N., and Cairns, B.R. (2005). Genome-wide dynamics of Htz1, a histone H2A variant that poises repressed/basal promoters for activation through histone loss. *Cell* 123, 219-231.
- Zhang, J., Shi, X., Li, Y., Kim, B.J., Jia, J., Huang, Z., Yang, T., Fu, X., Jung, S.Y., Wang, Y., *et al.* (2008). Acetylation of Smc3 by Eco1 is required for S phase sister chromatid cohesion in both human and yeast. *Mol Cell* 31, 143-151.

References

Zhao, R., Bodnar, M.S., and Spector, D.L. (2009). Nuclear neighborhoods and gene expression. *Curr Opin Genet Dev* 19, 172-179.

Zhao, X., and Rothstein, R. (2002). The Dun1 checkpoint kinase phosphorylates and regulates the ribonucleotide reductase inhibitor Sml1. *Proc Natl Acad Sci U S A* 99, 3746-3751.

Zhou, Z., Feng, H., Hansen, D.F., Kato, H., Luk, E., Freedberg, D.I., Kay, L.E., Wu, C., and Bai, Y. (2008). NMR structure of chaperone Chz1 complexed with histones H2A.Z-H2B. *Nat Struct Mol Biol* 15, 868-869.

Zhu, Z., Chung, W.H., Shim, E.Y., Lee, S.E., and Ira, G. (2008). Sgs1 helicase and two nucleases Dna2 and Exo1 resect DNA double-strand break ends. *Cell* 134, 981-994.

Zierhut, C., and Diffley, J.F. (2008). Break dosage, cell cycle stage and DNA replication influence DNA double strand break response. *EMBO J* 27, 1875-1885.

Zlatanova, J., and Thakar, A. (2008). H2A.Z: view from the top. *Structure* 16, 166-179.

Zou, L., and Elledge, S.J. (2003). Sensing DNA damage through ATRIP recognition of RPA-ssDNA complexes. *Science* 300, 1542-1548.

7 ABBREVIATIONS

3D	three-dimensional
5'FOA	5-fluoroorotic acid
53BP1	p53 binding protein 1
aa	amino acids
ABC	ATP binding cassette
AD	transcriptional activation domain used in Y2H
Ade	adenine
ADH	alcohol dehydrogenase
ADP	adenosine 5'diphosphate
Ala	alanine
Amp	ampicillin
APC/C	anaphase-promoting complex
ARPs	actin-related proteins
Asf1	anti-silencing function 1
Asp	aspartate
AT-rich	adenine and thymine rich
ATM	ataxia-telangiectasia mutated
ATP	adenosine 5'triphosphate
ATR	ATM and Rad3 related
BARD1	BRCA-associated ring domain-1
Bbd	bar body deficient
BD	DNA binding domain used in Y2H
Bdf1	bromodomain factor 1
βGal	β-galactosidase
BIR	break-induced replication
BIR-domain	baculovirus inhibitor of apoptosis repeat domain
BLM	Bloom syndrome
βME	beta-mercaptoethanol
bp	base pairs
BRCA1	breast cancer tumor suppressor 1
BSA	bovine serum albumine
C-terminal	carboxyterminal
C-terminus	carboxyterminus
CAF-1	chromatin assembly factor 1
CARs	cohesion-associated regions
cc	coiled coil
cdc	cell division cycle
Cent	centromere
CentpA	centromere protein A
CHD	chromodomain, helicase, DNA binding
ChIP	chromatin immunoprecipitation
ChIP-on-chip	ChIP followed by hybridization on a DNA microarray
Chk	CSK-homologous kinase
Chr	chromosome
Chz	chaperone for H2A.Z
CKII	casein kinase 2
CLB	cyclin B
CLN	cyclin
CSK	C-terminal Src kinase

Abbreviations

ctf7	chromosome transmission fidelity mutant 7 (Eco1)
D	aspartate
DDR	DNA damage response
DEAD/H box	(Asp-Glu-Ala-Asp/His)-box
DMSO	dimethylsulfoxide
DNA	deoxyribonucleic acid
dNTPs	deoxynucleotide triphosphates
DSB	double-strand break
dsDNA	double stranded DNA
DTT	dithiothreitol
E	glutamate
<i>E. coli</i>	<i>Escherichia coli</i>
e.g.	<i>exempli gratia</i> , for example
E1	activating enzyme
E2	conjugating enzyme
E3	ligase
Eco1	establishment of cohesion 1
EDTA	ethylenediaminetetraacidic acid
Esco1/2	establishment of cohesion (Eco1 homologs)
FACS	fluorescence-activated cell sorting
FHA	forkhead associated
FISH	fluorescence in situ hybridization
g	gram
G1	gap 1 phase of the cell cycle
G2	gap 2 phase of the cell cycle (interphase)
GAL	galactose
GFP	green fluorescent protein
γ H2AX	phosphorylated H2AX
Glu	glutamate
GST	glutathione-S-transferase
h	hour(s)
H1	histone 1 (linker histone)
H2A	histone 2A
H2A.Z	histone 2A.Z
H2AX	histone 2AX
H2B	histone 2B
H3	histone 3
H4	histone 4
HA	hemagglutinin epitope: YPYDVPDYA
HAT	histone acetyltransferase
His	histidine
HML	hidden <i>MAT</i> left, silent mating type locus
HMR	hidden <i>MAT</i> right, silent mating type locus
HO-endonuclease	homothallic switching endonuclease
HP1	heterochromatin protein 1
<i>hphNT1</i>	gene conferring resistance to hygromycin
HR	homologous recombination
HRP	horse radish peroxidase
Htz1	yeast H2A.Z
HU	hydroxyurea
i.e.	<i>id est</i> , that is
INO80	inositol requiring 80

IP	immunoprecipitation
IR	ionizing radiation
IRIF	ionizing radiation-induced foci
ISWI	imitation switch
K	lysine
Kan	kanamycine
<i>kanMX6</i>	gene conferring resistance to G418
kb	kilo base pairs
kD	kilo Dalton
kV	kilo Volt
l	liter
lacI	lactose repressor, lac inhibitor
lacO	lactose operator (lacI binding site)
LB	Luria-Bertani
LEM domain	LAP2, emerin, MAN1 domain
leu	leucine
LMU	Ludwig-Maximillians-University Munich
log	logarithmic
M	molar
m	milli ($\times 10^{-3}$)
μ	micro ($\times 10^{-6}$)
M	mitosis phase of the cell cycle
<i>MAT</i>	mating type locus
MBT	malignant brain tumor
Mcd1	mitotic chromosome determinant 1 (Scc1)
MDC1	mediator of DNA damage checkpoint 1
min	minute(s)
MMS	methyl methanesulfonate
MNase	micrococcal nuclease
MPIB	Max Planck Institute of Biochemistry
Mps3	monopolar spindle 3
MRN	mammalian Mre11/Rad50/Nbs1
mRNA	messenger RNA
MRX	sacharomyces cerevisiae Mre11/Rad50/Xrs2
MW	molecular weight
myc	epitope derived from the c-myc protein: EQKLISEEDL
n	nano ($\times 10^{-9}$)
N	asparagine
N-terminal	aminoterminal
N-terminus	aminoterminus
<i>natNT2</i>	gene conferring resistance to nourseothricin
NBS	Nijmegen breakage syndrome
NEM	N-ethylmaleimide
NHEJ	non-homologous end-joining
nt	nucleotides
°C	degrees celsius
OD _x	optical density at x nm
ORF	open reading frame
PAGE	polyacrylamide gel electrophoresis
PBS	phosphate buffered saline
PCNA	proliferating cell nuclear antigen
PCR	polymerase chain reaction

Abbreviations

PDB-ID	protein databank (www.pdb.org) identification number
PEG	polyethylene glycol
Pgk1	phospho-glycerate kinase
PHD-finger	plant homeo domain-finger (Zn finger like motif)
PI-3K	phosphoinositide-3-kinase
PIP	PCNA interacting protein
PML	promyelocytic leukaemia
Pol	polymerase
PolII	RNA polymerase 2
pQ	poly glutamine
ProA	protein A
ptc	phosphatase two C
PTMs	post-translational modifications
Q	glutamine
Rad	radiation
Rap80	receptor-associated protein 80
rDNA	DNA coding for ribosomal RNA
RE	recombination enhancer
Rfa	replication factor A
RFC	replication factor C
RFP	red fluorescent protein
RIDDLE	Radiosensitivity, immunodeficiency, dysmorphic features, learning disabilities
RNA	ribonucleic acid
RNAi	RNA interference
RNF	ring finger protein
RPA	replication protein A
rpm	rounds per minute
RSC	chromatin structure remodeling
RT-PCR	real time PCR
S	serine
s	second(s)
S-phase	DNA synthesis phase of the cell cycle
<i>S. cerevisiae</i>	<i>Sacharomyces cerevisiae</i>
SC	synthetic complete
Scc	sister chromatid cohesion
SDS	sodium dodecylsulfate
SDSA	synthesis-dependent strand annealing
SEM	standard error of the mean
Ser	serine
SIM	SUMO interacting motif
SMC	structural maintenance of chromosomes
Srs2	suppressor of rad6 #2
SSA	single-strand annealing
ssDNA	single stranded DNA
ssRNA	single stranded RNA
SUMO	small ubiquitin like modifier
SUN domain	Sad1p, UNC-84 domain
SUP	supernatant
SWI/SNF	switching defective/sucrose nonfermentable
SWR	SWI/SNF-related
T	threonine
TBST	tris-buffered saline with Tween-20

TCA	trichloro acidic acid
TE	Tris EDTA
Tet	tetracycline
TM	transmembrane
TPE	telomere positioning effect
Tris	Tris(hydroxymethyl)aminomethane
Trp	tryptophane
Ubc	ubiquitin conjugating
UIM	ubiquitin-interacting motif
Usp	ubiquitin-specific proteases
UV	ultraviolet light
V	Volt
v/v	volume per volume
VDJ	variable, diversity and joining genes
Ω	Ohm
WB	western blot
WCE	whole cell extract
WT	wild type
Y2H	yeast two hybrid
YPD	yeast bactopectone dextrose
Zn	zinc
ZnF	zinc finger

8 ACKNOWLEDGEMENTS

I would like to express my sincere gratitude and appreciation to my PhD thesis supervisor, Stefan Jentsch, whom I admire for his tenacity and devotion to science, the enthusiasm he exhibits in supervising students and his great intellect, which is characterized by an unconventional and individualist way of thinking. Stefan, next to being an outstanding scientist, you are also really good company, always open to discussion and new ideas, but also to ones concerns and worries. Thank you!

Next I would like to thank Peter Becker, not only for agreeing to co-referee this thesis work but also for his continuous support, advice and experimental suggestions over the past years as part of my thesis advisory committee (TAC).

Along these lines I would like to express my gratitude to the other members of the LMU doctoral thesis committee for refereeing this dissertation, especially Angelika Böttger and Thomas Cremer for taking the time to participate in my oral PhD examination. Additional thanks goes to the other IMPRS TAC-members, Zuzana Storchova in particular, but also to Olaf Stemmann and Erich Nigg. In addition, I would like to thank the coordination office of the International Max Planck Research School, especially Hans-Jörg and Maxi, for all their support over the years.

Many thanks to all members of the Jentsch lab, especially Steven, Michi, Kenji, Tim and the two Dirks, for making the lab a more fun place to work! A lot of this thesis work owes to the many insightful scientific discussions I had with Steven Bergink, and in the beginning of this work also with Lucian Moldovan. You are both brilliant scientists and I am certain you will succeed in your future scientific careers!

I would also like to acknowledge the technical help I had from various practical students over the years: Nina Suhartha, Caroline Haas, Elisabeth Weidinger, Birgit Schuster, Mathis Camerer, and Sybille Pfender. It was a great experience to teach, instruct and finally see you all thrive!

This thesis work was generously supported by a PhD scholarship of the Boehringer Ingelheim Fonds (BIF). Besides exceptional personal and financial support, the BIF-fellowship gave me the chance to participate in outstanding Abcam-, Keystone- and Titisee-conferences. Thank you Claudia, Sandra, Monika and Herrmann for all your help and generosity!

This dissertation is dedicated to my parents, Inge and Hans Hiller, for their never-ending love, confidence and encouragement. They have kindled and share my love for science, music and perfection. Finally my sincere thanks and love go to Axel, for his patience, understanding and support – not only in day-to-day happenings – but without whom my life just wouldn't be complete.

Kontakt: Plinganserstr. 59
81369 München
Telefon: 089-72015072
E-Mail: natalie.j.hiller@web.de

Geburtsdatum: 19.09.1984
Geburtsort: Mannheim
Nationalität: Deutsch

AKADEMISCHE AUSBILDUNG:

2006-2010: **Promotion** an der Ludwig-Maximilians-Universität München
International Max Planck Research School (IMPRS)
In der Arbeitsgruppe von Prof. Dr. Stefan Jentsch
am Max Planck Institut für Biochemie, Martinsried

2001-2006 **Studium der Biochemie** an der
Eberhard-Karls-Universität Tübingen

1994-2001 **Gymnasium:** Werner-Heisenberg-Schule, Leverkusen

1990-1994 **Grundschule:** German School New York

FORSCHUNGSTÄTIGKEIT VOR DER PROMOTION:

2006 **Diplomarbeit** am Max Planck Institut für Biochemie
im Labor von Prof. Dr. Stefan Jentsch
Thema: „Studies on SUMO E3-Ligases“

2004-2005 **Fulbright Enterprise Scholarship**
Forschungsjahr im Labor von Prof. Dr. Günter Blobel
Rockefeller University, New York, USA

2003-2004 **Hilfswissenschaftliche Mitarbeit**
Im Labor von Prof. Dr. Andreas Mayer,
Friedrich Miescher Laboratorien, Tübingen

STIPENDIEN:

2007-2009 Boehringer Ingelheim Fonds, Doktorandenstipendium
2002-2006 Studienstiftung des deutschen Volkes
2004-2005 Fulbright Enterprise Scholarship, Vollstipendium
2001-2003 Fonds der Chemischen Industrie, Jubiläumsstipendium

PUBLIKATIONEN:

Kalocsay M.*, Hiller, N.J.* and Jentsch S. (2009). Chromosome-wide Rad51 spreading and SUMO-H2A.Z-dependent chromosome fixation in response to a persistent DNA double-strand break. **Mol. Cell.** 33, 335-43. **these authors contributed equally*

Takahashi Y., Dulev S., Liu X., Hiller N.J., Zhao X. and Strunnikov A. (2008). Cooperation of sumoylated chromosomal proteins in rDNA maintenance. **PLoS Genet.** 4, e1000215.